MICROCOPY RESOLUTION TEST CHART
NATIONAL BUREAU OF STANDARDS-1963-A

AD-A134146

A GENERAL FIELD THEORY FOR VORTEX

STRUCTURE AND INTERACTION

Prepared by:

Francis H. Nicholson, Ph.D.

Prepared for:

Office of Naval Research

Under Contract No:

N00014-80-C-0026

3 OcTOBER 1983

DTIC
ELECTE
OCT 27 1983
B

DTIC FILE COPY

This treatise is dedicated with
love and admiration to

KEVIN JOSEPH MURPHY

whose support and encouragement
made the impossible possible

TABLE OF CONTENTS

I.   INTRODUCTION

The purpose of this work is to present ~~to the scientific commun-ity~~ a general field theory describing the structure and interaction of vortices, both atmospheric and extraterrestrial. This field theory is characterized by four main elements:

(1)   New laws of physics,

(2)   New mathematical expression for these laws,

(3)   A conceptual framework for application of these laws to vortex structure,

(4)   Data for partial verification of these laws.

Such a general field theory is also termed a "paradigm", Kuhn (1970). After consideration of the field theory, if the scientific community accepts the newly proposed paradigm, this acceptance is termed a "paradigm shift." According to Kuhn a paradigm is a "scientific achievement that some particular scientific community acknowledges for a time as supplying the foundation for its further practice." This achievement is "sufficiently unprecedented to attract an enduring group of adherents away from competing modes of scientific activity." Simultaneously it is "sufficiently open-ended to have all sorts of problems for the redefined group of practicioners to resolve."

Kuhn (1970) cites paradigms as examples of scientific practice which include law, theory, application and instrumentation. The paradigm here introduced incorporates such laws, theory and application, and is inspired by recently developed scientific instrumentation, the spin-scan camera of the geosynchronous meteorological satellite. This paradigm further proposes an expansion of mathematical systems and a theory for the structure of a wide range of vortex phenomena for the utilization and application of these laws. Lastly, the paradigm proposes a theory incorporating two further laws to describe the behavior

1

of interacting vortices.

The proposed laws are cast into a predominantly methematical
form which may then be checked in part through observation via
this new instrumentation which was the touchstone for the
paradigm articulation. Kuhn states (p. 26) that "seldom (are
there) many areas in which a scientific theory, particularly
if it is cast in a predominantly mathematical form, can be
directly compared with nature."

The Anomaly of Band Behavior

Kuhn says further that "discovery commences with the awareness
of anomaly, i.e., with the recognition that nature has some-
how violated the paradigm-induced expectations that govern
normal science." (p. 52). The anomaly in this case is the
behavior and structure of synoptic scale vortices seen in
their entirety by the geosynchronous meteorological satellite.
The presence and behavior of the spiral bands of clouds in
both tropical and extratropical vortices was an event for
which satellite meteorologists were not adequately prepared.
The seemingly contradictory behavior of these bands in these
two types of storms only deepens the puzzle.

These phenomena have not been explainable in simple and
concise terms. Such an explanation of the structure of at-
mospheric vortices seen from meteorological satellites seems
to require a new body of theory. But as Kuhn says (p. 46)
"A new theory is always announced together with applications to
some concrete range of natural phenomena; without them it
would not even be a candidate for acceptance." And rightly
so, for otherwise the scientist pursuing the research of
"normal science" would be too easily distracted by trivial
exceptions to the paradigm under which he operates, and
thereby be unable to continue his own work.

The theory advanced here has been developed to explain the vortex structure (including spiral bands) and behavior of these vortices observed from meteorological satellites. This theory must then be accompanied by application to a concrete range of natural phenomena. The field theory, or paradigm, which explains the presence and behavior of spiral bands in part by specifying the lateral flow field in the vortex, is correlated with flow fields of vortices ranging in size from fifteen centimeters in radius, in a laboratory Dines vortex cage, all the way up to the stellar velocities in the spiral galaxy, M31, a range of 21 orders of magnitude.

THE GENERAL FIELD THEORY - AN OVERVIEW

By its very nature a general field theory is complex and extensive. It is not surprising, therefore, that a road map through the theory is needed. Such a road map is provided in the form of three sets of flow diagrams. In these accompanying diagrams the Field Theory is divided initially into Theory and Application (See Set I). The first set details the Theory, the second and third sets detail the Application, Set II, the Vortex Structure and Set III, the Vortex Interaction. Let us now consider Set I.

From Set I we see that the Theory is further divided into Field Physics and Mathematics. The Field Physics is comprised, in turn, of five new field laws governing the structure and interaction of vortices. The Mathematics provides a systematic expression for these laws applicable to a host of natural phenomena. These mathematical systems include both extent and newly discovered coordinate systems separable in three dimensions in Laplace's equation and the various kinds (up to three) of solutions available in each coordinate system.

GENERAL FIELD THEORY

Theory — **Application**

<u>Field Physics</u>   <u>Mathematics</u>   <u>Vortex Structure</u>   <u>Vortex Interaction</u>

THEORY

<u>Field Physics</u>   <u>Mathematics</u> (Solutions to Laplace's Eq.)

Structural Laws   Interaction Laws   Ellipsoidal Coordinates   Cyclidal Coordinates

FIELD PHYSICS

<u>Structural Laws</u>   <u>Interaction Laws</u>
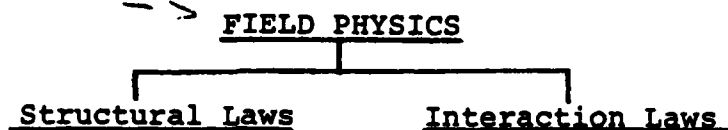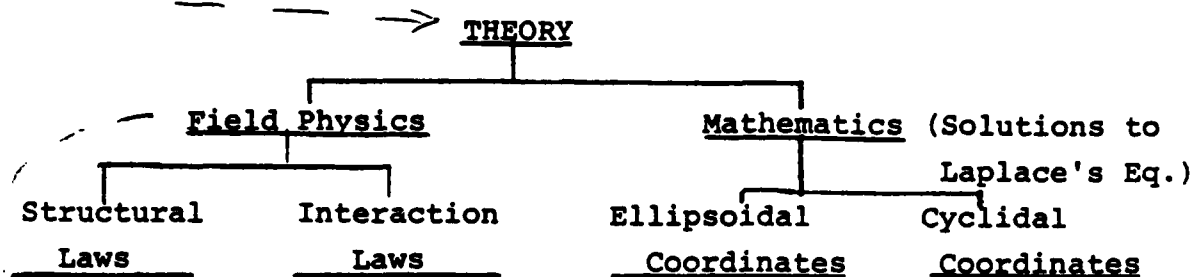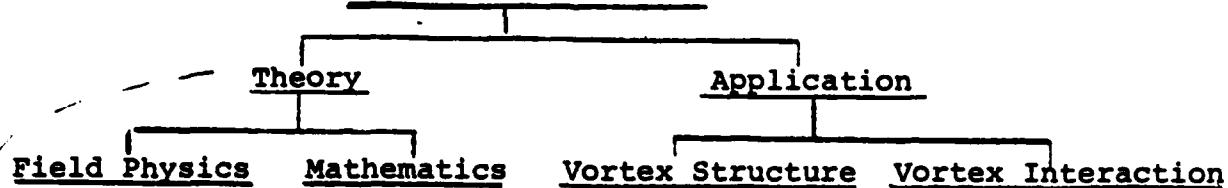
$$\text{I-III} \left\{ \nabla_2^2 \begin{pmatrix} \zeta \\ \delta \\ p \end{pmatrix} = 0, \infty \right.$$

(Lateral with regard to either vertical axis or axial circle)

$$\text{IV-V} \left\{ \begin{array}{l} \Gamma_t = \sum\limits_{i=1}^{n} \Gamma_i \\ Q_t = \sum\limits_{i=1}^{n} Q_i \end{array} \right.$$

MATHEMATICS

Ellipsoidal Coordinates (Spiral Variants)   <u>Cyclidal</u>

<u>Euclidean</u>   <u>Non Euclidean or Hyperbolic</u>

<u>Cylindrical</u>   <u>Spherical</u>   <u>Hyperbolic</u>
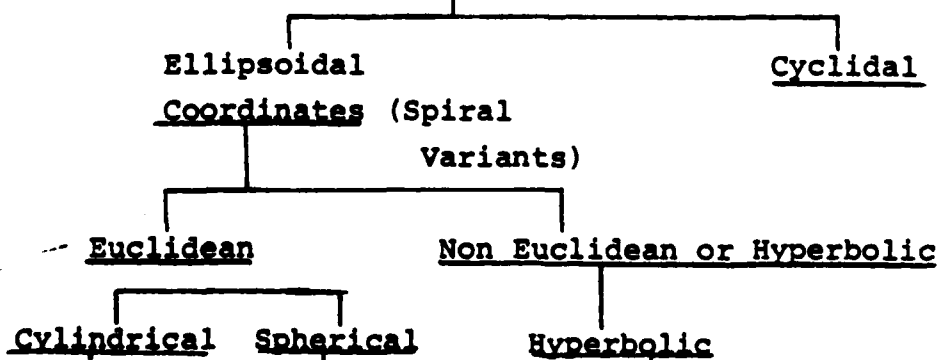
Curvature = 0,   positive constant,   negative constant

Application is divided into Structure and Interaction. The vortex structure includes such diverse phenomena as tornado funnels, nuclear fireballs, the banded structure of the Jovian atmosphere, the movement of stars and the shape of spiral arms in galaxies and the winding spiral frontal systems of terrestrial extratropical storms. The vortex interaction includes the mutual interaction of hurricanes known as the Fujiwhara effect, looping and cycloidal hurricane paths, and abrupt path changes. We will now look at the Field Physics in greater detail.

FIELD PHYSICS

Field Physics implies the utilization of tensors. According to Lanczos (1970),

> "During the nineteenth century, when the importance
> of tensors became increasingly manifest, the evo-
> lution of physics tended to turn more and more deci-
> sively from the particle physics of Newton to a
> field physics, advocated by Fresnel, Faraday, Max-
> well, and their followers. Here our attention is
> focused on the entire space, or some limited portion
> of it, without bias to certain small regions, the
> 'particles', which in Newton's time were designated
> as the seats of physical action. Now the realization
> came that the 'field strength' existed everywhere
> and it was a mere accident that the material particle
> was needed for the demonstration of its existence.
> The concept of a 'field' thus came in use, in which
> physical action is present in all points of space.
> The Maxwellian equations, which describe the action of
> electromagnetic forces, are partial differential
> equations which involve the space and time derivatives
> of the electric and magnetic field strengths."

The field laws proposed here are partial differential equations involving the space and time derivatives of the frictional and pressure field strengths. The field physics is composed of five physical laws, three governing the structure of vortices and two their interaction.

Structure

The laws governing the structure of vortices are all expressed in the two dimensional form of Laplace's equation. The two dimensions in question are orthogonal to the axis of reference of the vortex in question, whether that axis is a central axis or constitutes the axial circle or a torus (cf. Figure 1.1). This distinction is made more clear in the Application part of the text. These laws state (in order) that the two dimensional Laplacian of the normal component vorticity (i.e. parallel to the axis), lateral divergence (within the surface of reference) and pressure all either satisfy Laplace's equation in two dimensions or else Laplace's equation is undefined. The undefined condition would occur at a field boundary of a piecewise continuous vortex.

Interaction

The interaction laws arise naturally out of the consideration of vortices as discrete field entities. How do vortices interact? Laws IV and V allow the vortices to remain as discrete field entities and still satisfy Stokes' and Gauss' theorems respectively. The partitioning of circulation, orbital and spin vorticity in Stokes' circulation theorem is the heart of the Fourth Law. The allocation of the general sink function and the local sink function, and its radial counterpart are the subject of the Fifth Law.

Solenoidal   Toroidal

Central axis

ζ

U_θ

U_θ

U_θ

U_θ

ζ

ζ

Cylindrical

Axial Circle

ζ

Central axis

U_ν
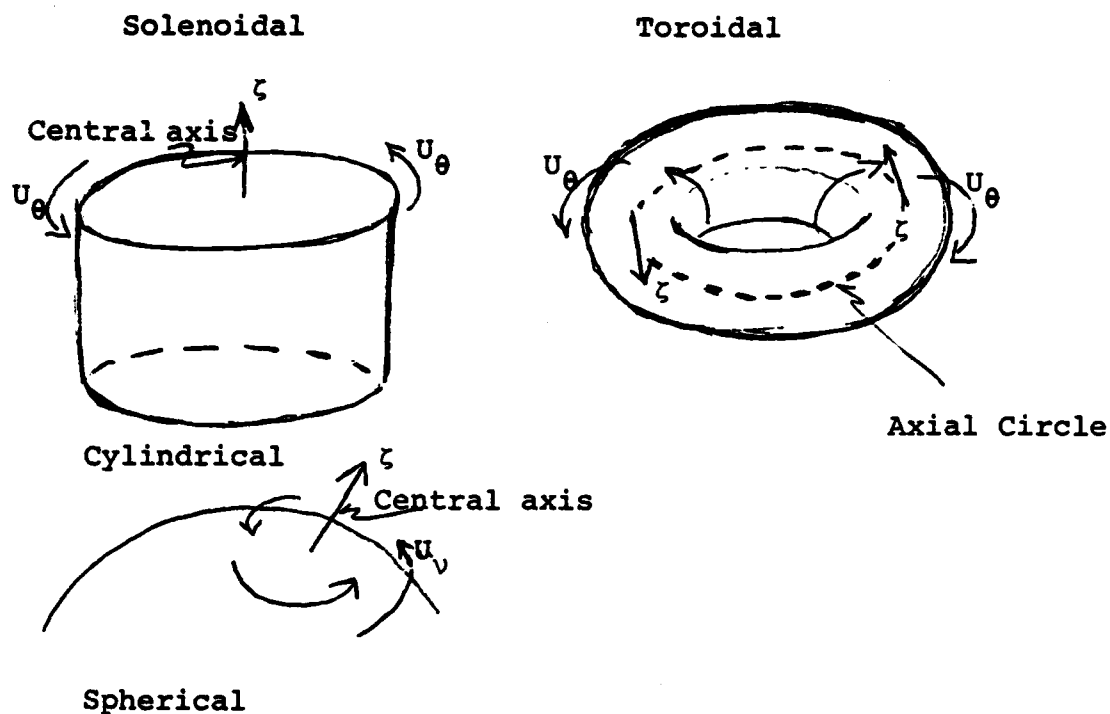
Spherical

Figure 1.1   Comparison of Solenoidal and Toroidal Vortices.
              Solenoidal vortices have a vertical central axis
              as in figures on left, cylindrical and spherical
              vortices. Figure on right has an axial circle.
              Vorticity is defined in relation to axis on left
              or axial circle on right. Solenoidal vortices
              have surface of constant curvature, either
              positive, zero or imaginary, and may have spiral
              mutations.   Toroidal vortices do not have
              constant curvature and therefore no spiral
              mutations. Schroedinger's and spatial wave
              equation are separable in the former, but not
              the latter.

Frictional Equivalents of Laws I and II

We may also restate Laws I and II: the lateral frictional
force possesses neither a curl nor a divergence, and though
it exists, it is so distributed as to locally alter neither the
circulation nor the sink function of the individual vortex.
As a consequence, the circulations and sink functions must
take on a specific form consonant with an integrated expression
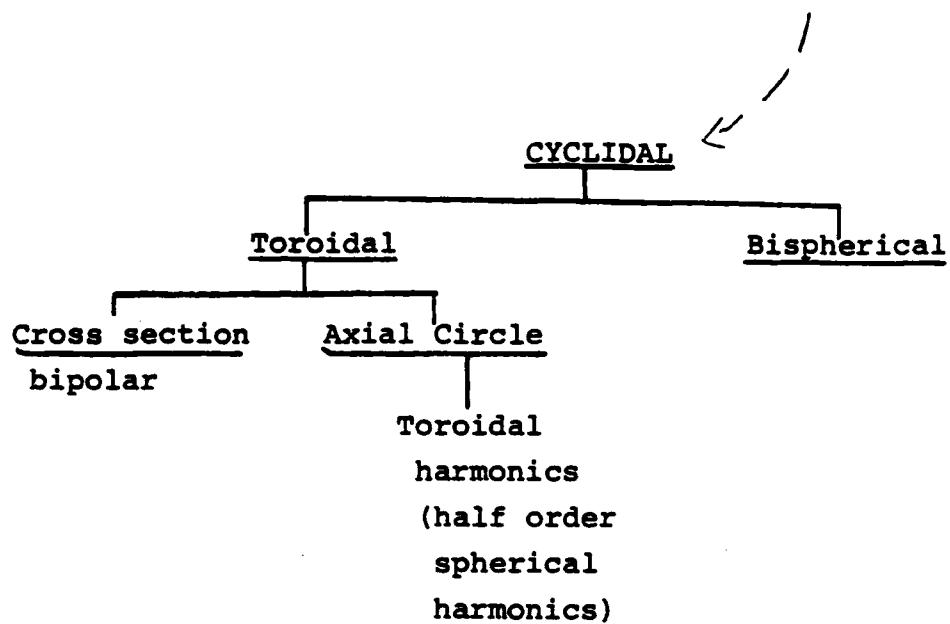of the first two laws.

The lateral frictional force is defined as having components
only within the surface of interest. There are no components
outside of the surface, nor any derivatives of those components
outside of the surface. Hence, in cylindrical coordinates,
there are no derivatives with respect to height, z, in the
lateral frictional force. All derivatives are with respect
to either radius (or its logarithm), or azimuth, or a linear
recombination of the logarithm of the radius and the azimuth.
This latter is the subject of the mathematical coordinate
systems both extant and new. The linear recombinations are
properly the subject of the logarithmic spiral coordinates.

MATHEMATICS

The mathematical part of the Theory provides a framework
for solutions to the first three laws. These solutions
occur in a number of extant coordinate systems and six
newly-discovered ones, which are more general expressions
of ones previously known. These coordinate systems are
termed ellipsoidal and cyclidal.

CYCLIDAL COORDINATES

Cyclidal coordinates are divisible into toroidal and bi-
spherical. The former are useful in describing one fluid

```
                                    CYCLIDAL
          ┌────────────────────────────┴────────────────────────────┐
       Toroidal                                              Bispherical
   ┌──────────┴──────────┐
Cross section        Axial Circle
   bipolar                  │
                         Toroidal
                         harmonics
                        (half order
                         spherical
                         harmonics)
```
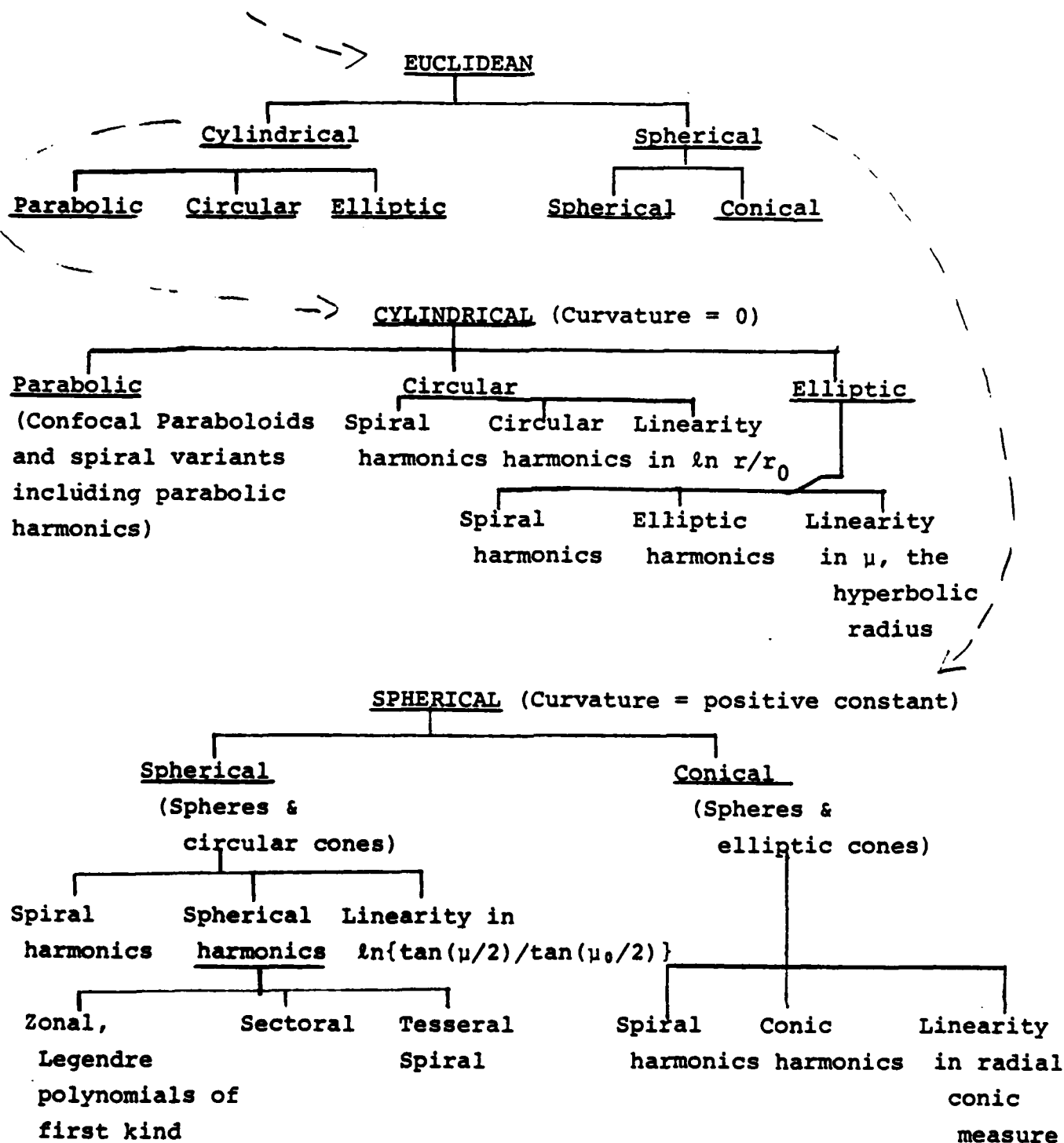
propogating as a pulse through another. This would include a smoke ring created by a playful smoker, a drop of blood falling as a ring in a Copper Sulfate solution, a rising cumulonimbus cloud or a rising nuclear fireball. It is the toroidal coordinates which display an axial ring. The surface normal to this ring is the proper forum for the two dimensional Laplacian.

Bispherical coordinates also possess an axial ring but at this writing a relevant application is not apparent to the author.

Toroidal coordinates are separable in Laplace's equation and possess solutions known as toroidal harmonics. The solutions in the "radial" components of the torus are combinations of half order spherical harmonics of the first and second kind on hyperbolic functions of the radial coordinate and sinusoidal functions of the azimuthal coordinate. Their cross sections are given in bipolar coordinates.

ELLIPSOIDAL COORDINATES

The ellipsoidal coordinates, on the other hand, are degenerate forms of more general spiral forms documented in Appendix A. The ellipsoidal coordinates may be divided into Euclidean and non-Euclidean, or hyperbolic. The former have surfaces of interest with curvature either a positive constant, or zero. These surfaces occur in cylindrical and spherical forms respectively. In non-Euclidean or hyperbolic coordinates, the surface of interest has a curvature with a negative constant and is a circular hyperboloid of one sheet. The Euclidean coordinates may be further subdivided into cylindrical and spherical types.

EUCLIDEAN

Cylindrical   Spherical

Parabolic   Circular   Elliptic   Spherical   Conical

CYLINDRICAL (Curvature = 0)

Parabolic   Circular   Elliptic

(Confocal Paraboloids   Spiral   Circular   Linearity
and spiral variants   harmonics harmonics in $\ln r/r_0$
including parabolic
harmonics)   Spiral   Elliptic   Linearity
                        harmonics   harmonics   in μ, the
                                             hyperbolic
                                             radius

SPHERICAL (Curvature = positive constant)

Spherical   Conical
(Spheres &   (Spheres &
   circular cones)   elliptic cones)

Spiral   Spherical   Linearity in
harmonics   harmonics $\ln\{\tan(\mu/2)/\tan(\mu_0/2)\}$

Zonal,   Sectoral   Tesseral   Spiral   Conic   Linearity
Legendre   Spiral   harmonics harmonics   in radial
polynomials of   conic
first kind   measure

CYCLINDRICAL COORDINATES

There are three types of cylindrical coordinates; parabolic, circular and elliptic. The parabolic coordinates consist of confocal paraboloids and possess spiral variants with spiral parabolic harmonics as solutions to Laplace's equation.

The circular coordinates consists of circular cylinders intersected by radial planes. These coordinates have solutions which are linear in $\ln r$, circular harmonics and log spiral harmonic solutions, consisting of a linear recombination of $\ln r/r_0 + i\theta$. The elliptical coordinates duplicate the results of the circular harmonics, consisting of elliptic cylinders intersected by confocal hyperboloids. Again, there are elliptic harmonics, spiral elliptic harmonics based on a linear recombination of hyperbolas and ellipses and solutions linear in the radial elliptic coordinate.

SPHERICAL SYSTEMS

The spherical systems may be divided into two classes, spherical and conical. Spherical coordinates have nodes defined by spheres intersected by circular cones, and partitioned azimuthally by planes intersecting at a common axis. Conical coordinates, on the other hand, have nodes composed of the intersection of spheres, elliptic cones and cylindrical hyperboloids of two sheets.

Each system has solutions to Laplace's equation which are either linear in the logarithm of the tangent of the half radial angle (suitably scaled), spherical harmonics or spherical log spiral harmonics in the case

12

of spherical coordinates, or their counterparts in conical coordinates. The spherical harmonics may also be subdivided into zonal, sectoral or tesseral harmonics. Zonal harmonics are a function of latitude only, sectoral of longitude only, and tesseral of both. The spiral harmonics may be considered to be a form of tesseral harmonics. Zonal harmonics have solutions which are Legendre functions of the first kind and yield bands of positive and negative solutions alternating as a function of latitude. It is interesting to note that solid rotation constitutes a solution of Laplace's equation, since the Coriolis parameter is a Legendre function of the first kind, and of order one, i.e. $\sin \phi$. As such, therefore, the Coriolis parameter, $2\Omega \sin\phi$, is a solution to the first Law, i.e., $\nabla_2^2 \zeta = 0$.

1.2   APPLICATION - VORTEX STRUCTURE

INTRODUCTION

In this section we deal with the Application of the General
Field Theory to Vortex Structure. In the preceding section
the Field Physics and Mathematics were outlined. Here, the
first three laws governing vortex structure are considered
along with their mathematical manifestations as they appear
in natural phenomena.

Just as there are two kinds of Euclidean Coordinate systems,
the ellipsoidal and cyclidal, there are also two kinds of
vortex systems. These corresponding systems are the
Solenoidal and Toroidal systems. A solenoidal system is
characterized by a central vertical axis. A toroidal system,
on the other hand, is characterized by an axial ring, as
the name would suggest. The solenoidal vortices have log
spiral harmonic solutions. The toroidal vortices do not.

Following the mathematical subdivision, the solenoidal vortices
may be divided into cylindrical and spherical types. The
cylindrical vortices, in turn, may be divided into three
further kinds, depending upon the fluid in which they appear
most prominently, the terrestrial atmsophere, the ocean, or in
the rarified reaches of space.

SPIRAL GALAXIES

The movement of stars in M31 and the spiral arms are a
manifestation of the circular cylindrical vortex in space.
The stellar motions display a double maximum, peculiar to
the three piece, cylindrical model called the "Double Vortex"
which is discussed at some length later in the text.

APPLICATION

Structure   Interaction

Solenoidal   Toroidal

Cylindrical   Spherical   Atmospheric   Plasma

Terrestrial   Galactic   Partial   Total
                                       Storms   General Circulation
                                                         & Climate
Atmospheric   Oceanic

ATMOSPHERIC

Mechanical   Devils   Waterspouts   Tornadoes   Hurricanes

Dines Vortex   Sand,   Lesser,   Hurricane   Hurri-
   Cage   Snow,   Tornadic   induced,   canes,
(Wilkins)   Fire,   Great Plains   Indean Ocean
                Dust   ordinary,   Cyclones,
                                             Great Plains   Pacific
                                                long path   Typhoons

GALACTIC

Pre-Solar System   Spiral Galaxies

Interacting   Spiral Arms   Double Vortex
   Spiral Arms   Structure

15

This double vortex, and others in the cylindrical genre, are three part vortices in which the vorticity and divergence fields are piecewise and continuous. Each piece satisfies Laplace's equation. At the juncture of the pieces the Laplacians of divergence and vorticity are undefined. The three parts of the vortex are the core, inner regime surrounding the core, and the outer regime exterior to the other two.

PREPLANETARY SOLAR SYSTEM

Using the spiral galaxy as a model of the preplanetary solar system, we may hypothesize how the formation of the sun and the planets might have occured from a dual vortex with spiral arms consisting of a solar system sized nebula. The dual vortex is characterized by two maxima in the tangential velocity field. These maxima arise out of a very steep concentration of vorticity. To be precise, a steep concentration of vorticity enclosing an even steeper concentration of vorticity. Since each concentration accounts for a velocity maximum, the term dual vortex.

The divergence pattern ordinarily follows the vorticity pattern so that the center of the vortex is characterized by an extremely high concentration of negative divergence, or in this case, the necessary matter for the formation of the central star of a solar system. Were the axially symmetric vortex the only allowable mode, then it would be doubtful that the outlying matter would achieve sufficient concentration to form planets. The presence of spiral solutions, and their orthogonal counterparts presents a possible mechanism for concnetration of planetary matter.

Just as in a hurricane, where the prominent divergence field is confined to the first three harmonics, so there may be

16

such a concentration in the preplanetary vortex. If a
higher order (wavenumber 10) orthogonal spiral appears,
then the mechanism for separation of the arm into appropriate
segments, each coallescing into its own planetary mass is at
hand. The phenomenon would be much like an interference
pattern in a ripple tank. In this case, however, the interfer-
ence pattern would arise out of two separate but overlapping
solutions to Laplace's equation in the gaseous divergence field,
orthogonal spiral arms.

The concept of an interference pattern is a logical extension
of combining axially symmetric with spiral asymmetric solutions
to the vorticity and divergence fields. Such a solution is not
a priori impossible if the boundary conditions are appropriate
and independent.

Thus a mechanism exists for planetary and solar creation
based on the hypothesis that the lateral frictional force
within the preplanetary vortex be incapable of sustaining
a divergence field. Or more precisely, the field wide lateral
frictional force is non-divergent.

Further support may be gleaned from the realization that the
bulk of the planetary masses for the outer planets - Jupiter,
Saturn, Uranus and Neptune - are composed of gases which, nearer,
would have been driven off in vast quantities by solar heating.
It is well known, for instance, that earth's atmsophere is
a secondary atmosphere. It is quite conceivable that if the
original mass of the earth's atmosphere were returned to the
earth, then its mass would be equal to if not greater than
Jupiter's. In that case, the divergence field creating the
masses of the respective planets, could very easily increase
in intensity in a manner consonant with the distribution
of divergence in the spiral arms of a hurricane.

OCEANIC VORTICES

Eddies shed by the Gulf Stream and other currents such as the
Kuroshio may also be described in cylindrical coordinates.
These eddies undoubtedly are far less vigorous than their
severe atmospheric counterparts, and as such probably are
describable by a single regime or "simple" vortex, also
described in more detail below.

ATMOSPHERIC VORTICES

The bulk of the latter section deals with cylindrical
atmospheric vortices. Data on their circulations has
been amassed, covering such divers phenomena as laboratory
Dines vortex cages, tornadoes, waterspouts and hurricanes.
Of the naturally occuring severe atmospheric vortices, all are
characterized by spiral phenomena of one sort of another.
Waterspouts have been observed to display spiral rain
curtains. Tornadoes show hook echoes on radar. Hurricanes
have spiral rain squalls preceding the main storm.

The dust devil, waterspout and tornado display funnels but
the winds exterior to the funnel are not accompanied by
characteristic optical phenomena except within the lower
reaches of the boundary layer. The only manifestation
of the winds, therefore is the debris kicked up in transiting
the earth's surface.

In the case of the waterspout, this amounts to spray droplets.
In the tornado, the debris can be considerably larger, includ-
ing lethal missiles such as lawnmowers, human bodies, flying
timber and even Volkswagons. The dustdevil funnel is made
obvious by the dust picked up from the surface of the earth.
The tornado funnel, on the other hand, is a manifestation of

the third law insofar as the funnel cloud itself is evidently
a lowering of the lifting condensation level, and as such,
assuming a vertically homogeneous mixing ratio, represents
a constant pressure surface. Since under appropriate condi-
tions the height of the pressure surface may be substituted
for a pressure variation then the shape of the funnel, the
lifting condensation level, is a logarithmic surface of revolu-
tion, thereby satisfying Laplace's equation. The radial com-
ponent of the height of the constant pressure surface is
linear (although possibly piecewise so) in the logarithm of
the radius such that

$$z = z_0 \ln(r/r_0)$$

where r_0 is a typical scaling dimension of the tornado funnel.
Since the Laplacian is two dimensional, then the height of the
pressure surface, and even the central axis itself may move
back and forth horizontally, giving the funnel a sinuous,
rope like stucture.

The tornadic winds may be described by the three part mature
vortex discussed at length later in the text. It is not
unusual for dust devils to have a lowering of the pressure
sufficient that a tuba cloud descends into the middle of the
dust devil vortex turning the dust devil into a tornado.
Waterspouts may also reach tornadic intensity. The three
kinds of vortices evidently occupy positions along a continuum
where the dividing line is an arbitrary phase change for water
vapor. The division is therefore phenomenological rather
than dynamic.

Less violent manifestations of these vortices are snow, sand
and fire devils. The snow devils most commonly occur over
freshly fallen snow, loosely packed and clean, the sanddevils over

white sandy beaches and firedevils over forest fires.

All of these are different natural manifestations of vortices
satisfying the first three laws in cylindrical coordinates.
The differences arise out of the funnel manifestation and the
causal energetics, but the overall dynamics are the same,
only the scale is different.

The largest atmospheric cylindrical vortex is the hurricane.
As the phenomena increase in size their duration is typically
longer. The hurricane may have a life cycle up to ten days
or longer, the tornado up to a half hour, the dust devil a
matter of five or ten minutes, and sand and snow devils a
matter of tens of seconds.

The funnel of the hurricane is invisible and manifest as the
eye, whereas the winds are underlined by clouds and rain.
Indeed the hurricane is divided into three parts, the eye,
convective ring and outer hurricane corresponding to the three
part mature vortex. The vortex structure of the divergence
field may, in the axially symmetric case, be described by a
double ring vortex or toroidal vortex. Thus the horizontal
and vertical components of the hurricane, and conceivably
other vortices, may represent the linking of toroidal and
solenoidal vortices. This would certainly be an interesting
point to pursue.

Thus the cylindrical vortices include, in roughly ascending
order of intensity, areal coverage and duration, sand and
snow devils, dust and fire devils, waterspouts, tornadoes
and hurricanes.

Sand and snow devils show no funnels and last less than a

minute. Their energetics arise out of a breakdown of the
surface superadiabatic lapse rate and usually occur over
snow or white sand, areas of high visible but low infrared
albedo. Dust and fire devils show a funnel like structure
due to the dust and flames and/or smoke incorporated into the
rising sleave or air and particulates in the "inner" vortex
in contrast to the clean and descending air in the core of
the vortex.

Dust devils commonly occur over superheated arid terrain and
may rise several thousand feet into the air possibly because
of the vast extent of superheated air in the lower planetary
boundary layer capable of feeding the dust devil's divergence
field.

Fire devils have been observed over volcanoes, forest fires
and may have been present in the firestorms over the burning
cities of Dresden, Hiroshima and Nagasaki. Firestorms are
conflagratory equivalents of min-hurricnaes, and like hurri-
canes are capable of spawning their own lesser vortices.
Hurricanes may spawn tornadoes which are weaker than their
Great Plains equivalents and fire storms may spawn firedevils.
Like hurricanes, it is conceivable that there may be spiral
characteristics to the burn patterns, but that remains to be
seen.

The largest vortex which can be treated in cylindrical
coordinates is the hurricane. Even this is borderline
since the larger hurricanes, or typhoons, approach the
dimensions of smaller extratropical storms. The hurricane is
characterized by three regimes and spiral rain bands which
include wind shifts first backing then veering and pressure
jumps. This is indicative of spiral patterns not only in the
divergence field, but the vorticity and pressure fields as
well. The three regimes, core, inner and outer regimes of

the mature vortex corresponds approximately with the hurricane eye, the convective ring and the outer storm. The spiral bands represent log spiral harmonic solutions of the low level divergence field to Laplace's equation. The larger vortices are more properly treated in spherical coordinates since the lateral dimension begins to display evidence of the curvature term. Since the effective atmosphere is only about ten miles thick, the outer portions of a larger vortex bend more than the thickness of the atmosphere, so that unless the earth's curvature is taken into account, horizontal coordinates become meaningless after a certain distance.

SPHERICAL VORTICES

Spherical vortices may be divided into two types. The first type, or storms, do not occupy the whole sphere and mathematically a scaling factor must be introduced into the spiral variation of spherical coordinates. The second type, or general circulation, does occupy the whole sphere and spiral phenomena centered at one or the other of the poles characterize both Earth and Venus.

Both partial spherical vortices and complete spherical vortices may be divided into vortices associated with the inner planets, Venus, Earth and possibly Mars, and the outer planets, Jupiter, Saturn, Uranus and Neptune. The inner planets are characterized by moderate to slow rotation rates and strong solar insolation resulting in pronounced radiation imbalances between poles and equators necessitating significant meridional heat exchange between equator and poles in the planetary atmospheres, and in the case of earth, the planetary oceans.

The outer planets, on the other hand, are characterized by weak insolation, rapid rotation rates and pronounced zonal characteristics. The general circulation of the inner planets

SPHERICAL

	Partial	Total
	Storms	Climate & General Circulation
Degenerate		Sphere in solid rotation, Coriolis Parameter
Terrestrial—	Extratropical Cyclones	Terrestrial Type Circulations, Piecewise absolute vorticity, Circumpolar spirals - meridional exchange, Venusian Spirals.
Jovian — —	Great Red Spot, Lesser Jovian Spots (high meridional shear environment)	Jovian Type Circulations, with zonal features in form of banding and circulations rapidly alternating with latitude, increasing toward equator. Intertropical Convergence Zone
Solar — —	Sun Spots	Solar Circulation

may be modelled by a combined vorticity and divergence field
with both spiral and axially symmetric characteristics.
The axially symmetric properties are discussed in greater
depth in Appendix B. Essentially, the planetary vorticity
fields are of two parts, polar and tropical. The absolute
vorticity of the polar region is constant. The absolute
vorticity of the tropics is linear in the logarithm of the
tangent of the half colatitude, or

$$\begin{bmatrix} \zeta \\ \delta \end{bmatrix} = \begin{bmatrix} \zeta_0 \\ \delta_0 \end{bmatrix} + \iota \, \ell n \, \tan(\phi/2 + \pi/4)$$

where ϕ is latitude and ι the gradient of ζ and δ with
respect to the logarithm of the tangent of the half
colatitude at $\phi = \phi_0$. The spiral asymmetries in the diver-
gence field are spherical log spiral bands which appear as
straight bands in Mercator projections in Kornfield (1969) and
as ordinary polar log spirals in stereographic projections
also in Kornfield (1969).

Terrestrial storms are characterized by spherical log spiral
bands in the cloud fields. These bands are also accompanied
by pressure jumps and backing and veering of the winds indica-
ting like spiral asymmetries in the pressure and vorticity
fields. The outer planets are distinguished by alternating
zones of banding in the atmosphere. These zones and the
accompanying circulation fields may be modelled by zonal
harmonics, solutions to Laplace's equation of the divergence
and vorticity fields dependent solely on latitude given by
Legendre polynomials in cos θ and cos 2θ and their corresponding
series, where θ is the colatitude, $\pi/2 - \phi$. This is treated
in greater detail in Appendix C.

The corresponding partial spherical vortex in the outer planets,
the Great Red Spot of Jupiter, is modelled by conical coor-
dinates and their spiral equivalent. This is an elliptical

24

vortex arising in a high shear environment.

The general circulations of Jupiter and Saturn and probably Uranus and Neptune are characterized by multiple peaks and valleys increasing in amplitude toward the equator. These peaks and valleys show promise of being described by the phase shift in the difference of two close Legendre polynomials of the first kind corresponding to the planetary vorticity field. Such a phase shift constitutes a Legendre series.

Thus the theory of solenoidal vortices describes both cylindrical and spherical vortices. The atmospheric cylindrical vortices are predominantly warm core, but also include oceanic eddies and spiral galaxies. The spherical vortices are cold core and cover partial spherical vortices, or storms, terrestrial extratropical and the Great Red Spot; and full spherical vortices, or general circulations. The latter are both mixed meridional and zonal for the inner planets and nearly exclusively zonal for the outer planets. These alternate soultions to Laplace's equation correspond to the different insolation and rotation rate requirements between the inner and outer planets.

The theory of solenoidal vortices would not be complete without reference to the atmospheric anticyclone, prevalant on earth. Since the anticyclone appears to have a cohesive structure, and interacts with other vortices in compliance with the fourth and fifth proposed Laws, there probably exists an adequate description of the vorticity, divergence and pressure fields of the anticyclone consonant with the first three laws in conical coordinates. Perturbations in the anticyclone shape may be accounted for by conical spiral asymmetries. While the author has not yet done this analysis, it is worth mentioning in the interests of completeness.

THE STRUCTURE OF TOROIDAL VORTICES

The final part of Set II details the structure or ring vortices.
Toroidal or ring vortices may be divided into two kinds,
atmospheric and plasma. Atmospheric toroidal vortices
describe pulses of one fluid through another. This may range
from synoptic scale, where tropical cloud clusters evolve into
cloud rings, to possible explanations of the structure of the
throat of the hurricane, all the way down to the mesoscale
cumulonimbus and cumulus families.

The ring vortex is characterized by minimal entrainment with
zero slip conditions on the lateral boundary of the rising
fluid pulse. The outer, downward circulation is exactly
compensated by the rate of rise of the ring vortex as a
whole. The ring vortex has a structure predetermined in
toroidal coordinates with a vorticity distribution such that
the frictional curl within the rising pulse is zero. Such a
constraint does not mean zero friction. The frictional force
is non-zero, but its distribution is such that the curl of
the frictional force is zero. By this means the ring circula-
tion is explicitly governed, yet allowing for an azimuthal
Fourier variation. These theoretical distributions include
the toroidal harmonics discussed in greater detail in Appendix
D.

Ring vortices may also be applied to a micrometeorological
and oceanic level. The smoke ring blown by the playful
smoker is one such vortex, and a drop of blood in a Copper
Sulfate solution is another such.

It is not inconceivable that in a larger ring vortex with
azimuthal harmonics that smaller ring vortices may form.
Laplace's equation may be satisfied in a piecewise manner.

```
                              TOROIDAL
                             /         \  ─ ─ ─ ─ ─ ─ ─
                            /            \              
                           /              \             
           Atmospheric             Plasma              Misc.
          /        \               /      \              |
         /          \             /        \             |
    Synoptic     Mesoscale                          Blood drop in
        |         /    \                             CuSO₄,
    Throat of  Single  Multi     Free     Contained  Smoke ring
    hurricane    |       |          |          \
        |        |       |          |           \
    Cloud      Cu's    Cb's      Nuclear       Fusion
    clusters                     Fireball      Plasma

                                High Explosive
                                Detonations
```

Misc. branch: Blood drop in $CuSO_4$, Smoke ring
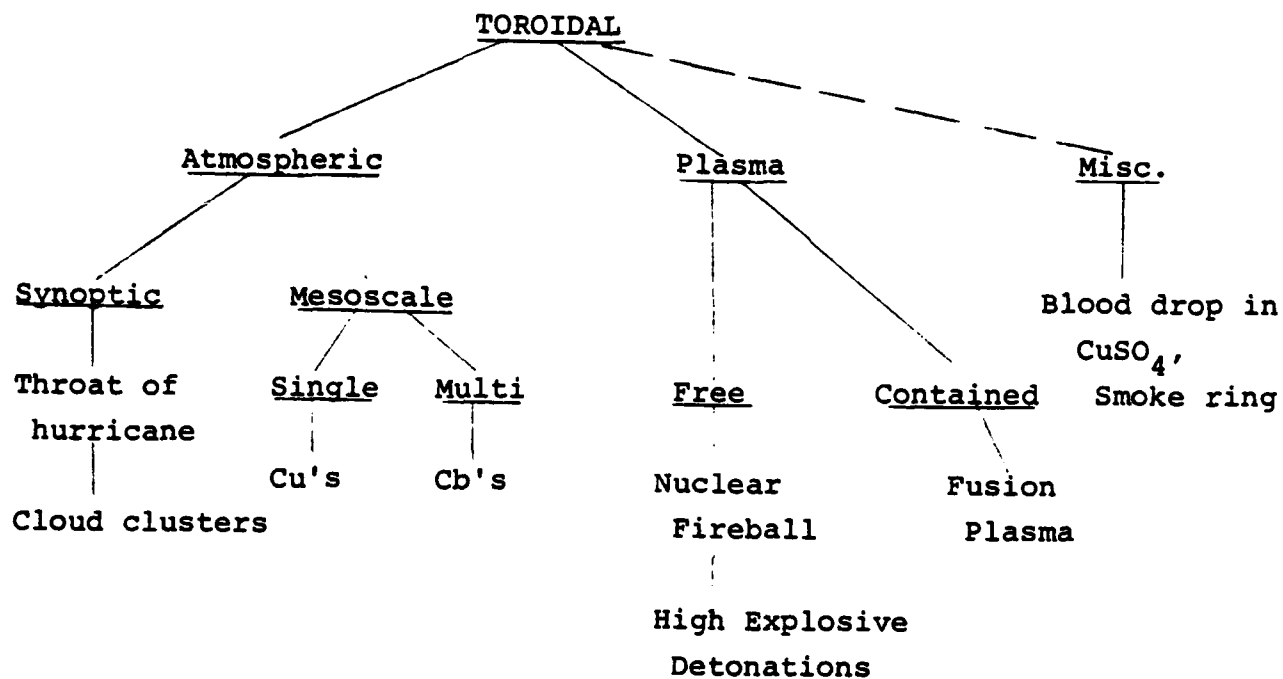
Hence, the Great Red Spot in the Jovian circulation and ring
cloud clusters in the Terrestrial tropics, composed of lesser
ring vortices, cumulonimbi.

PLASMA VORTICES

Both nuclear fireballs and toroidal fusion reactors fall under
this category, being directly addressed in Appendix D.
The mushroom cloud is merely a rising ring vortex with its
main propogation in the center. The outer falling component
of the vortex is exactly compensated by the rate of ascent of
the vortex as a whole. The rising fireball literally eats
its way through the atmosphere pulling a tail of debris behind
it. As is true in any active vortex, a distinct circulation
and sink field is accompanied by a characteristic pressure
distribution. Creation of a vortex in a toroidal containment
vessel by electromagnets will invariably alter the pressure
field in the plasma, possibly pushing the internal pressures
locally beyond the crictical values necessary to sustain a
continuous fusion reaction.

MISCELLANEOUS VORTICES

Under this category falls vortices produced by airfoils
and the ring vortices produced by the downwash from the
blades of a helicopter. The lift of an airfoil is given by the
cross product of the oncoming airstream into the vorticity of
the airfoil. Knowledge of the distribution of the vorticity
about the airfoil which is itself a potential boundary in
Laplace's equation may contribute to an understanding of
the relevant phenomena. Likewise, the circulation distribution
for downwash from both moving and hovering helicopters may
be useful in maximizing their efficiency.

STRUCTURAL REVIEW

We have now reviewed the kinds of toroidal vortices describable
by the field theory thus far. The atmospheric toroidal vortices
range from droplets of blood in Copper Sulfate, to smoke rings,
rising cumuli and cumulonimbi and possibly the throat of the
hurricane to cloud clusters in the tropics. The plasma
torodial vortices include those which are free, i.e. nuclear
fireballs and their non plasma little cousins, high explosive
detonations, and those which are contained, the toroidal
plasmas in fusion containment vessels.

In review, then, the Structural Application encompasses both
toroidal (or ring vortices) and solenoidal (or vortices with
central axes). The latter may be either cylindrical or
spherical, and each of these has elliptical variants. All
of the solenoidal vortices have both spiral and partial
variants which account for the new branch of mathematics out-
lined in Appendix A.

1.3 APPLICATION - VORTEX INTERACTION

The final application of the Model Theory is given in
Vortex Interaction discussed at greater length in Chapter VII.
As shown in Set III, the vortex interaction is conveniently
divided into phenomena predominantly associated with either
Law IV or Law V. The Vortex Interaction may be either
dual or multiple vortices.

Dual Vortices

The dual circulations are given by interactions between a
set of cyclones or a cyclone and an anticyclone. The latter
is most predominantly displayed with a hurricane rotating
about the center of mass of the cyclone-anticyclone pair.
This phenomenon was suggested by Riehl in 1956. The speed of
rotation, however is determined through the fourth Law so
that the translational circulation of the hurricane is less
than the ambient speed of the anticyclonic steering current.
The presence of the cyclone diminishes the anticyclonic
vorticity budget so that the net circulation is a difference
of the circulations of the two vortices.

In the case of two hurricanes the fourth Law provides for
the Fujiwhara effect. Both hurricanes rotate about one
another at a speed greater than the ambient steering current
would suggest. If one of the hurricanes is replaced with
an extratropical storm, then not only does the hurricane
rotate about the other storm, or their common center of mass,
to be precise, but it also spirals in toward the center of
the extratropical storm. Thus is introduced Law V, which
accounts for radial movements much in the same manner that
Law IV accounts for tangential movements.

VORTEX INTERACTION

Dual Vortex   Multiple Vortex

Hi-Low   Low-Low
(Riehl's Center
of Mass)   Dual Hurricanes   Extratropical
              (Fujiwhara Effect) Storm- Hurricane
Translation   Translation greater
less than   than ambient current
ambient current

        Gyre Formation   Gyre Exchange   Gyre Trans-
                                                  lation

    Hi-Low   Dual Hcns.   Movement of storm
    (1013 mb   (Minimal Approach from one high to
     isopleth)   Distance)   another
Abrupt Path Change

                                        Cycloidal Paths

Law V dominates the multiple vortex interactions, more from
a stylistic standpoint rather than a phenomenological one.
A group of multiple vortices is termed a 'gyre'. This
term is borrowed from both Oceanography where a large
oceanic body of water rotating is called a gyre, and from
Lewis Carrol's Jabberwocky,

> "Twas brillig and the slithey toves
>   did gyre and gimble in the wabe."

Hopefully a new general field theory will not be significantly
less entertaining than Alice in Wonderland, and will be perceived
as having somewhat more information content.

The Multiple Vortex part of the Field Theory taxonomy falls
into three catagories dealing with Gyre Formation, Gyre
Exchange, and Gyre Translation.

Gyre Formation

Gyre formation involves the creation of a hurricane bearing
group due to the approach of a hurricane to close enough
proximity for the group to act as an integral unit. In this
case the hurricane encountering an anticyclone will not
appreciably be affected until the 1013 mb isobar wraps at
least half way around the storm. The hurricane must there-
fore be lodged in the anticyclone. Otherwise the hurricane
would continue to follow a great circle route.

Upon approaching another hurricane, the two have a minimal
distance, usually about 600 miles before they interact
in the manner prescribed by the Fujiwhare effect and
explained in greater detail in the seventh chapter.

Gyre Exchange

Just as hurricanes may enter a group to form a gyre, they may also leave a group to join another, undoubtedly through the interaction governed by the fifth Law. In this way, hurricanes may be passed form one group to another, like a football from one player to another. This coupled with the following phnomenon will lead to some interesting hurricane paths.

Gyre Translation

Not only will a hurricane rotate about the common center of mass of a gyre, but it will also translate with the gyre. Thus, rotation and translation may produce some very interesting hurricane paths, among which are cycloidal paths characterized by looping.

Summary

In summary, therefore, the vortex may interact with one other or several other vortices. The hurricane may simply rotate about the common center of mass, as with an anticyclone, or may actually spiral into the center of the other vortex, as with an extratropical storm. The hurricane may lodge in the edge of another vortex, as the 1013 mb isobar of an anticyclone, or approach to a minimum distance as in the Fujiwhara effect. Finally, the hurricane may make an abrupt path change due to gyre formation, may loop due to gyre exchange and translation, or may simply translate along a great circle due to lack of any other interfering vortices.

The fourth and fifth Laws are necessary for the vortices to retain their own internal field characteristics. The fourth and fifth Laws enable interacting individual vortices to individually and independently satisfy Laws I-III inclusive.

33

EXPOSITION OF THE PARADIGM

The remainder of this paper will deal with the exposition of
the new paradigm which addresses, inter alia, spiral band
structure and behavior. The exposition of the paradigm deals
with the new laws, their mathematical formulation (including
the new mathematical systems discovered for articulation of
these laws) and the incorporation of these laws into a theory
of vortex structure, which is then correlated with data.

Chapter II deals with the new laws of vortex structure and
their interpretation and understanding. Chapter III discusses
the paradox of spiral behavior and the new spiral mathematics
which results. Chapter IV and Appendix A discuss the mathe-
matics of orthogonal log spiral coordinate systems and solutions
for Laplace's equation separable in these coordinates.
Chapter V deals with the theory of the structure of vortices
and provides application of the laws. Appendix B is a
monograph detailing the application of a simple two part vortex
to a model of the two dimensional general circualtion for
the inner planets, including earth. Appendix C outlines
a proposal for studying the general circulation of the outer
planets, specifically Jupiter and Saturn. Appendix C also
discusses the circulation of earth as being a possible
intermediate case between the circulation of the inner planets
and the outer ones, and proposes a simple explanation of the
phenomenon of the Inter Tropical Convergence Zone.

Chapter VI deals with the correlation of the vortex theory to
observed data. This includes the axially symmetric version
of the first Law, and the spiral asymmetric version of the
second Law. Data in support of Law III is also presented.
Appendix D presents a discussion of the solutions to Laplace's
equation in toroidal coordinates and its application to
ring vortices in general and toroidal plasmas in particular.

Appendix E details the computer code used in the correlation
of the data with the axially symmetric version of the first
Law. Chapter VII presents the hypothesis of vortex interaction,
including its two governing laws. Appendix F presents prelim-
inary results to orthogonal spiral analyses of hurricane David.
The evidence suggests that Law II does indeed obtain and mathe-
matically describes the divergence field resulting in cloudiness
in the hurricane vortex. A summary with suggestions for future
articulation of the paradigm is then presented in Chapter VIII.

II.   THREE LAWS PROPOSED FOR GOVERNING
THE STRUCTURE OF VORTICES

The introduction of a general field theory has new physical laws as its first main element. This chapter introduces the laws for vortex structure and discusses their physical meaning. The laws then become fundamental building blocks from which the rest of the field theory may be constructed. In this section then three laws that govern vortex structure are proposed.

The first two laws are presented first in their most general form. The laws are then recast in a more dynamical and mathematical from, giving three separate but complementary physical interpretations of the first law based on a common factor in the explanation. The third advance of these laws involves a mathematical transformation at which point the laws are joined by the third law and displayed in matrix form with the ramifications for the mathematics examined in some detail.

The laws Related To Overall Vortex Properties

The first two laws are stated in the context of their effect on the two most fundamental properties of the atmospheric vortex. These two properties are the circulation function, Γ , and the sink function, Q. The circulation function is simply another way of indicating that in a vortex the flow has a component of closed circulation. The sink function simply means that the flow has a component moving in at one level, up and out at another level. In an atmospheric vortex this component results in clouds and precipitation. More simply stated Γ and Q bring wind and rain.

The first three laws may be stated most simply in terms of the effect of the lateral frictional force on these two

properties of the vortex, and the countermanding effect of the pressure gradient force. The laws may be stated as follows:

I.   The lateral frictional force in a vortex either does not exist, or if it does, changes the circulation in a manner independent of radius.

II. The lateral frictional force in a vortex (if it exist) changes the sink function, Q, of the vortex in a manner independent of radius.

III. Since the frictional operation on the circulation and sink functions constitute forms of work, then the pressure gradient force* (if it exists) does work against one or both of the other two forces, on Γ and/or Q, also in a manner independent of radius.

Thus, the atmospheric vortex, which is a combination of an atmospheric sink and a circulation has both of these properties changed by a force in a manner independent of radius.

The lateral frictional force is usually ignored in contemporary thinking, especially in the science textbooks which present the old paradigm. Either the force is assumed to be trivial by order of magnitude considerations, or it does not exist to begin with. The order of magnitude considerations are interesting in that the lateral coefficient of eddy viscosity, a component of the lateral frictional force, is not measureable and can only be estimated indirectly from numerical models or simply guessed. In any event, the researcher ordinarily choses to concentrate on the vertical component of friction instead.

Further examination of the nature of vortices and attempts to simulate them have led to disquieting indictments of the validity of the assumptions given above that are used to dismiss the lateral frictional force. The underlying assumption is that if a force is zero it is therefore irrelevant. In severe vortices, especially hurricanes, the role of lateral friction in the maintenance of components of vortex structure has been recognized as essential both by numerical modelers, such as Anthes (1970) and tropical meteorologists such as Malkus (1960).

---

*assuming constant specific volume with radius. This assumption is relaxed further into the text.

This being the case, it is apparent that a deeper understanding
of the laws proposed is needed.

Lateral Frictional Curl and Divergence

A more specifically dynamic way of looking at the first two
laws is to state them with reference to their most evident
physical implications:

I.   The lateral frictional force is either undefined or
- (a)   if the vortex were to be divided into a series of
concentric annuluses, each annulus in the flow
field would exert an identical fricional drag upon
the adjacent annuluses immediately interior and
exterior to it,

- (b)   the lateral frictional force exerts a torque on
the angular momentum field independent of radius or

- (c)   the lateral frictional force exerts no curl, i.e.
neither creates nor destroys vorticity
irrespective of considerations of axial symmetry
or azimuthal averaging of the vortex properties.

These three statements will now be examined in greater detail.
The common factor to all three versions of the first law is that
the lateral frictional force is an hyperbolic function of radius
except in (c) where it may assume other forms which we will come
to presently.

Since the lateral area of an annulus of vanishingly small
thickness is directly proportional to the mean radius of the
annulus, $\bar{r}$, by $2\pi\bar{r}h$, where h is height, then the increase
of annular radius is directly compensated by the hyperbolic
decrease of the frictional force per unit area. The first

version of Law I states that the drag per unit area on the annulus wall, when integrated over the entire annulus is identical from annulus to annulus, regardless of annulus size. Hence, the lateral frictional force neither speeds up nor slows down any given annulus at the expense of the others.

The second version of Law I states that the torque on the angular momentum field due to the lateral frictional force is independent of radius. This implies that a parcel travelling from the outer limits of the vortex toward the center will have its angular momentum constantly modified as it passes through. The only exception to this occurs when the frictional force ceases to exist, even if only for an instant, in which case the frictional torque changes to a new but constant value. In the mature hurricane, as we shall see later, this event happens twice at locations roughly equivalent to major phenomenological changes encountered while traversing the storm inward, the entrance to the wall cloud, and the entrance into the eye. The torque, T, is given by $k \cdot r \times F$ where r is the radial distance from the center of the vortex coordinates to the force, F. If T is to be constant, independent of radius, F must be hyperbolic in r.

The final version of the First Law involves the curl of the frictional force C. The form of the curl for axially symmetric flow is given by $C = \frac{1}{r} \frac{\partial}{\partial r} r F$. If F is hyperbolic with radius then the curl is zero. Analogously to vorticity the shear term is equal and opposite to the curvature term, so that if

$$\nabla_2 \times F = 0$$

then

$$\frac{1}{r} \frac{\partial}{\partial r} r F = \frac{F}{r} + \frac{\partial F}{\partial r} = 0 \text{ or}$$

$$\frac{F}{r} \text{ (curvature term)} = -\frac{\partial F}{\partial r} \text{ (shear term)}$$

The second Law may be reexamined in a more specifically dynamic way.

39

II.   The lateral frictional force either exerts no
divergence or is undefined.

We now examine an alternate statement of the second Law
comparable to those of the first.

Laws II and III deal, in the axially symmetric case, with
the actual dimensions of the annulus itself. The second Law
states that the component of the lateral frictional force normal
to the annular wall is non divergent. The same may be said for
the component of the pressure gradient force which does not
involve the toroidal acceleration, i.e. $\nabla \cdot -\alpha \nabla p = -\nabla \alpha \cdot \nabla p - \alpha \nabla^2 p$.
So, the first right hand term is the toroidal acceleration (to
differentiate it from the lateral, solenoidal acceleration). The
second right hand term, when set to zero, constitutes the third
law.

Law II states that the lateral frictional force normal to
the annular wall resists contraction of the annulus into a
smaller annulus in a manner independent of radius. Thus each
annulus is democratically entitled to the same protection from
forces seeking to shrink (or expand) it. Of necessity, the
tensor describing such behavior is non divergent.

This democratic resistance to outside influences would be
meaningless if there were not a compensating distribution of
counteracting forces inimical to the resisting frictional force.
Law III provides such a force with such a behavioral pattern.
The toroidal acceleration counteracts other frictional
components. The Laplacian of pressure provides a distribution
for the pressure such that the fields are similar, but identity
depends on boundary values. The similarity is limited to each
axially symmetric field being a logarithmic surface of
revolution. Laws II and III are not to be construed as
indicating that these forces are equal and opposite to one
another. As we shall see in Chapter VI, they may even act in
concert. In any event, each force component acts upon the
annular surfaces in a manner independent of radius.

Both the first and second laws may be represented
mathematically by

$$\text{I} \quad \underset{\sim}{k} \cdot \nabla_2 \times \underset{\sim}{F} = 0, \infty$$

$$\text{II} \quad \nabla_2 \cdot \underset{\sim}{F} = 0, \infty$$

It is relevant now to examine the Navier-Stokes (read
Newtonian applied to a fluid) formulation for lateral friction.
The frictional force, $\underset{\sim}{F}$, is usually given by

$$\underset{\sim}{F}_2 = \nabla_2 \cdot K_h \nabla_2 \underset{\sim}{U}$$

where K_h is the coefficient of eddy viscosity. K_h is
often assumed constant for the sake of convenience, but only with
much trepidation and innumerable caveats. If K_h is assumed
constant, then

$$\underset{\sim}{F}_2 = K_h \nabla_2^2 \underset{\sim}{U}$$

and we may then rewrite the first two laws one more time and
finally add the third Law.

Since the order of operation for the cross or dot product of
the del operator and the Laplacian upon a scalar or vector field
is immaterial, so that

$$\underset{\sim}{k} \cdot \nabla_2 \times \nabla_2^2 \underset{\sim}{U} = \nabla_2^2 (\underset{\sim}{k} \cdot \nabla_2 \times \underset{\sim}{U}) \text{ and } \nabla_2 \cdot \nabla_2^2 \underset{\sim}{U} = \nabla_2^2 (\nabla_2 \cdot \underset{\sim}{U})$$

then the curl or divergence of the Laplacian of velocity is
identical to the Laplacian of the curl or divergence of the
velocity or

$$\text{I} \quad \nabla_2^2 \zeta = 0, \infty \quad \text{where } \zeta = \underset{\sim}{k} \cdot \nabla_2 \times \underset{\sim}{U}$$

$$\text{II} \quad \nabla_2^2 \delta = 0, \infty \quad \text{where } \delta = \nabla_2 \cdot \underset{\sim}{U}$$

and by adding pressure we obtain Law III

$$\text{III} \quad \nabla_2^2 p = 0, \infty$$

Succinctly, then, all three laws may be expressed simultaneously in matrix form by

$$\nabla_2^2 \begin{pmatrix} \zeta \\ \delta \\ p \end{pmatrix} = 0, \infty$$

or the horizontal divergence, vertical component vorticity and pressure either satisfy the two dimensional Laplace's equation, or their Laplacians are undefined. From a statement concerning the effect of the lateral frictional force on the two major characteristics of a vortex we have arrived at three atmospheric parameters which satisfy a homogeneous, linear, second order partial differential equation whose solution is uniquely determined by boundary conditions.

Hence, these force components do not simply modify major vortex characteristics, they specify their distributions.

Since the vorticity, divergence and pressure fields either satisfy Laplace's equation or do not have a definable Laplacian, these two characteristics determining the types of fields governed by the new laws. The emphasis now shifts from the fields themselves to the field boundaries. We are concerned not only with their values but also with the boundary shapes, locations and orientations.

*While the divergence of the pressure gradient force, $-\alpha \nabla p$, is given by

$$-\nabla_2 \alpha \cdot \nabla_2 p - \alpha \nabla^2 p,$$

the proposed law addresses only the second term. Strictly speaking, then, only one component of the pressure gradient force operates in opposition to lateral friction, the other component must compensate for the vertical shear component of friction.

III. MATHEMATICAL APPLICATIONS OF THE PROPOSED LAWS

The application to the real world of the proposed laws requires an understanding of the atmospheric vortex's salient features; spiral bands of cloudiness, precipitation and water vapor seen by the meteorological satellites. This understanding includes not only their geometry, but also their behavior. Further, we need a grasp of their underlying dynamics. Geosynchronous time lapse pictures assist the exploration of the nature of the bands. The satellite sees a wide range of synoptic scale vortices, from the Aleutian Low churning in the Gulf of Alaska to tropical hurricanes spinning off of the Intertropical Convergence Zone (ITCZ). This separation in geography parallels the separation in behavior of spirals in the extratropical and tropical cyclone.

The two kinds of vortices exhibit contradictory, even paradoxical behavior. In the midlatitude storm, a product of the clash betwen two sharply contrasting air masses, the occluded front winds itself around, as a spiral band into tight, nearly concentric rings. In contrast, in the hurricane, the offspring of vast stretches of the homogeneous, maritime tropical atmosphere, wild tightly turning winds blow thunderheads <u>through</u> stationary spiral bands. Cumulonimbi, born on one edge of the band, arc inward and across the band only to die at the other edge. The bands themselves, however, neither rotate nor wind up.

Band Behavior Reconciliation

The reconciliation of the band behavior in the presence of two different kinds of vortex flow gives birth to a theory of vortex structure that applies these laws to the flow.

43

The laws applied to the extratropical flow field yield information for flow in hurricanes. The behavior of the flow in extratropical storms producing these spiral fronts is now examined.

Timeline Behavior In Occluded Fronts of Extratropical Storms

Occluded fronts in midlatitude storms wind up into almost concentric rings. The front acts as a "time line" indicating the progress of a group of streamlines over a series of time intervals. Figure 3.1 shows how the front not only rotates but changes its shape at successive times. Timeline I at time I displays slight curvature. Curve II at time II has rotated and increased its curvature. Curves III and IV show progressive stages of the line winding up. These curves represent the movement of the front and its distortion by winding. We may simplify this process by transforming the spirals into semilog coordinates. The mathematical transformation of the curves into the artificial, but mathematically relevant coordinates of azimuth vs. the logarithm of the radius replots log spirals as straight lines, shedding light on their interaction. Figure 3.2 shows the front at the various stages. Here, all log spirals are straight lines, including the frontal position. Assuming the streamlines are also logarithmic spirals, then Figure 3.3 presents the schematic movement of trajectories in semilog coordinates.

Spiral Slope As A Function of Time

This geometric representation yields its mathematical form upon inspection. From the azimuthal and logarithmic components of the streamlines in Figure 3.3 we may formulate the velocity components. The azimuthal velocity, $\dot{\theta}$, and logarithmic radial velocity, $d \ln r / dt$, may be written by inspection,

44
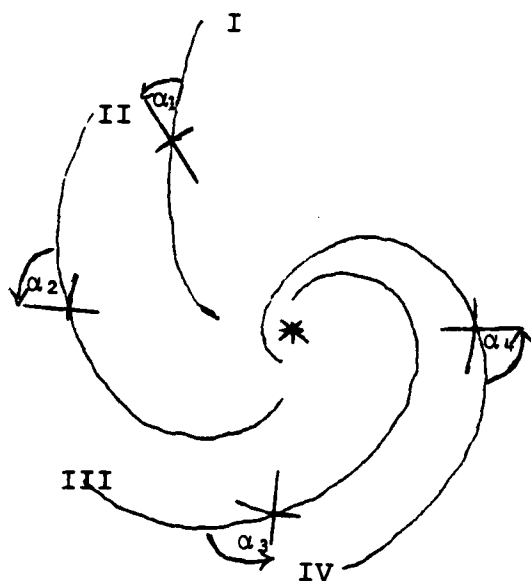
Figure 3.1 Movement of
log spirals in simple
vortex. Note both rota-
tion and tightening of
spirals under influence
of flow field. The spiral
tangent angles, α_{1-4}, increase
counterclockwise. Tra-
jectories are parallel in
next projection, Fig. 3.2.
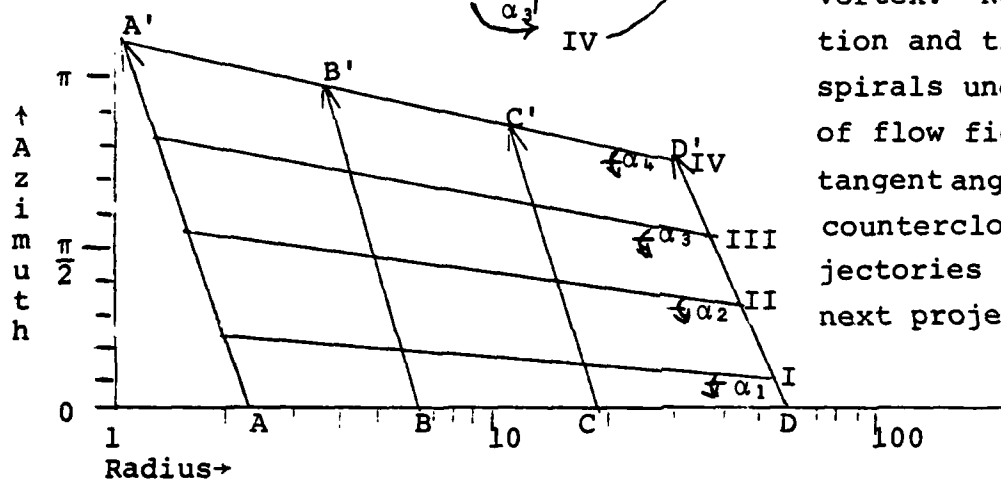
Figure 3.2 Movement of log spirals of Figure 3.1 in semilog coor-
dinates under influence of spiral trajectories, A-A',
B-B', C-C', D-D'. Bands I-IV behave as time lines.
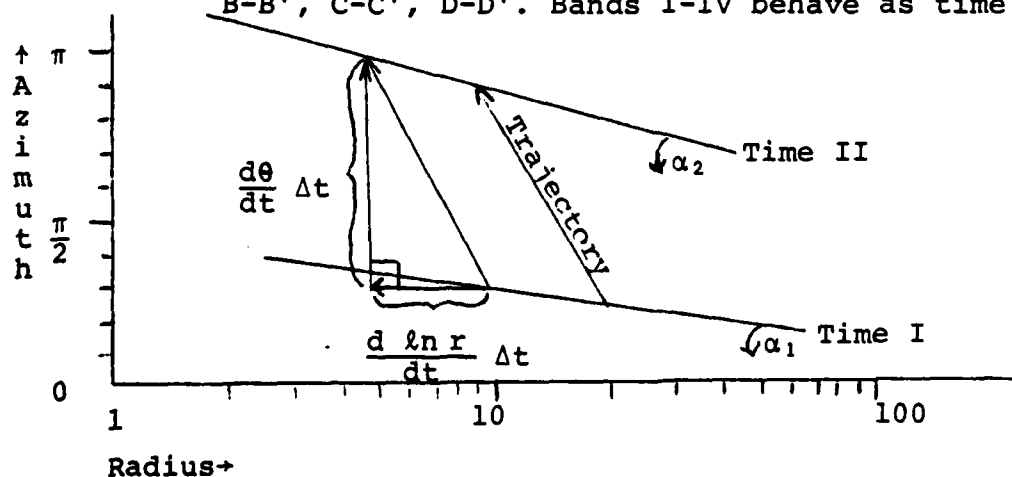
Figure 3.3 Components of trajectories moving Spiral Time
Line from Time I to Time II. Note that the
magnitude of the trajectory increases linearly
in the abscissa from right to left in order to
steepen the slope of the spiral from Time I to
Time II. The components, $d\theta/dt$ and $d\ln r/dt$, do too.

45

$$\dot{\theta} = A + B \ln r/r_0 \tag{3.1}$$

and

$$d \ln r/dt = A' + B' \ln r/r_0 \tag{3.2}$$

where A, B, A' and B' are constants.

Multiplying (3.1) and (3.2) by r yields the tangential and radial velocities, U_θ and U_r, respectively

$$U_\theta = r A + rB \ln r/r_0 \tag{3.3}$$

and

$$U_r = r A' + r B' \ln r/r_0. \tag{3.4}$$

VELOCITY AS A FUNCTION OF ITS MAXIMUM

Eq. 3.3 supports a maximum such that

$$\frac{\partial U_\theta}{\partial r} = A + B \ln r_x/r_0 + B = 0 \tag{3.5}$$

where r_x is the radius of the maximum velocity. B may be expressed in terms of the maximum angular velocity $\dot{\theta}_x$ by $B = -\dot{\theta}_x$.

We may rewrite (3.3) as

$$U_\theta = r \, \dot{\theta}_x (1.0 + \ln r_x/r) \tag{3.6}$$

or

$$U_\theta = \frac{rU_{\theta_x}}{r_x} \ln(\underline{e} \, r_x/r) \tag{3.7}$$

where $\underline{e}$ is the base of the natural logarithms. Thus the tangential velocity is expressed entirely in terms of its maximum U_{θ_x}, and the location of the maximum r_x, and the location of the velocity itself, r.

46

Vorticity and Divergence of Simple Flow

Further derivatives which combine the shear, (3.5), and curvature, (3.1) terms utilized above are the vorticity, ζ, and divergence, δ, fields. The vorticity and divergence fields of both of these flows satisfy Laplace's equation. Thus,

$$\zeta = \frac{1}{r} \frac{\partial}{\partial r} r U_\theta \tag{3.8}$$

combined with (3.3) yields

$$\zeta = 2(A + B \ln r/r_o) + B \tag{3.9}$$

and likewise for

$$\delta = \frac{1}{r} \frac{\partial}{\partial r} r U_r \tag{3.10}$$

combined with (3.4) yields

$$\delta = 2(A' + B' \ln r/r_o) + B' \tag{3.11}$$

From (3.10) and (3.11) it is evident that both ζ and δ are linear in the logarithm of the radius, a sine qua non for an azimuthally averaged function to satisfy Laplace's equation. Moreover, the linearity is evident not as a line, but as a line segment beginning at r_o.

The Laplacian for axially symmetric flow is given by

$$\nabla_2^2 = \frac{1}{r} \frac{\partial}{\partial r} r \frac{\partial}{\partial r} \tag{3.12}$$

Then $\nabla_2^2 \zeta$ may be written

$$\frac{1}{r} \frac{\partial}{\partial r} r \frac{\partial}{\partial r} (2(A + B \ln r/r_o) + B) \tag{3.13}$$

which yields

$$\frac{1}{r} \frac{\partial}{\partial r} 2B = 0.$$

Reintegration and Boundary Values

Linearity in the logarithm of the radius presents new opportunities. Reintigration of the Laplacian of vorticity must take into account boundary conditions so that the integration occurs between r_o and r. Consequently three derivatives of the velocity field resulting in zero must integrate to three constants describing the field, not just the two which describe the flow field in equat'n3.4. Thus the velocity field may now be written

$$U_\theta = r\ C_1 + r\ C_2\ \ell n\ r/r_o + C_3\ r^{-1*} \qquad (3.14)$$

where C_3 is a new and puzzling element attributable to boundary conditions.

In the extratropical storm C_3 may indeed be zero, but need not be. For C_3 to be zero is actually a special and limited case. Equation (3.14) may be further expanded for n regimes where the linear fragments of vorticity join at r_1, $r_2, \ldots, r_{n-2}$ to r_{n-1}. The vorticity looks like a stick figure with a series of breaks in it, shown in Figure 3.4 (The same may be said for the divergence distribution). We express vorticity as

$$\int_{r_0}^{r} \frac{\partial r\ U_\theta}{\partial r} dr = \int_{r_0}^{r_1} r\ \zeta_1\ dr + \int_{r_1}^{r_2} r\ \zeta_2 \ldots + \int_{r_{n-1}}^{r_n} r\ \zeta_n dr^*$$

$$(3.15)$$

where

$$\zeta_1 = 2\ A_1 + 2\ B_2\ \ell n\ r + B_2 \text{ up to}$$

$$\zeta_n = 2\ A_n + 2\ B_n\ \ell n\ r + B_n$$

---

*The relation of the C's to A's and B's are made clear at Eq. (3.18).
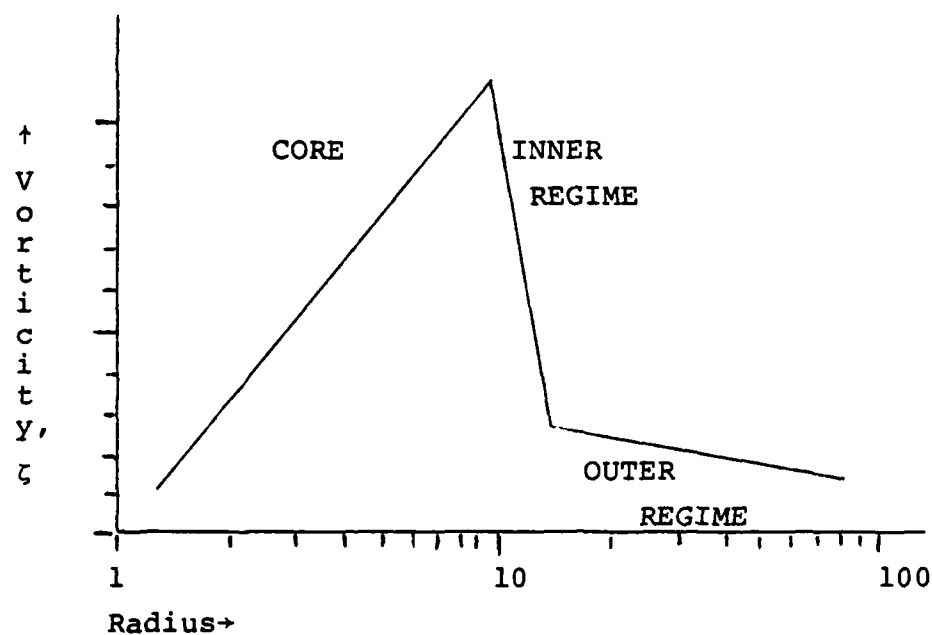
Figure 3.4 Piecewise, continuous distribution of
vorticity showing core, inner and outer
regimes. Since vorticity is linear in
the logarithm of the radius, it satis-
fies Laplace's equation.

The C_3's are functions of the boundary values and locations of the boundaries interior to the point of interest.

The Nature of C_3

Integration of circulation from one end of the vorticity fragment to the other makes the nature of C_3 explicit. The value of C_3 plays a critical role in the difference between the hurricane and extratropical storm. Thus,

$$\int_{r_o}^{r} \frac{\partial r U_\theta}{\partial r} dr = \int_{r_o}^{r} r\zeta dr = \int_{r_o}^{r} (2 r A + 2rB \ln r + rB) dr \quad (3.16)$$

becomes

$$r U_\theta - r_o U_{\theta_o} = r^2 A \Big|_{r_o}^{r} + r^2 B \ln r \Big|_{r_o}^{r} \quad (3.17)$$

$$r U_\theta = r_o U_{\theta_o} + r^2 A - r_o^2 A + r^2 B \ln r - r_o^2 B \ln r_o$$

or

$$U_\theta = r A + r B \ln r + \frac{r_o U_{\theta_o}}{r} - \frac{r_o^2 A}{r} - \frac{r_o^2 B}{r} \ln r_o \quad (3.18)$$

Letting $C_1 = A$, $C_2 = B$ and $C_3 = r_o U_{\theta_o}$

$$- r_o^2 A - r_o^2 B \ln r_o$$

We obtain (3.14). Eq. (3.18) may be further expanded where the subscripts 1, 2, 3 refer to the values in the core, inner and outer regime, respectively with boundaries given by r_o, r_1, r_2 and r respectively.

50

Again:

$$\int_{r_o}^{r} \frac{\partial r \, U_\theta}{\partial r} \, dr = \int_{r_o}^{r} r \zeta_1 \, dr + \int_{r_1}^{r_2} r \zeta_2 \, dr + \int_{r_2}^{r} r \zeta_3 dr \quad (3.19)$$

so that

$$r \, U_\theta - r_o \, U_{\theta_0} = r^2 A_1 \Big|_{r_o}^{r_1} + r^2 B_1 \ln r \Big|_{r_o}^{r_1} + \quad (3.20)$$

$$r^2 A_2 \Big|_{r_1}^{r_2} + r^2 B_2 \ln r \Big|_{r_1}^{r_2}$$

$$+ r^2 A_3 \Big|_{r_2}^{r} + r^2 B_3 \ln r \Big|_{r_2}^{r}$$

which yields

$$(3.21)$$

$$r \, U = r_o \, U_o - r_o^2 A_1 + r_o^2 B_1 \ln r_o \qquad \ldots \ldots 1$$

$$+ r_1^2 (A_1 - A_2) + r_1^2 (B_1 - B_2) \ln r_1 \ldots 2$$

$$+ r_2^2 (A_2 - A_3) + r_2^2 (B_2 - B_3) \ln r_2 \ldots 3$$

$$+ r^2 A_3 + r^2 B_3 \ln r \qquad \ldots 4$$

Eq. (3.21) may be expanded or contracted to fit any number of regimes. Line 1 contains all the terms which constitute C_{31} i.e. C_3 in regime 1 which may be zero. Line 2 contains the terms for C_{32} and line 3 for C_{33}. If there are only two regimes then line 3 is dropped and the subscript 3's in line 4 become 2's.

The winding occluded front implies a flow which in turn satisfied the first stated law. The flow field implied by the behavior of the occluded fron* is only one of many possibilities

51

allowed by a reintegration of the law. The flow field of the hurricane, as will be seen in Chapter V satisfies the law in a piecewise fashion. In two of the pieces, C_3 (the boundary value term resulting from integration of the vorticity field) is the most significant term. Spirals of the occluded type cannot coexist with a flow field in which C_3 is non zero. Yet, exist they do, seemingly in spite of the flow field rather than because of it, since they do not rotate or windup. Another solution to this puzzle must then be found. This brings us simultaneously to both the second law and spiral solutions to Laplace's equation; in this case spiral harmonics in the low level divergence field. We now look at the component of this problem.

First, since the phenomena of interest are log spirals we shall examine the meaning of the term. Then the relationship of log spirals to formulations of Laplace's equation in six new spiral coordinate systems is examined. Secondly, the spiral solutions to Laplace's equation are applied to the second law to seek a solution to the puzzle of the spiral cloud bands in hurricane which "defy" the flow field.

Finally, the circular motion and moving spiral fronts are accounted for by considerations of Law I. It is by considering Law II that the stationary spiral bands in hurricanes are explained, while the tangential winds, piecewise compiled from Law I blow through them.

Summary

In summary, the flow field which produces logarithmic spiral bands that rotate and wind up has the following properties. There is a velocity maximum. Indeed, the entire flow field may be specified as a function of the maximum and its location. The divergence and velocity fields are linear functions in the logarithm of the radius, satisfy Laplace's equation, and

therefore the first and second laws. For divergence and
vorticity distributions comprised of linear fragments the
C_3's are functions of the boundary values and locations of the
boundaries interior to the point of interest. The fragmentation
itself satisfies both laws. The fields exhibit first order
discontinuities at their joints-there, the Laplacians are undefined.

$$\nabla^2_2 \begin{pmatrix} \zeta \\ \delta \\ p \end{pmatrix} = \infty$$

IV.   THE RELEVANCE AND MATHEMATICS OF LOG SPIRAL
COORDINATE SYSTEMS

As we saw in Chapter III, the winding occluded front of an
extratropical storm implies a flow which in turn satisfied the
first stated Law. The flow field implied by the behavior of the
occluded front is only one of many possibilities allowed by a
reintegration of the law. The flow field of the hurricane, as
will be seen in Chapter V satisfies the law in a piecewise
fashion. In two of the pieces, C_3 (a boundary condition term)
is the most significant term. Spirals of the occluded type
cannot coexist with a flow field in which C_3 is non zero.
Yet, exist they do, seemingly in spite of the flow field rather
than because of it, since they do not rotate or windup. Another
solution to this puzzle must then be found. This brings us
simultaneously to both the second Law and spiral solutions to
Laplace's equation, in this case spiral harmonics in the low
level divergence field. We now look at the component parts of
this problem.

First, since the phenomena of interest are log spirals we
shall examine the meaning of the term. Then the relationship of
log spirals to formulations of Laplace's equation in five new
spiral coordinate systems is examined. Finally, the spiral
solutions to Laplace's equation are applied to the second Law to
seek a solution to the puzzle of the spiral cloud bands in
hurricanes which "defy" the flow field.

Nonsatellite Observed Spiral Phenomena

There are, however, other atmospheric vortices not seen from
the geosynchronous satellite harboring spiral bands. Indeed, the
universe of vortices is replete with spiral phenomena. Spiral
bands occur in waterspouts (Golden, 1974), as hook echoes in
tornadoes, spiral rainbands in hurricanes and extratropical
storms as mentioned above, as spiral bands on the elliptically

54

shaped Great Red Spot on Jupiter, and even as spiral bands of
star clusters in spiral galaxies, a range of 18 orders of
magnitude. The careful bather will also note that spiral
standing waves in the surface of the water appear about a vortex
funnel in draining bathtubs. These are spiral waves which appear
upon the surface of the water in conjunction with the formation
of a particularly vigorous bathtub funnel. This phenomenon
expands the range of interest to 21 orders of magnitude and the
third proposed Law.

What accounts for these spiral phenomena, and what has all
of this to do with Laplace's equation or the three proposed laws?

These are questions which will now be addressed. First, let
us examine more closely the meaning of the term "logarithmic
spiral."

Logarithmic Spirals

Even the name, logarithmic spiral, is ambiguous. The spiral
in question may just as easily be called an exponential spiral
since the relationship which defines the parameters may be
validly expressed in either of two forms

$$1) \quad \ell n \, \rho = a\theta \qquad\qquad\qquad (4.1)$$

or

$$2) \quad \rho = e^{a\theta}$$

where ρ is the dimensionless radius. Dimensionless, perhaps,
but expressible in radians, nevertheless. The fundamental
characteristic of the logarithmic spiral, that which
distinguishes it from every other spiral, is that the spiral's
slope (sometimes called its inflow angle) is a constant, or

if $\ln \rho = a\theta$,

$\quad\quad\quad \partial\theta / \partial \ln \rho = a$ (4.2)

or $\rho \, \partial\theta/\partial\rho = a.$

The slope mentioned above is defined in polar coordinates, and is therfore <u>coordinate dependent</u>. The slope in Cartesian coordinates is given by $\partial y/\partial x$, and when the slope is constant for a curve, there exists a family of straight lines that satisfies the slope.

For example, the gradient in ξ coordinates is given by

$$\left(1/f \left(\xi_1, \xi_2, \xi_3 \right) \right)\left(\frac{\partial}{\partial\xi_1} \underset{\sim}{i} + \frac{\partial}{\partial\xi_2} \underset{\sim}{j} \right)$$ (4.3)

and the slope of a logarithmic spiral in those coordinates is given by

$$\partial\xi_2/\partial\xi_1 = \text{constant}$$ (4.4)

The gradient in polar coordinates is given by

$$\nabla = \frac{\partial}{\partial r} \underset{\sim}{i} + \frac{1}{r} \frac{\partial}{\partial\theta} \underset{\sim}{j} \quad \text{or} \quad \nabla = \frac{1}{r}\left(\frac{\partial}{\partial \ln r} \underset{\sim}{i} + \frac{\partial}{\partial\theta} \underset{\sim}{j}\right)$$ (4.5)

and the Laplacian by

$$\nabla^2_2 = \frac{1}{r^2}\left(\frac{\partial^2}{\partial \ln r^2} + \frac{\partial^2}{\partial\theta^2}\right)$$ (4.6)

The slope of a log spiral is given by $\partial \ln r/\partial\theta = \text{constant}$ likewise, the gradient in spherical coordinates is given by (holding r constant)

$$\nabla_2 = \frac{1}{r} \frac{\partial}{\partial\theta} \underset{\sim}{i} + \frac{1}{r} \sin\theta \, \frac{\partial}{\partial\phi} \underset{\sim}{j}$$ (4.7)

Factoring out $1/r \sin\theta$ yields

$$\nabla_2 = \frac{1}{r} \sin\theta \left(\sin\theta \, \frac{\partial}{\partial\theta} \underset{\sim}{i} + \frac{\partial}{\partial\phi} \underset{\sim}{j} \right)$$ (4.8)

or

$$\nabla_2 = \frac{1}{r \sin \theta} \left(\frac{\partial}{\csc\theta\ \partial\theta} + \frac{\partial}{\partial\phi}\ \underset{\sim}{j} \right) \qquad (4.9)$$

and since in (4.9),

$$\int \csc\theta\ d\theta = \ell n \tan (\theta/2)\ , \text{then}$$

and the Laplacian may be expressed as

$$\nabla_2^2 = \frac{1}{r^2}\ \sin^2\theta \left(\frac{\partial^2}{\partial\ \ell n \tan\ (\theta/2)^2} + \frac{\partial^2}{\partial\phi^2} \right) \qquad (4.10)$$

and the slope of the spherical log spiral by

$$\partial\ell n \tan\ \frac{\theta}{2}\ /\partial\phi = \text{constant} \qquad (4.11)$$

If the spiral is expressed in semi-log coordinates, then it too may be expressed as a straight line. In point of fact, by rotation of the semi-log coordinate axes one may obtain a coordinate system where the axes are themselves logarithmic spirals and the coordinates of any point may be defined in terms of spiral coordinates yielding a spiral space. There are other coordinate systems besides the polar or circular cylindrical where this is possible.

For example, the definition of the slope on the surface of a sphere, given in spherical coordinates is, as given above,

$$\partial\theta/ \sin\theta\ \partial\phi = a\ (\text{constant}) \qquad (4.12)$$

or

$$\partial\ \ell n \tan\ \frac{\theta}{2}\ /\partial\phi = a.$$

For small angles $\theta = \tan(\theta/2)$ so that $\partial\ \ell n\theta\ /\partial\theta \sim a$ but not so for large θ .

We may immediately construct another semilog coordinate system for the surface of spheres which upon rotation yields a spiral spherical space. Therefore, any point on the sphere may be redefined in terms of this spiral spherical space.

Any coordinate system in which one coordinate may be held constant and upon which the slope depends only on the other two coordinates* is subject to rotation into spiral form, and has a Laplacian (the dot product of the gradient into itself), which may also be expressed in this form.

Laplace's Equations In Spiral Systems

Laplace's equation is a classic elliptic equation with complex characteristics. The axially symmetric solution (linearity in $\ln r$) is not the only solution to Laplace's equation. The asymmetric solution is the product of an exponential and periodic function such that the Laplacian in Cartesian coordinates is given by

$$\nabla_2^2 \, a = \frac{\partial^2 a}{\partial x^2} + \frac{\partial^2 a}{\partial y^2}$$

then if

$$a = \gamma(n) e^{nx} \cos ny \text{ or}$$

$$a = \gamma(n) e^{ny} \cos nx \text{ or}$$

$$a = \gamma(n) e^{nx} \sin ny \text{ or}$$

$$a = \gamma(n) e^{ny} \sin nx \tag{4.13}$$

where n may be an integer in a Fourier series, and $\gamma(n)$ is a Fourier amplitude dependent on n,

$$\nabla_2^2 \, a = 0 \tag{4.14}$$

The relevance of the solution to the asymmetric vortex is now addressed.

*i,e., where the curvature of the surface containing the spiral is a real or imaginary constant (positive, negative or zero).

In Cartesian coordinates it is axiomatic that rotation of coordinates implies a direct transformation of the form of the Laplacian from the old coordinate axes to the new ones (Figure 4.1). The Laplacian before rotation is expressed as

$$\nabla_2^2 = \frac{\partial^2}{\partial x^2} + \frac{\partial^2}{\partial y^2} \tag{4.15}$$

and after rotation as

$$\nabla_2^2 = \frac{\partial^2}{\partial x'^2} + \frac{\partial^2}{\partial y'^2} \tag{4.16}$$

In polar coordinates the Laplacian is written

$$\nabla_2^2 = \frac{1}{r} \frac{\partial}{\partial r} r \frac{\partial}{\partial r} + \frac{1}{r^2} \frac{\partial^2}{\partial \theta^2} \tag{4.17}$$

by multiplying the radial term by r/r, recombining and factoring out $1/r^2$ the Laplacian may be rewritten as

$$\nabla_2^2 = \frac{1}{r^2} \left(\frac{\partial^2}{\partial \ell n r^2} + \frac{\partial^2}{\partial \theta^2} \right) \tag{4.18}$$

Laplace's equation may dispense with the $1/r^2$ to give

$$r^2 \nabla_2^2 a = \left(\frac{\partial^2}{\partial \ell n r^2} + \frac{\partial^2}{\partial \theta^2} \right) a = 0 \tag{4.19}$$

Thus, any linear solution in θ and $\ell n r$ satisfies (4.19) as well as the product of an orthogonal set of exponential and periodic functions. As can be seen in (4.16) rotation of the coordinate system θ, $\ell n r$ by angle α in Figure 4.2 would give a new expression for Laplace's equation

$$r^2 \nabla_2^2 a = \frac{\partial^2}{\partial S_r^2} a + \frac{\partial^2}{\partial S_\theta^2} a = 0 \tag{4.20}$$
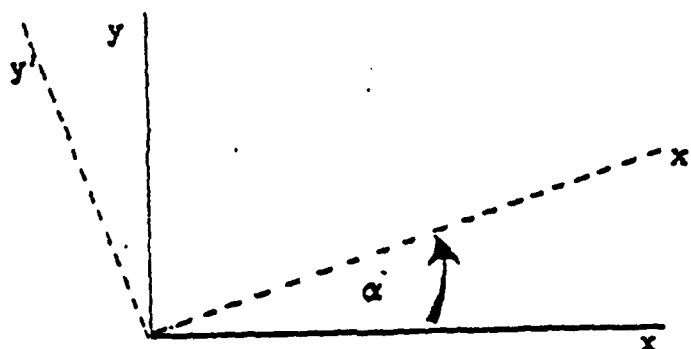
Figure 4.1   Rotation of Cartesian coordinates x,y
             to produce new coordinates x',y'. The
             Laplacian is independent of the rotation,
             since it is the dot product of the gradient
             upon itself.
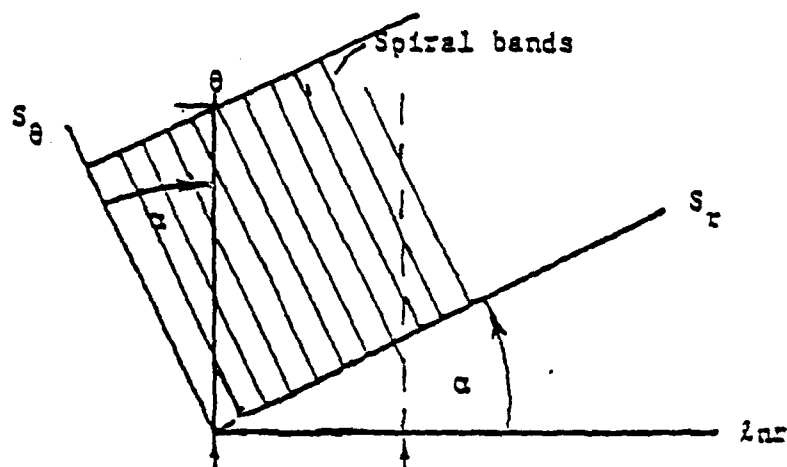
Figure 4.2   Rotation of semilog coordiantes to produce
             log spiral coordinates. The ray and circle
             are actually degenerate types of logarithmic
             spirals.

where S_r and S_θ are the new coordinate axes illustrated in Figure 4. . This rotation brings the cloud bands parallel to S_θ and periodic in S_r. Since both S_θ and S_r satisfy (4.4) they are log spirals, and the

new coordinate system e^{S_θ} and e^{S_r} are log spiral coordinates. S_θ and S_r are in units of radians. They vary in the model from 0 to $2\pi\cos\alpha$ and 0 to $2\pi\sin\alpha$ respectively.

The scalar transformations between θ, $\ln r$ and S_θ, S_r are

$$S_r = \ln r \cos\alpha + \theta \sin\alpha \qquad (4.21)$$

$$S_\theta = \theta \cos\alpha - \ln r \sin\alpha \qquad (4.22)$$

Thus (4.13) may be written in S_θ and S_r as

$$a = \gamma(n) e^{n(S_\theta)} \cos(nS_r), \text{ etc., being exponential}$$

in S_θ and

periodic and linear in S_r.

Spiral Space

Spiral space is represented pictorially in Figure 4.3 below. The spirals are defined by S_r and S_θ being constants.

For

$$S_r = K = \ln r \cos\alpha + \theta \sin\alpha \qquad (4.23)$$
and

$$S_\theta = K' = \theta\cos\alpha - \ln r \sin\alpha \qquad (4.24)$$

the orthogonal log spirals which define spiral space are given by

$$r = \exp \frac{K - \theta\sin\alpha}{\cos\alpha} \qquad (4.25)$$

for constant S_r, i.e., the coordinate along which S_θ only changes and

and

$$r = \exp \frac{\theta\cos\alpha - K'}{\sin\alpha} \qquad (4.26)$$
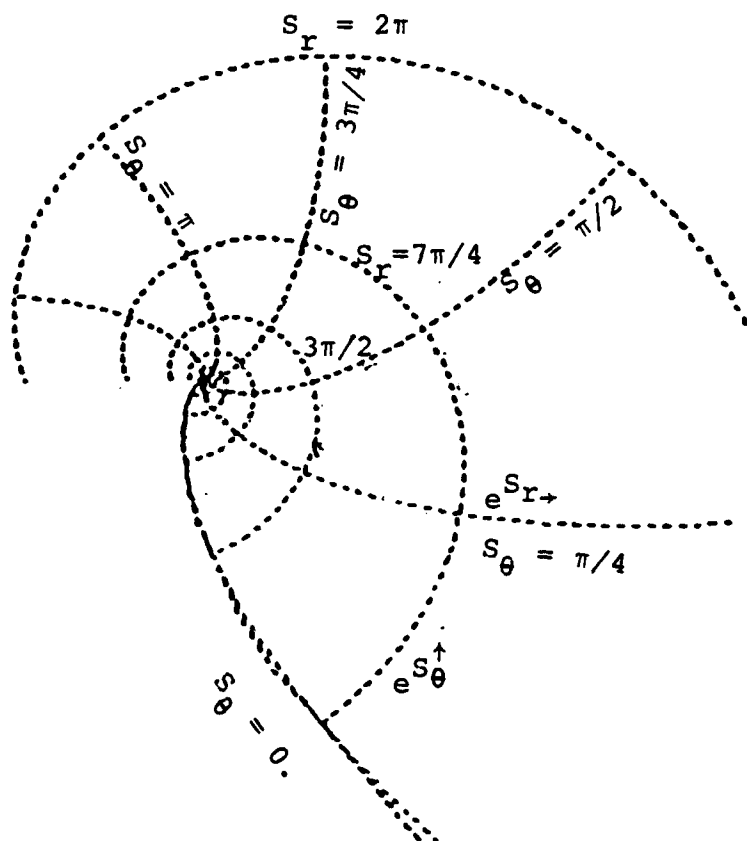
Figure 4.3 Real space in orthogonal log spiral coordinates, e^{S_θ} and e^{S_r}, with angle of rotation $20°$. The spirals occur at every $\pi/4°$. The range of S_θ is from 0 to $2\pi \cos 20°$, and that of S_r, 0 to $2\pi \sin 20°$.

for constant S_θ, i.e., the coordinate along which only S_r changes. Thus any point in spiral space may be defined in terms of values of the log spirals e^{S_θ} and e^{S_r}, or simply S_r and S_θ.

Spherical Coordinates

Spiral space may also be defined in geographic or spherical coordinates, so that all algorithms applicable to polar coordinates may be applied to spherical ones as well. The two dimensional Laplacian in geographic coordinates ϕ, λ is given by

$$\nabla_2^2 = \frac{1}{r^2} \frac{1}{\sin\phi} \frac{\partial}{\partial\phi} \sin\phi \frac{\partial}{\partial\phi} + \frac{1}{r^2} \frac{1}{\sin^2\phi} \frac{\partial^2}{\partial\lambda^2} \qquad (4.27)$$

rearranging terms gives

$$\nabla_2^2 = \frac{1}{r^2 \sin^2\phi} \left(\frac{\partial}{\csc\phi \, \partial\phi} \frac{\partial}{\csc\phi \, \partial\phi} + \frac{\partial^2}{\partial\lambda^2} \right) \qquad (4.28)$$

or

$$\nabla_2^2 = \frac{1}{r^2 \sin^2\phi} \left(\frac{\partial^2}{\partial(\ln \tan\frac{\phi}{2})^2} + \frac{\partial^2}{\partial\lambda^2} \right) \qquad (4.29)$$

Rotating the coordinate system $\ln \tan\frac{\phi}{2}$, λ through the angle α produces

$$\nabla_2^2 = \frac{1}{r^2 \sin^2\phi} \left(\frac{\partial^2}{\partial S_\phi^2} + \frac{\partial^2}{\partial S_\lambda^2} \right) \qquad (4.30)$$

where S_ϕ and S_λ are log spirals on a sphere conforming

to the equation

$$\tan\alpha = \frac{r \sin\phi \, \partial\lambda(\phi)}{\partial\phi} = \frac{r \partial\lambda(\phi)}{\partial\ln \tan\frac{\phi}{2}} = \text{constant.} \qquad (4.31)$$

63

The elliptic solution

$$e^{(S_\theta + i\, S_r)}$$ may equally be applied to $e^{(S_\lambda + i\, S_\phi)}$

where

$$S_\phi = \ln(\tan \tfrac{\phi}{2}) \cos\alpha + \lambda \sin\alpha \qquad (4.32)$$

and

$$S_\lambda = \lambda \cos\alpha - \ln(\tan \tfrac{\phi}{2}) \sin\alpha \qquad (4.33)$$

The spherical space is defined in terms of spherical log spirals so that

$$S_\phi = 2 \tan^{-1} \left(\exp \frac{K - \lambda \sin\alpha}{\cos\alpha}\right) \qquad (4.34)$$

for constant S_λ and

$$S_\lambda = 2 \tan^{-1} \left(\exp \frac{\phi \cos\alpha - K'}{\sin\alpha}\right) \qquad (4.35)$$

for constant S_ϕ.

Transformations in Complex Space

The transformation from polar to spiral coordinates involves the successive transformations of shortening, rotation, scaling and stretching.

By considering complex space

$$z = re^{i\theta} \qquad (4.36)$$

and its conjugate

$$\bar{z} = re^{-i\theta} \qquad (4.37)$$

then by the transformation of shortening (operating on the conjugate in the northern hemisphere) we obtain

$$\ln\bar{z} = \ln r - i\theta \tag{4.38}$$

Scaling by i and n where $i = \sqrt{-1}$ and n is an integer produces

$$ni \ln\bar{z} = n(\theta + i \ln r) \text{ (semilog coordinates)} \tag{4.39}$$

Scaling by the versor, $e^{i\alpha}$ (equivalent to rotating the semilog coordinates), produces

$$nie^{i\alpha} \ln\bar{z} = n(\theta + i\ln r)e^{i\alpha} = n(S_\theta + iS_r) \tag{4.40}$$

Restretching to obtain real space curvilinear coordinates produces

$$\bar{z}^{nie^{i\alpha}} = \exp\left[n(\theta + i \ln r) e^{i\alpha}\right] \tag{4.41}$$

$$= \exp\left[n(S_\theta + iS_r) \right] \tag{4.42}$$

The Laplacian in complex coordinates is given by

$$\nabla_2^2 = 4 \frac{\partial}{\partial z} \frac{\partial}{\partial \bar{z}} \tag{4.43}$$

so that

$$4\frac{\partial}{\partial z} \frac{\partial}{\partial \bar{z}} (\bar{z}^{nie^{i\alpha}}) = 0 \tag{4.44}$$

SPIRAL COORDINATE SYSTEMS

Laplace's equation and the three laws are expressible in spiral coordinates. Of the thirteen systems mentioned by Morse and Feschbach (1953) which are separable in Laplace's equation, only five (of the non Cartesian* systems) can be changed into spiral form. That is to say, that five of the coordinate systems given by Morse and Feshbach are actually degenerate forms of more general spiral systems.

Three of these degenerate systems are cylindrical, with unit surface curvature $k = 0$, while the other two are spherical, with unit surface curvature, $k = 1$. There are four of relevance to meterology and vortex studies.

The first is the circular cylindrical coordinate system where the gradient is taken with the cylindrical axis held constant. This coordinate system is, of course, a degenerate form of the elliptic cylindrical coordinate system, just as a circle is an ellipse whose two foci have merged into a common origin. The coordinates orthogonal to ellipses are hyperbolas which in a circular form degenerate into rays.

Both of these coordinate systems are degenerate forms of the even more general spherical and conic systems respectively. The spherical system has coordinates described by the intersection of circular cones, vertically intersecting planes and spheres. The conic system is created by elliptic cones and conic hyperboloids with a sphere. The slopes of the latter two are taken on the surface of a sphere and are a function of only the other two coordinates. This is not so of the various toroidal, bispherical, spheroidal and paraboloidal coordinate systems. The only exception is the cylindrical parabolic coordinates, where

---

*There is a sixth, non-Euclidean spiral coordinate system obtained by substituting i for the radius of the sphere in spherical coordinates.

the horizontal coordinates are given by confocal orthogonal parabolas. Explicit derivations are given in Appendix A.

Therefore Laplace's equation can be expressed in five separate spiral coordinate systems. Just as circular harmonics are solutions to Laplace's equation in polar coordinates, so are spiral harmonics solutions to Laplace's equation in the pressure, velocity and divergence fields of vortices. The reader need only ask himself which spiral phenomena in a waterspout (spiral rainbands), a tornado (hook echo), hurricane (spiral bands of severe thunderstorms), an extratropical storm (spiral occluded front), spiral arms of galaxies (where stars are born as they enter the spiral arms) can definitely be excluded from any relationship with spiral harmonics or bands. The zero Laplacian condition may obtain just as easily for low level divergence fields complemented by upper level convergence fields, and vice versa.* It is only on the vertical distribution of divergence that the phenomenon producing (rain clouds, cb's) vertical velocity may be postulated. The proposed law specifies only the horizontal divergence distribution.

In summary, we have examined spiral behavior in both tropical and extratropical storms. This examination has led to an understanding of flow behavior and characteristics. Piecewise linear distributions of divergence and vorticity are complemented by spiral harmonic distributions. In the next section we will construct various models of atmospheric vortices based on these solutions to the proposed laws. In Section VI, following the exposition of the models in Section V, data will be correlated with the models from an array of atmospheric vortices. The fidelity of the fit to the models will be the linchpin of the new paradigm.

---

* In the case of spiral galaxies, spiral harmonics may be a solution to Newton's expression for gravitational potential satisfying Laplace's equation, in a relative sort of way.

V. THE THEORY OF VORTEX STRUCTURE

In Chapter II we dealt with the new laws of physics. Chapter III presented the mathematical application of these laws. Chapter IV and Appendix A discussed the mathematics of orthogonal log spiral coordinate systems, and solutions for Laplace's equation separable in these coordinates. In Chapter V we present the theory of vortex structure. This theory incorporates four different sub "models" for fitting the vortex structure together. These models will later be applied to appropriate naturally occurring atmospheric vortex data and contrasted with other, competing vortex models arising out of a different field theory and a different paradigm.

The vortex models presented in this section are two dimensional models of divergence, vorticity and pressure fields utilizing the solutions of the structural laws discussed in the previous chapter. The models display correllary flow fields of tangential and radial velocities. These are the components of circulation, Γ , and sink function, Q, mentioned in Section II. First we will deal with the axially symmetric models in ascending order of complexity. We will then address the asymmetric spiral model components.

Symmetric Models

One Piece - Simple Model

The first simple model, shown in Figures 5.1a and 5.1b, is one piece. The vorticity field in 5.1a is linear in the logarithm of the radius. The velocity field in 5.1b has a maximum. The tangential velocity field may be expressed entirely in terms of the wind maximum and its location. A ray in this field will deform into an evertightening log spiral. This is the

Radius →
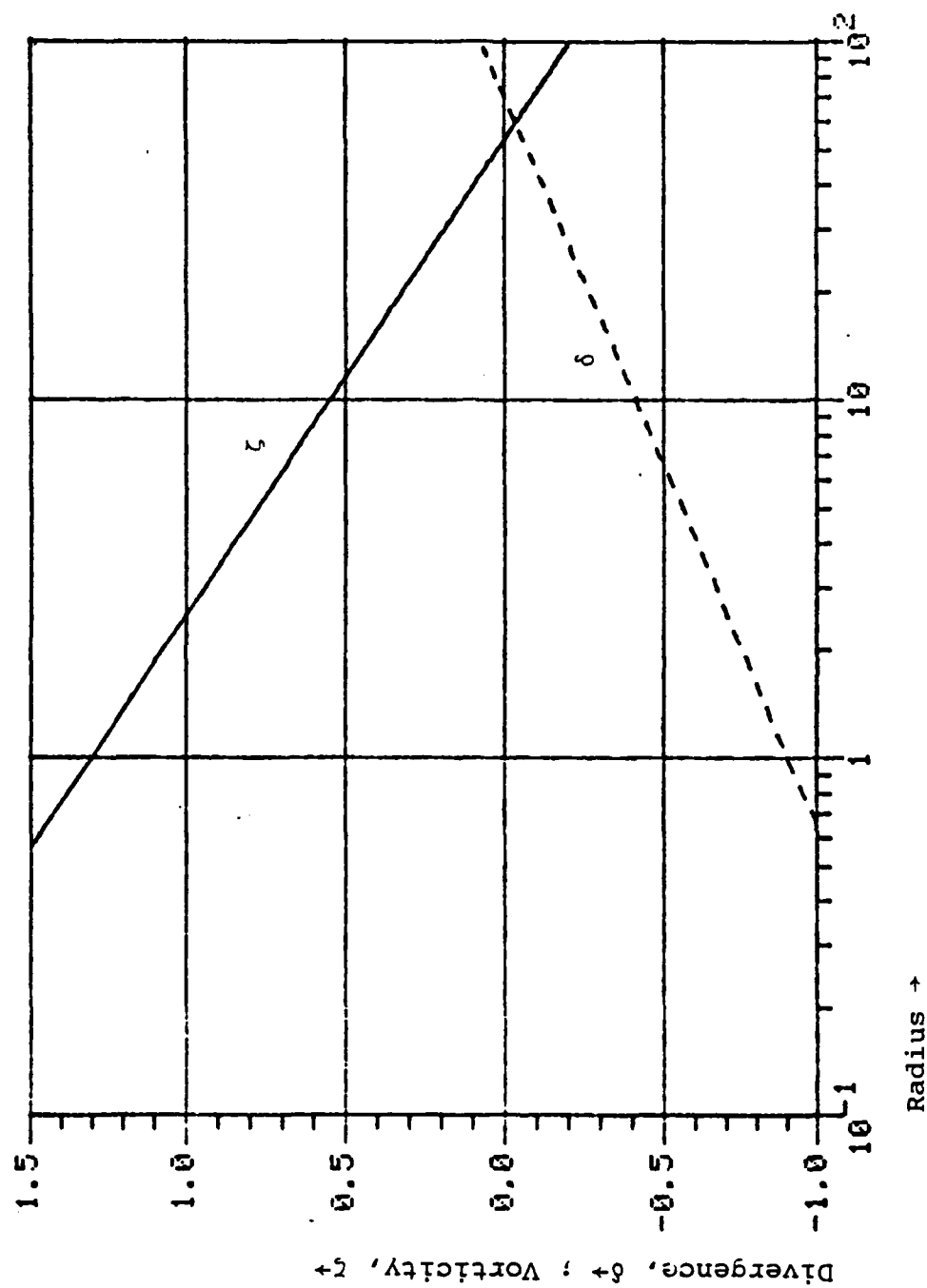
Figure 5-1a: Vorticity and Divergence of simple, one part vortex.

69

Radius →
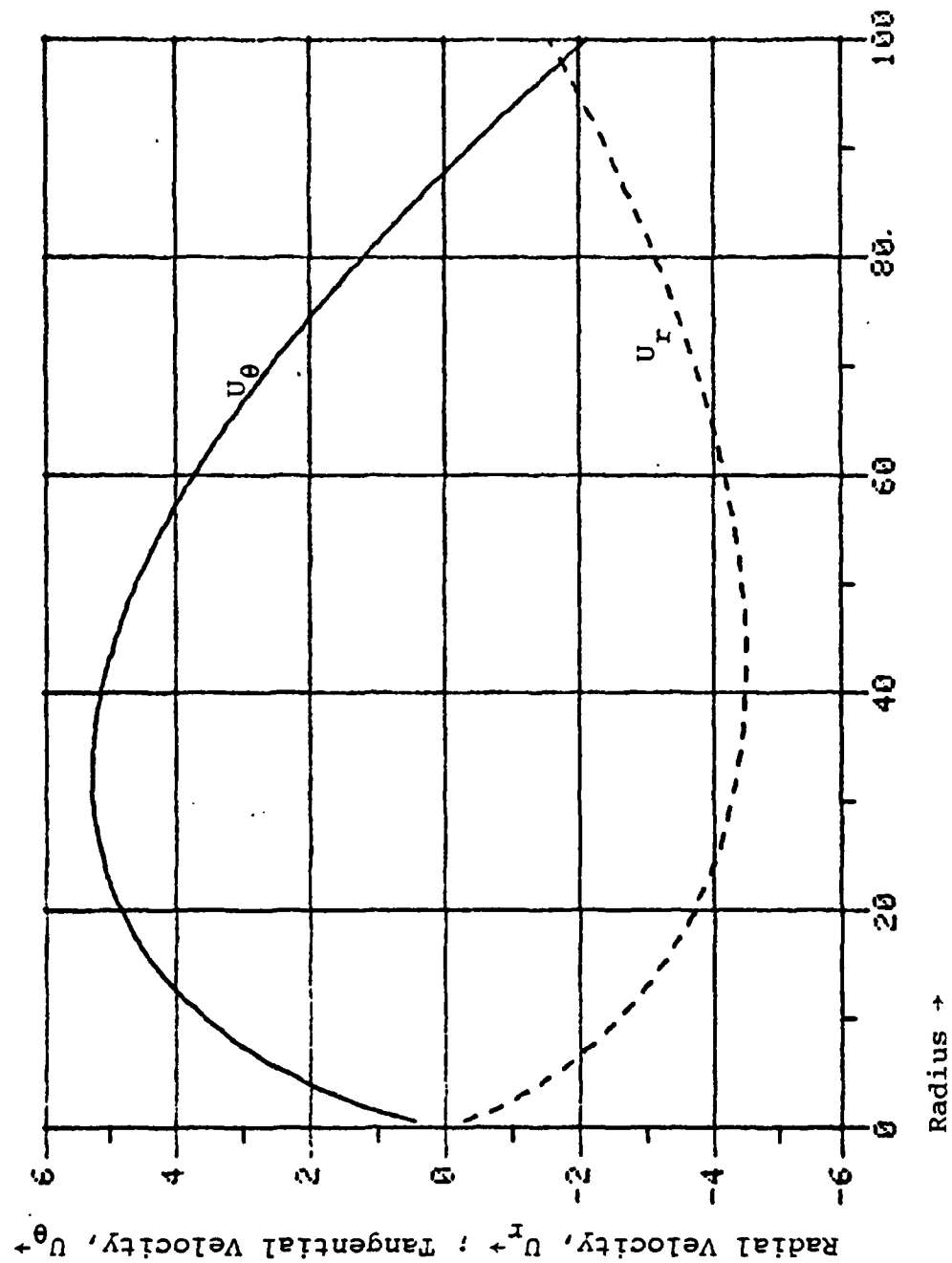
Figure 5-1b: Tangential and radial velocities corresponding to vorticity and divergence in 5-1a.

70

classic field of the extratropical storm, or the stirred coffee
cup. The same is true of the divergence and radial velocity
fields.

Two Piece - Compound Model

From the elementary one piece model we now discuss the two
part model. The inner portion we shall call the inner regime,
the outer, the outer regime.

In Figure 5.2a and 5.2b the vorticity field has been broken
into two parts with the majority of the vorticity crowded into
the inner regime. The same holds for the divergence field. The
consequences in the velocity fields have been a sharpening of the
flow field maxima with a displacement inward. Several of the
data sets are fit to the tangential velocity of this model
because of data density inadequate to define a further innermost
field, the core evident in the mature vortex in Figures 5.3a and
5.3b.

Three Piece - Mature Vortex

The mature vortex is characterized by the presence of a core
regime. Here the vorticity rises from a small value increasing
to the boundary of the core, whereas the divergence field starts
at a positive value descending through zero to a negative value
at the edge of the core. From there outward the vortex is
similar to the compound vortex structure. The tangential
velocity field, however, has a deeper and wider eye structure.
The radial velocity is initially positive, becoming large and
negative and then approaching a small negative absolute value.

The creation of the core regime and the corresponding core
pressure field suggest the "bomb" concept of Sanders.

Radius →
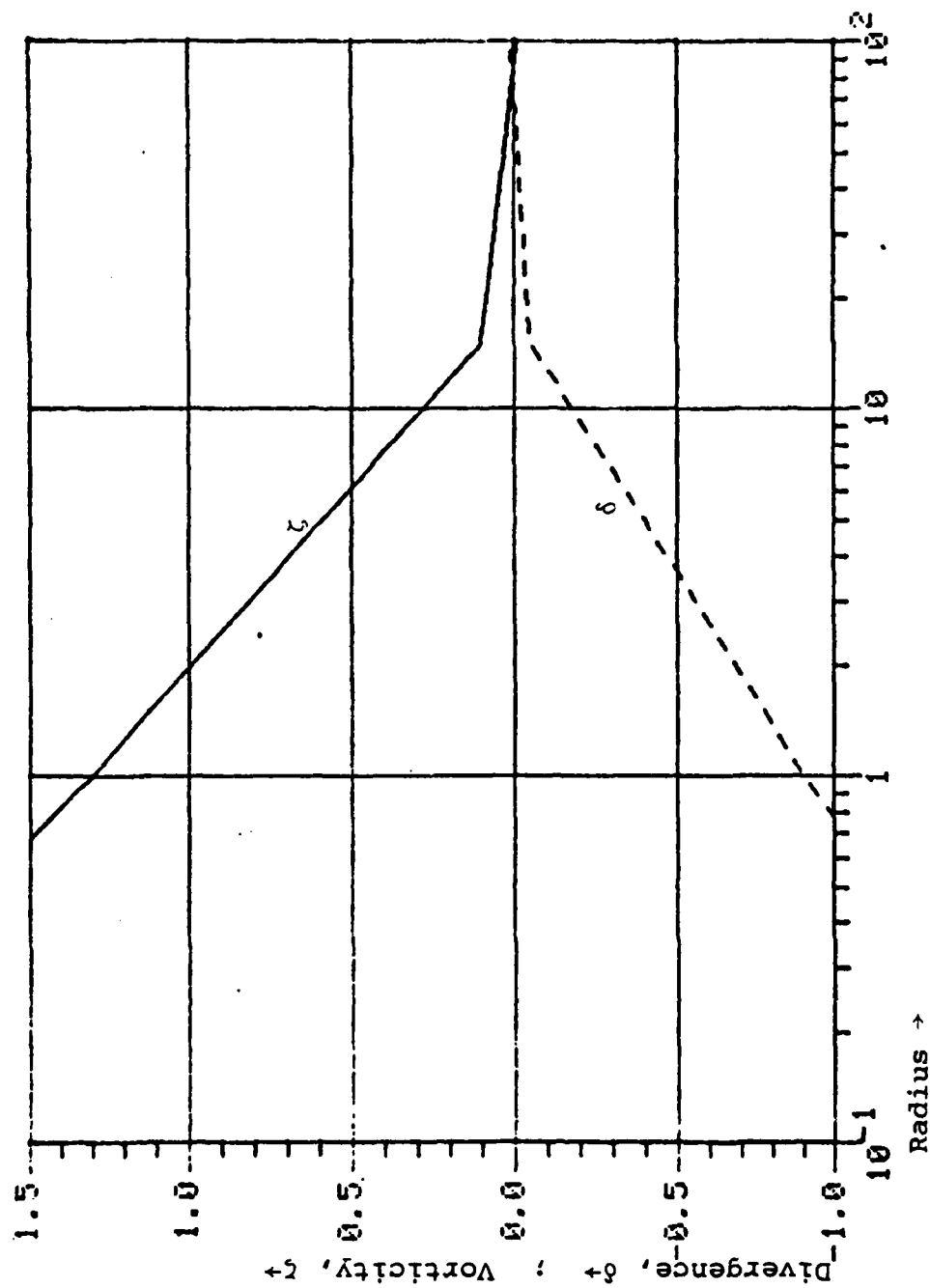
Figure 5-2a: Vorticity and divergence of complex or two part vortex with boundary at r = 15.

Radius →
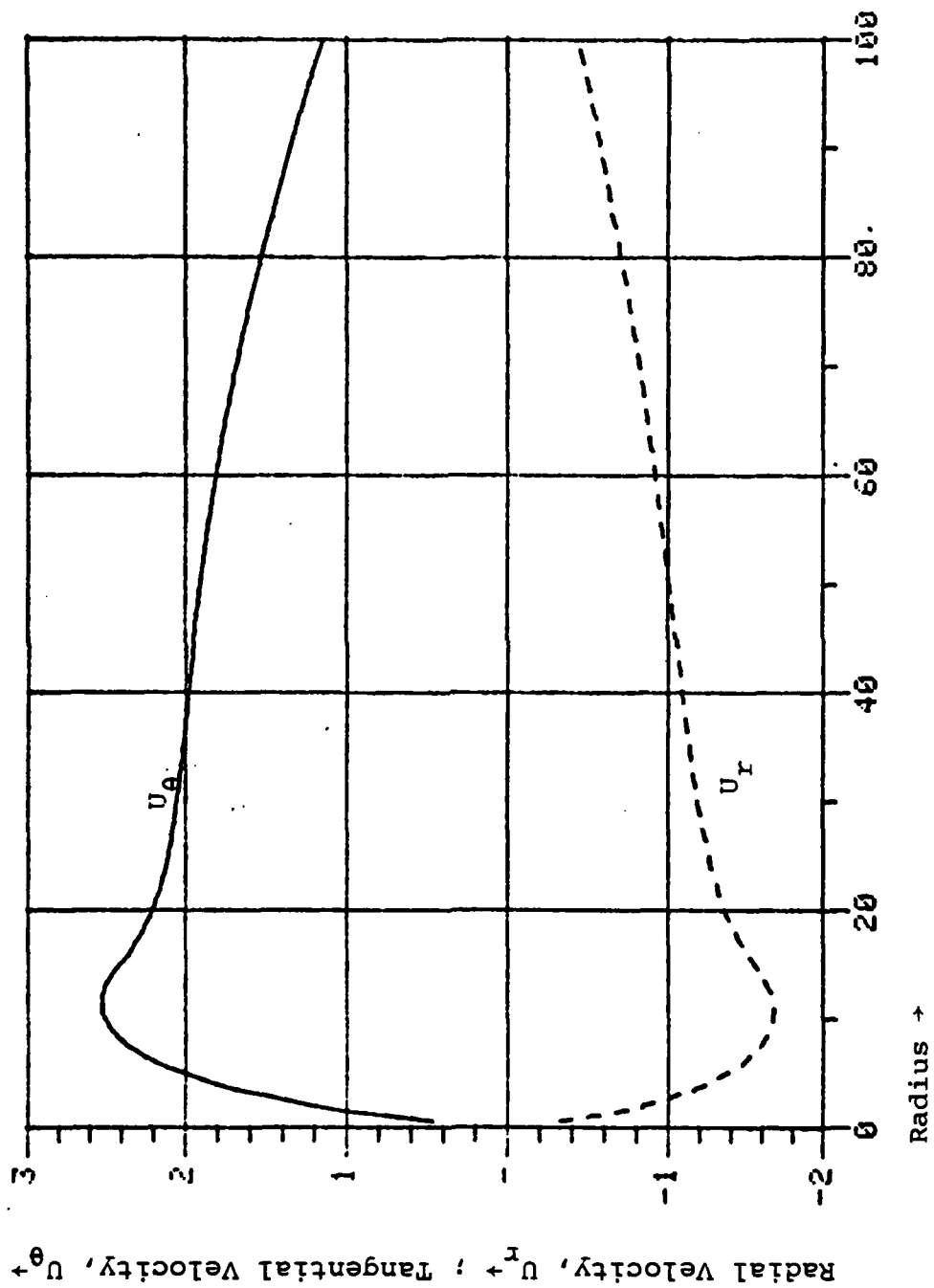
Figure 5-2b: Tangential and radial velocities corresponding to vorticity and divergence fields of Figure 5-2a.

Radial Velocity, U_r→ ; Tangential Velocity, U_θ→

Radius→
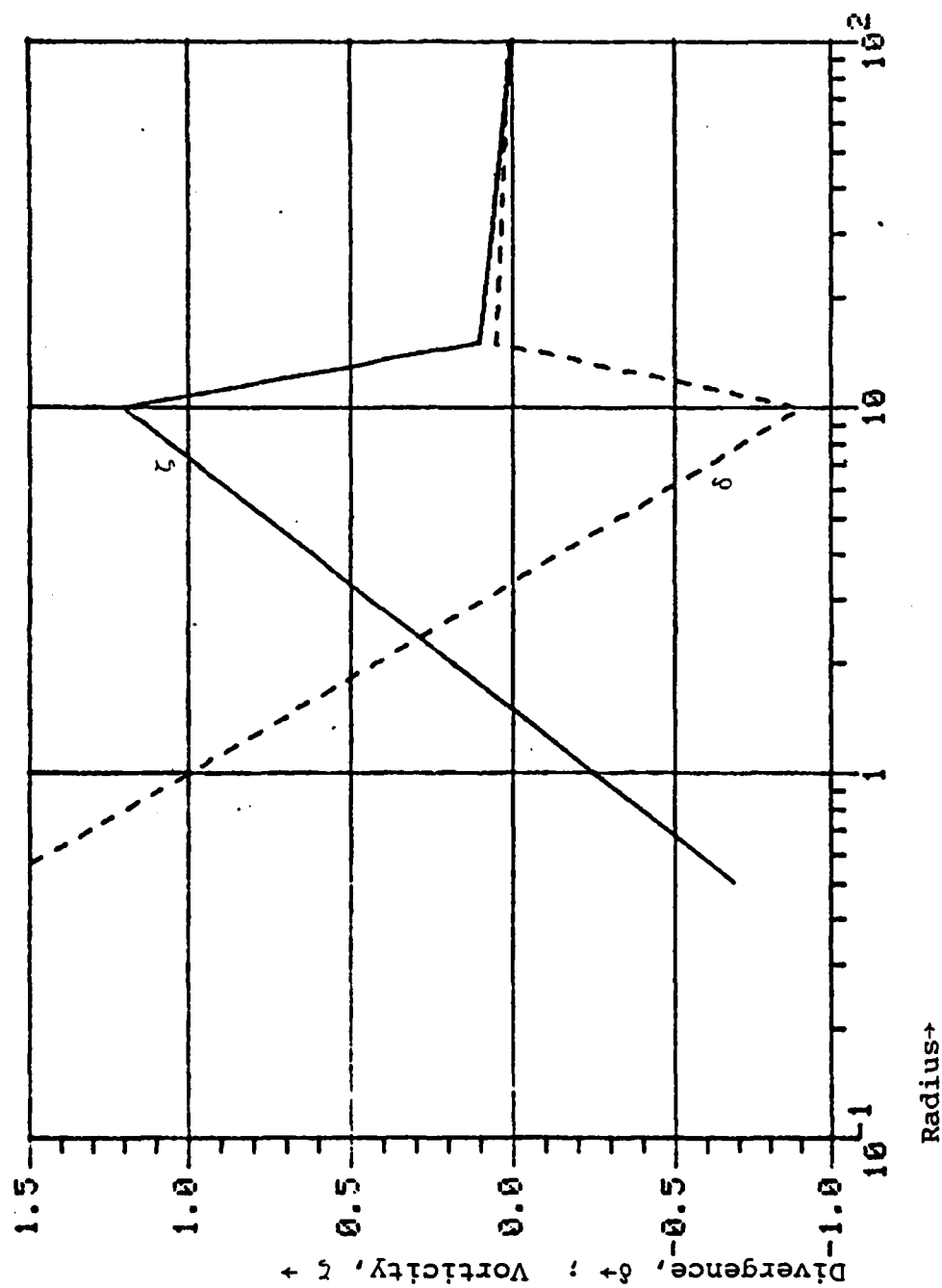
Figure 5-3a: Vorticity and divergence fields for mature, or
three part vortex. Radii of regimes at r = 10, 15.

74
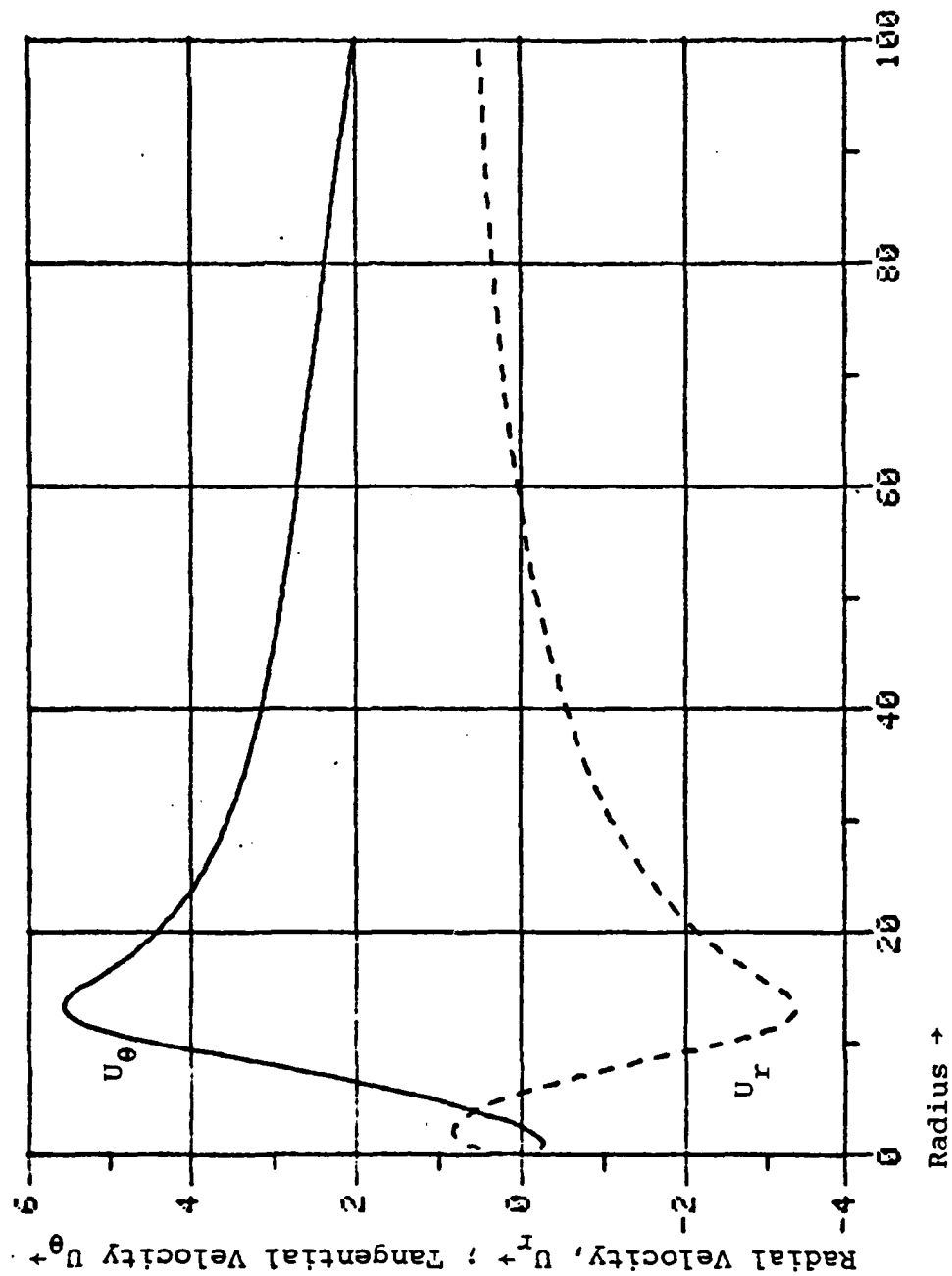
Figure 5-3b : Tangential and radial velocities corresponding to
vorticity and divergence fields in 5-3a. Note
positive radial velocity in the eye.

75

Three Piece - Double Vortex

One final vortex completes the roster of the axially symmetric vortices. This is the double vortex. The data supplies one example of this particular vortex shown in Figures 5.4a and 5.4b. The vorticity field has a core beginning with a very large, rather than a low, vorticity value. This field then decreases to the boundary of the core regime, there to join with the field of the inner regime. The velocity field is unique in having two maxima separated by a minimum. The outer maximum is always the greatest.

Composite Vortex Structure

The atmospheric vortex is a composite of symmetric and asymmetric components. The tropical hurricane is a composite of the "mature vortex" and the spiral vortex with wave numbers one, two and often higher. The preponderance of data collected for this paper displays a correlation with three of the four symmetric vortices, the compound, mature and double vortex. Further work is being done to perform a Fourier analysis of hurricane bands in spiral space. Is is now appropriate to examine the data in these three categories to assess the goodness of fit of the model.
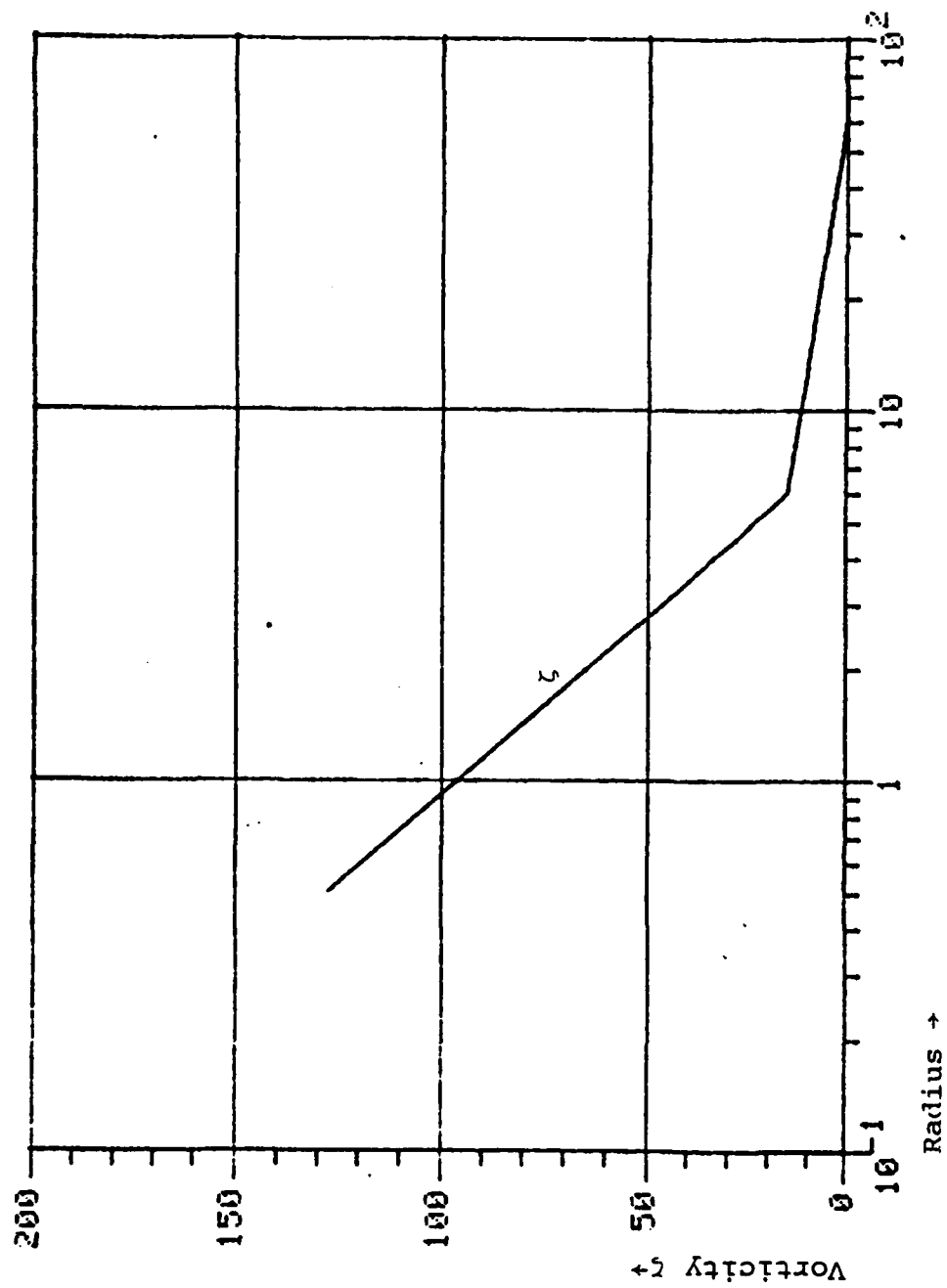
Figure 5-4: Vorticity field for double, or two part vortex. Radii of core and inner regimes at r = 6, 60.

77
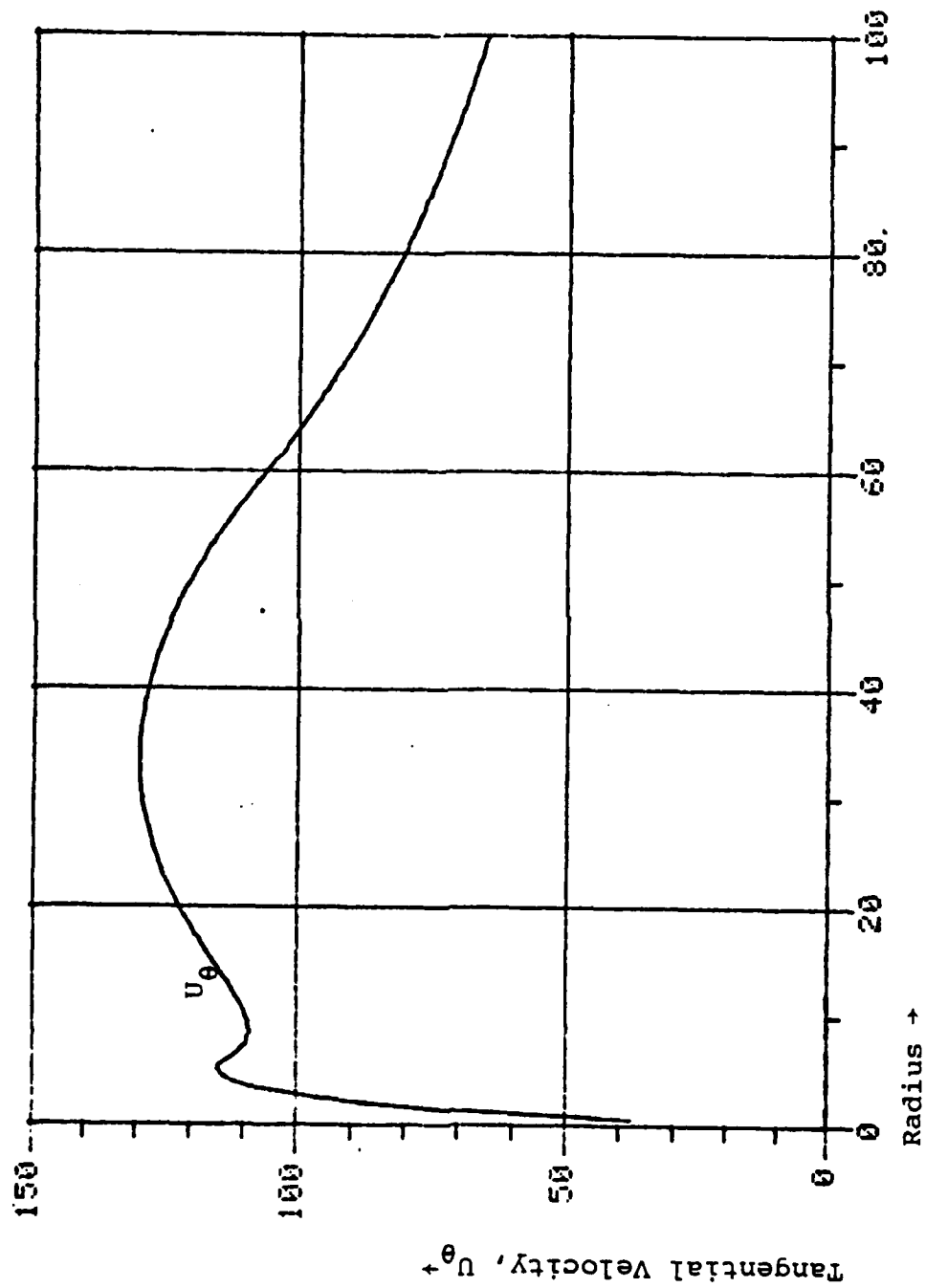
Figure 5-4b: Tangential velocity field corresponding to vorticity field of 5-4a. Reference Figure 5-18 for data.

78

VI. THE VERIFICATION OF THE AXIALLY SYMMETRIC PORTION
OF LAW I.

Chapter VI is devoted to verification of a small but significant part of the new paradigm. First we shall examine that aspect of the paradigm to be verified. Following that will be a brief explanation of the extant models of the vortex structure competing with those advocated by the paradigm. Then the extant models and the paradigm models will be compared. The criteria for utilization of the various paradigm models will be set forth based mainly on availability of data. The variety and range of data instrumentation and vortex types will then be examined.

The mathematical procedures for fitting the paradigm models (also called the zero Laplacian vortex, or zLv) are then outlined. The question of extrapolation of the data inward to the center of the vortex is addressed. Boundary layer vortices are examined first. Since two of these vortices are the lower sections of the Dallas tornado, the remaining portion of the tornado is then examined, followed by an examination of three consecutive days in the life of hurricane Daisy including a period of most intense winds.

There follows an examination of four hurricanes which are dissimilar in their wind fields but are rich in data and similar in their vorticity fields. There then follows two days in the life of hurricane Carrie, interesting from the standpoint of watching a hurricane organize.

We then switch to hurricane Camille with data provided by the movement of thunderstorms vertically integrating the momentum fields through which they travel(Bradbury 1971). In wrapping up,* from the far reaches of space we examine the behavior of the spiral galaxy in the Andromeda Nebula, M31.

---

*in a spiral sort of way, naturally.

Finally a summary of the data results and interpolation is presented.

Law I - Symmetric Part

Verification of the three laws requires analysis for both azimuthally averaged and spiral asymmetric components. Full verification of all three laws is well beyond the scope of this work and must be left for future work, a task characteristic of a new paradigm, i.e., that it be "sufficiently open-ended to leave all sorts of problems for the redefined group of practitioners to resolve." (Kuhn, p. 10). In this paper the investigation is confined to verification of the azimuthally averaged version of the first law. The first law in this form,

$$\frac{1}{r} \frac{\partial}{\partial r} \; r \frac{\partial \zeta}{\partial r} \; = 0, \infty \quad \text{or} \quad \frac{1}{r^2} \frac{\partial^2}{\partial \ln r^2} \; \zeta \; = 0, \infty \quad (6.1)$$

is satisfied when the velocity field fitting the data has a corresponding vorticity field which is a piecewise, continuous and linear function of the logarithm of the radius. In the previous chapter the kinds of vortex models to be fit to the data were examined. In this chapter the data is examined for its conformity to one or other of these models and the competing models of Herbert Riehl (1963) and Rankine (1888).

The Riehl and Rankine Models of the Symmetric Vortex

The Riehl and Rankine models have similarities and differences to one another in the tangential velocity field. The similarity lies in the interior vortex (interior to the maximum wind) being in solid rotation, an assumption which provides a significant portion of the root mean square error of these models when fit to the extant data. The difference is that the Rankine model is irrotational in the outer vortex. The frictional force and hence frictional curl are zero. The Riehl model follows an

inverse square root law based on bulk aerodynamic considerations of conservation of potential vorticity. Here the lateral frictional curl is zero, but for a vertical component of friction only. The lateral frictional force is assumed zero. Vertical integration of an hyperbolic frictional curl yields

$$r\tau_{\theta_S} = \text{constant} \tag{6.2}$$

where τ_{θ_S} is the surface tangential stress component. This stress is commonly expressed as proportional to the square of the surface wind

$$\tau_{\theta_S} = C_D \rho_S v_{\theta_S}^2 / \cos \alpha \tag{6.3}$$

where C_D is the drag coefficient, ρ_S is the surface density, v_{θ_S} is the tangential wind component measured at ship's deck level, and α is the inflow angle. Riehl sets $\cos \alpha = 1.$, based on observations by Ausman (1959).

Combining (6.2) and (6.3) yields $rv_\theta^2 = \text{constant}$, or,

$$v_\theta r^{0.5} = \text{constant}. \tag{6.4}$$

81

Riehl combines this exterior wind profile with an interior one of solid rotation. Unfortunately, the resultant juncture exhibits a first order discontinuity and a zero order vorticity discontinuity. The same is true of the Rankine vortex, which suffers from dynamical inconsistencies as well (Nicholson, 1972). Not only do these vortices have velocity discontinuities between their inner and outer portions, but discontinuities in the physics behind the choice of an inner vortex to match the outer one. If the physics is good enough for the outer vortex, it should be valid for the inner vortex as well. Interestingly, the Rankine vortex is nearly a degenerate form of the zero Laplacian vortex since in both the inner and outer vortex vorticity is constant, thereby satisfying Laplace's equation. Again, however, neither for the Rankine nor the Riehl vortex model are there piecewise continuous distributions of vorticity linear in the logarithm of the radius.

It was found that for hurricanes Riehl's vortex model was superior to Rankine's. For non hurricane cases, Rankine's was superior to Riehl's. In all cases both models had a higher root mean square error than did the zero Laplacian vortex (zLv). This was the case despite the fact that the zLv labors under the constraint of first order discontinuities in the vorticity field,

while the other two exhibit the dynamically difficult, but less constraining zero order discontinuities. The velocity field is smooth and continuous in the zLv while the other velocity fields exhibit first order discontinuities. Lastly the zLv has smooth maxima and minima in its velocity field, whereas the other two possess no minimum whatsoever and no true maximum but rather an artificial maximum created by the juncture of two velocity fields which occur at the union of two separate regimes. In the zLv the maxima and minima occur within the regimes, not at their borders, thus satisfying the part of the law which requires the Laplacian of vorticity to be zero rather than to be undefined.

Model Choice

The mathematical niceties of the data fit to the model are reserved for Appendix E. The models are chosen strictly on the availability of the data for the various regimes, specifically the innermost or core regime. Depending upon this data availability, either a two part (compound) or three part (mature, and in one case double) vortex is chosen. The three part model differs from the two part primarily by the introduction of a core regime. The mature and the double vortices are determined strictly by the same computational procedure, i.e., the only specification initially is for a three part rather than a two part regime.

Data Variation

The range of vortices from which the data are gleaned is vast. Vortices are analyzed from the laboratory, the free, maritime tropical atmosphere and the far reaches of outer space. The extent of the size difference is from 15 cm to 120 minutes of celestial arc. Maximum velocities vary from less than 20 m /sec to greater than 300 km/sec. Data was taken by a wide range of

instrumentation. In the laboratory a combination of stagnation pressure velometers and small three cup anemometers were used. Stellar velocities from H_α at a dispersion of 135 Å/mm and $N_{II}\lambda 6583$ emission lines were determined with accuracy of 10 km/sec in the spiral galaxy in Andromeda, M31. The gas in the galaxy is assumed to move with the speed of the stars. Photogrammetry was employed in the analysis of spray from the ocean surface in the winds of the Lower Matecumbe Key waterspout and flying pieces of lumber and other debris in the Dallas tornado. Clover leaf fly throughs from the National Hurricane Research Labs (NHRL) were supplemented by the observed motion of cumulonimbi on radar PPI scopes in hurricane Camille. Data was taken in the first few centimeters of the boundary layer in the Dines vortex cage, at 15 m in the waterspout and 150' and 300' in the Dallas tornado. The NHRL reconnaisance flights varied from 5500' to 15,600 ft. In the spiral galaxy in the Andromeda Nebula there is no "bottom" boundary layer. Needless to say this data collection has been taken from a variety of authors nearly as extensive as the vortex kinds and instrumentations. First we will examine the data taken from vortices in the planetary boundary layer. Before this, however, it is important to consider how the velocity and vorticity fits were made.

Least Squares Fit of Circulation

In Chapter III the velocity as a function of a piecewise vorticity structure was presented in equation (3.2). For a given set of data corresponding to a segment of the vorticity within a regime a least squares fit of the circulation for three or more points may provide both upper and lower values of circulation for the regime. If only two data points are available, then the lower value needs to be specified. For the core regime this indicates that $C_3 = 0$, eq. (3.14) that the "y intercept" exists at $r_0 = 1$, or is otherwise specified (e.g., by the

84

upper bound of the adjacent, inner regime. For the outer
regimes, the lower boundary and value of circulation is identical
to the upper boundary and circulation of the regime interior to
the regime of interest.

Thus, in the core, if three data points are available, then
an additional degree of freedom is provided so that the
circulation at the lowest datum may not be extrapolated to the
center of the vortex. This is true for the vortex data sets with
even numbers in parentheses ( ) after their titles, indicating
that the number of parameters includes the circulation value
interior to the innermost datum. Otherwise, it is assumed that
the circulation extends to $rU_\theta = 0$ at $r = 0$. A curiosity of
the latter assumption is a small but discernable anticyclonic
velocity at short radii in such vortices where the core
circulations extrapolate to zero at the center. The velocity in
"even" vortices becomes rapidly large indicating an hyperbolic
dependence upon a positive C_3. In others it becomes zero at
$r \neq 0$ indicating a negative C_3.

The data are indicated by "x's." The zLv velocity and
vorticity are both given by the solid lines. The values
corresponding to the Riehl vortex, are given by a simple dashed
line. The Rankine is given by the dashed-dot line. The velocity
for the Riehl and Rankine vortices interior to the maximum datum
are solid rotation, linear with radius. Both are represented by
the Riehl vortex interior to the maximum datum. The vorticity
for this solid rotation is also represented by a constant value
for both in the inner vortex. The Rankine vortex is irrotational
in the outer vortex - its vorticity is therefore zero. Only the
Riehl vorticity is indicated in the outer vortex. Both the Riehl
and Rankine vortices exhibits zero order discontinuities in the
vorticity field.

Boundary Layer Vortices

Let us first examine the vortices in the boundary layer. These are the Dines vortex cage, Figure 6.1; the Lower Matecumbe Key waterspout, Figure 6.2; and the Dallas tornado at 150 and 300 feet respectively, Figures 6.3 and 6.4. Two of these are odd vortices, the vortex cage and waterspout. Two are even, the Dallas tornado at 150 and 300 feet. All four exhibit a slight negative vorticity at the juncture between the outermost regime and the regime immediately interior to it. The zLv has a lower root mean square error than either of the other two models.

The waterspout exhibits slight anticyclonic velocity when extrapolated inward which may either be real or simply a result of fixing the lower boundary of the core arbitrarily. The Riehl vortex model fares worse than the Rankine model in all of these cases. With the exception of the two part Dines vortex cage, where there is not enough data the boundary layer vortices exhibit a sharp rise in vorticity in the core, and a plunge in the interior regime to a negative value, followed by a rise to ambient values in the outer regime.

Dines Vortex Cage (Figure 6.1) (Wilkims, 1962)

The data from this laboratory vortex are thoroughly critiqued in Nicholson (1972). The inner data are from stagnation pressure velometers. The outer from small, three cup anemometers. The outer data had to be corrected in order to remove a bias introduced by assumptions of conservation of angular momentum in the data presentation. The zLv rms for the Dines vortex was just over 1 m sec^{-1}, 1.049. The Riehl and Rankine errors were __?__ and __?__ respectively. The boundary of the inner regime is within a half a centimeter of the radius of the fan opening at the top of the cage, indicating a dynamical rationale for the boundary placement.

86

Radius→centimeters
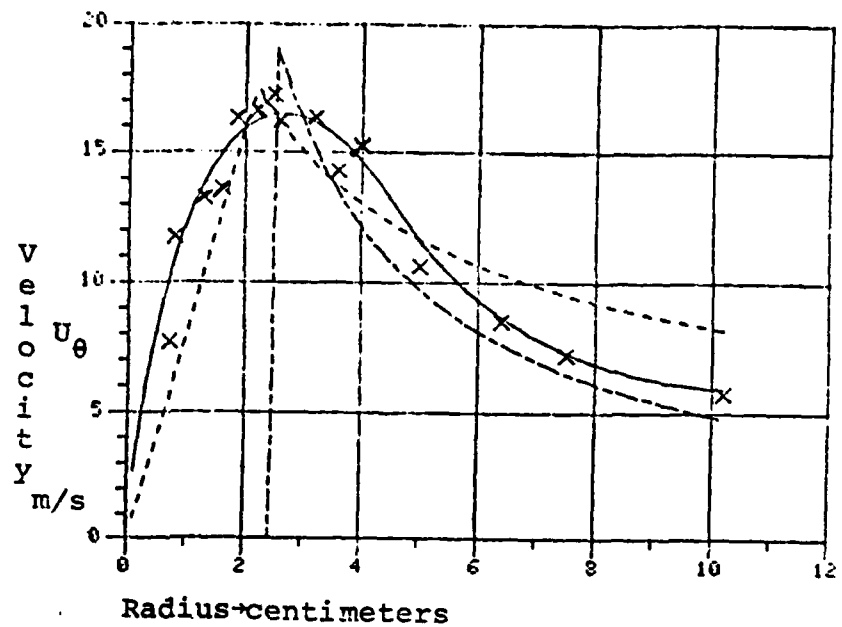
Figure 6-1a: Tangential Velocity in
Wilkins' Dines Vortex Cage.(3)
x = data, ——— = zLv, ----- = Riehl's,
— · — = Rankine's vortex models. RMS = 2LV
root mean square error, RMSL =

Radius→
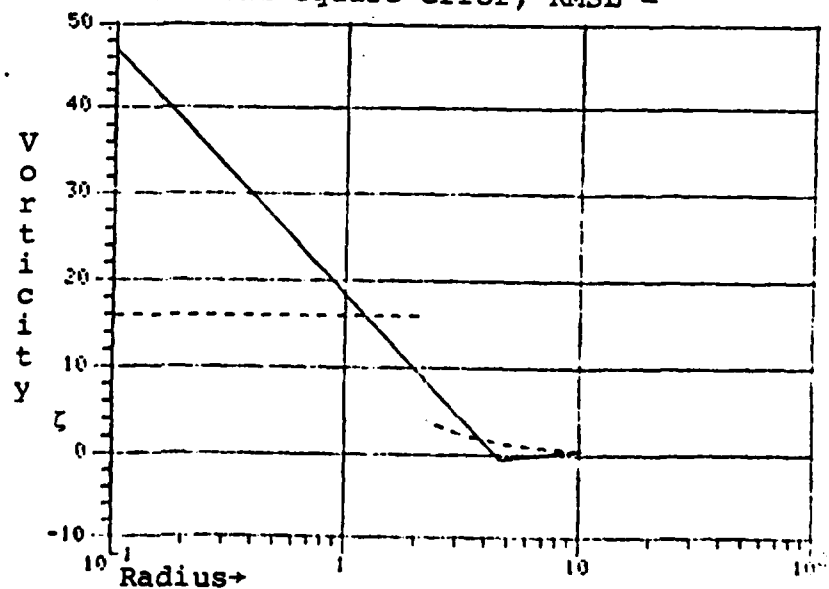
Figure 6-1b: Vorticity in zLv and Riehl
models. Note discontinuity
in Riehl vorticity.

87

Lower Matecumbe Key Waterspout (Figure 6.2) (Golden, 1974)

This boundary layer vortex data analyzed by Golden is taken by photogrammetric analysis of flying water droplets at 15 meters height. The z_{Lv} rms is just under 3 m sec^{-1}, with a maximum wind of almost 65 m sec^{-1}. Riehl's error was 9.058 m sec^{-1} and the Rankine error, 5.998 m sec^{-1}. It is evident that the collar of maximum convection occurs between about a 6 and 16 meter radius.

BOUNDARY LAYER TORNADOES (Moecker, 1960)

The Dallas data, though ingenious, exhibit the greatest possibility for error since they are based on interpolation of observations of flying debris which are averaged over a time period of 17 minutes. At the 300' level, two suspect observations were dropped at a radius of about 220'. This is based on the lack of data supporting the distribution of isopleths at this level, coupled with the enhanced fit of each of the vortex models.

Dallas Tornado at 150' (Figure 6.3)

The Dallas tornado at 150' has a z_{Lv} rms of 8.926 mph and a maximum wind of 190 mph at about 125'. Both the Riehl and Rankine vortices underestimate the wind maximum, the Riehl by 50 mph and the Rankine by 25 mph.

Dallas Tornado at 300' (Figure 6.4)

At 300' the wind maximum decreases by about 10 mph, and the Riehl error is about 25 mph. The rms for the z_{Lv} is 10.83 mph out of 175 mph maximum, 12.74 for the Rankine vortex and 25.44

*In Riehl's model $v_\theta = cr^{-0.5}$ and $\zeta = 0.5cr^{-1.5}$.
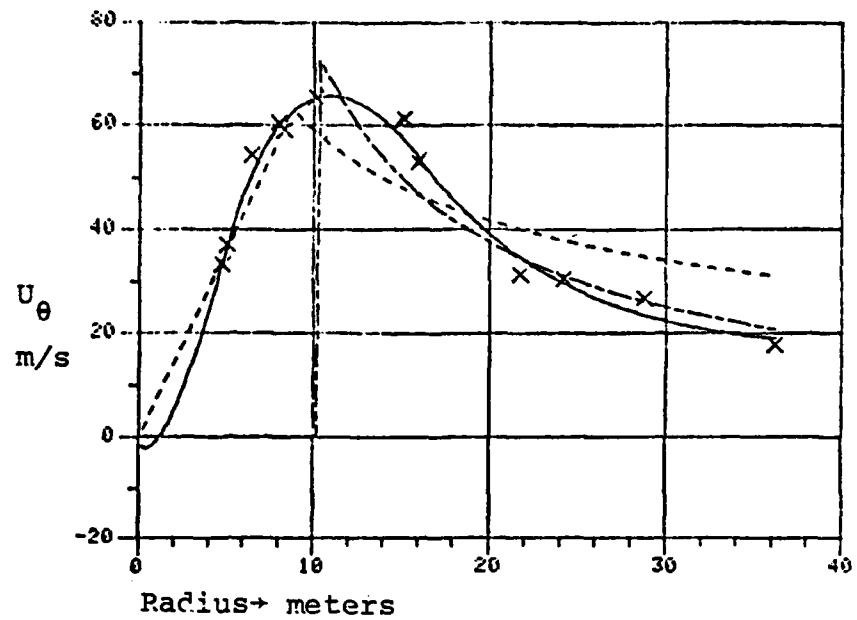
Figure 6.2a: Lower Matecumbe Key water-spout tangential velocity. Key as in 6.1.
(5)

RMS=2.931, RMSL=9.058, RMSK=5.998
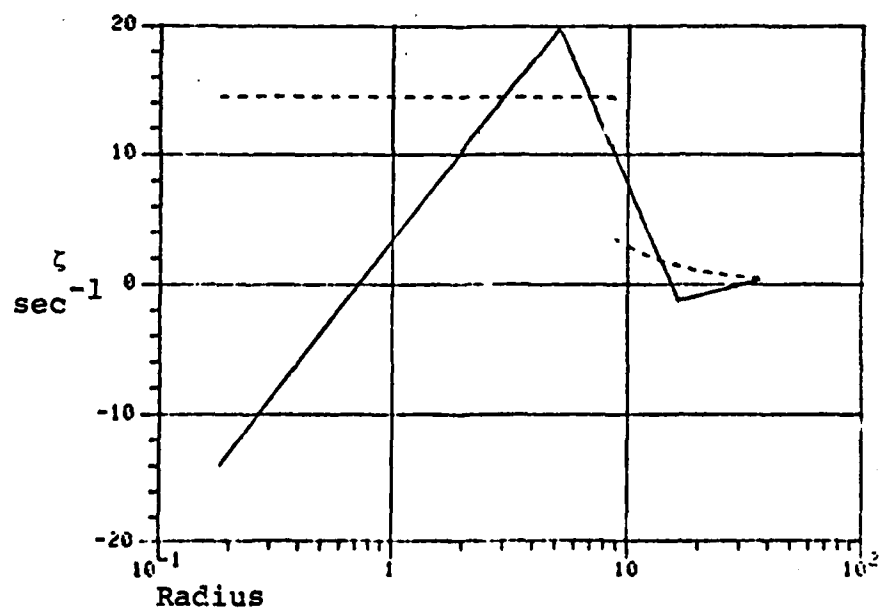
Figure 6.2b: Vorticity field of L.M.Key waterspout

89
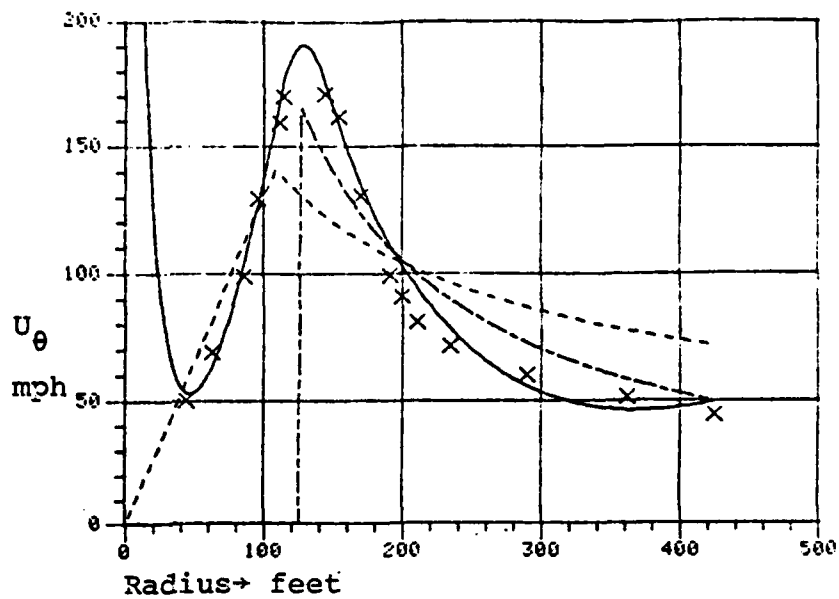
Radius→ feet

Figure 6.3a: Dallas Tornado at 150' tangential velocity profile. Key as in 6.1.
(6)

RMS=8.926, RMSL=27.38, RMSK=16.74
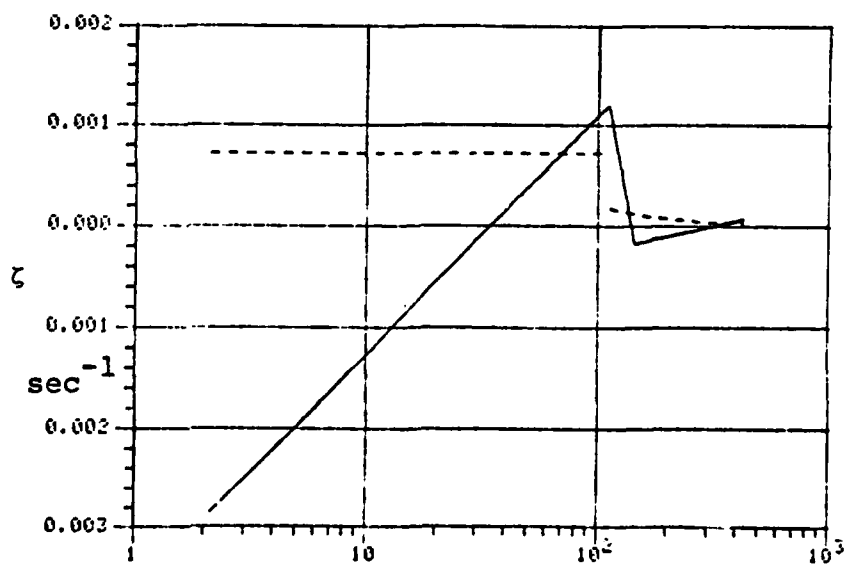
Radius

Figure 6.3b: Dallas Tornado at 1~0'
vorticity profile.
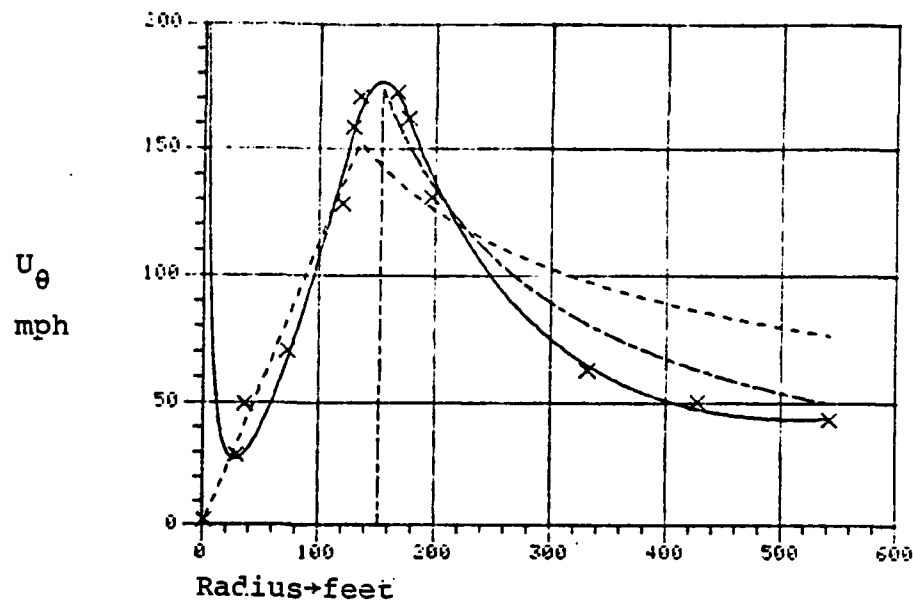
Radius→feet

Figure 6.4a: Dallas Tornado at 300'
tangential velocity profile. Key as in 6.1.
(6)

RMS=10.83, RMSL=25.44, RMSK=12.74
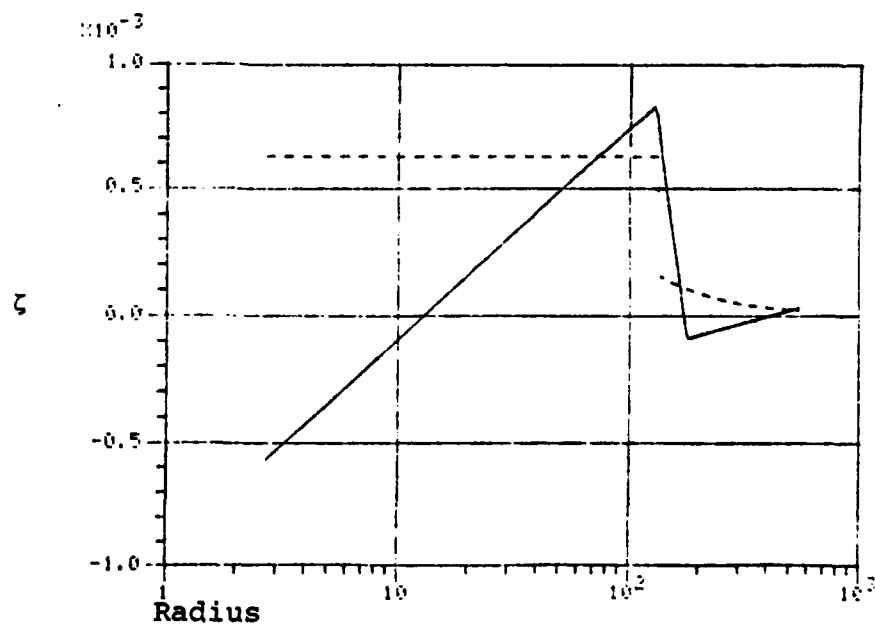
Figure 6.4b: Vorticity profile of Dallas
tornado at 300'.

for the Riehl vortex. The necessarily poor quality of the data due to temporal averaging and spatial interpolation precludes curve extrapolation inward of the innermost datum.

According to Bozart (personal communication) the presence of negative relative vorticity in the vortex is indicative of intense convective activity. This juncture occurs just beyond the radius of maximum winds (not at it, as in the Riehl and Rankine vortices). This is the location where classically the ring of most intense convection occurs in a hurricane, and quite possible in other severe vortices.

Dallas Tornado at 1000' (Figure 6-5) (Hoecker, 1960)

At the lowest level in the Dallas tornado, 150', the maximum vorticity is 12×10^{-4} sec $^{-1}$. This vorticity is cut to 8 x 10^{-4} at 300' and 4.5×10^{-4} at 1000'. The vorticity concentration is up to an order of magnitude greater than ambient vorticity. The two data at the maximum appear to be the most suspect, although the distributution of the isopleths in Hoecker's analysis appears reasonable. The zero value for both the 300 and 1000 ft level isdiscarded by virtue of the theoretical difficulty of incorporating a circulation value at or near a mathematical singularity and the relative uncertainty of the exact position of the vortex center. The zLv rms for the Dallas tornado at one thousand feet (away from the flying lumber) was 5.919 mph, the Rankine 7.182 and Riehl 16.44. The zLv was 5 mph short of the maximum data, whereas the Rankine is 10 mph in excess. Riehl is 15 mph short.

Hurricane Daisy (Figures 6.6, 6.7, 6.8) (Riehl, 1963)

Riehl's model came in a poor third for the vortices in the boundary layer. In all fairness his model was designed for vortices in the free atmosphere. Let us then examine his fit to

92
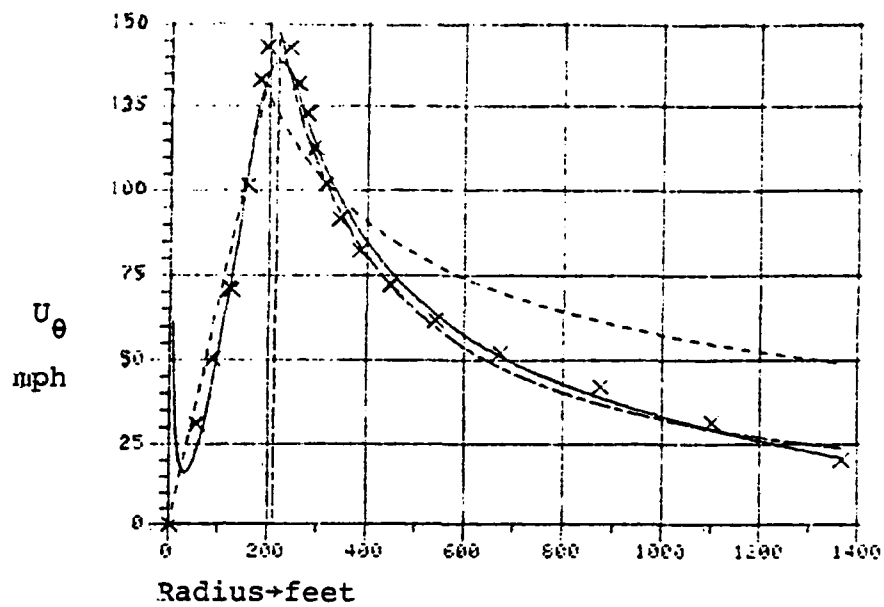
Figure 6.5: Dallas Tornado at 1000'
tangential velocity profile. Key as in 6.1.
(6)

RMS-5.919, RMSL=16.44, RMSK=7.182
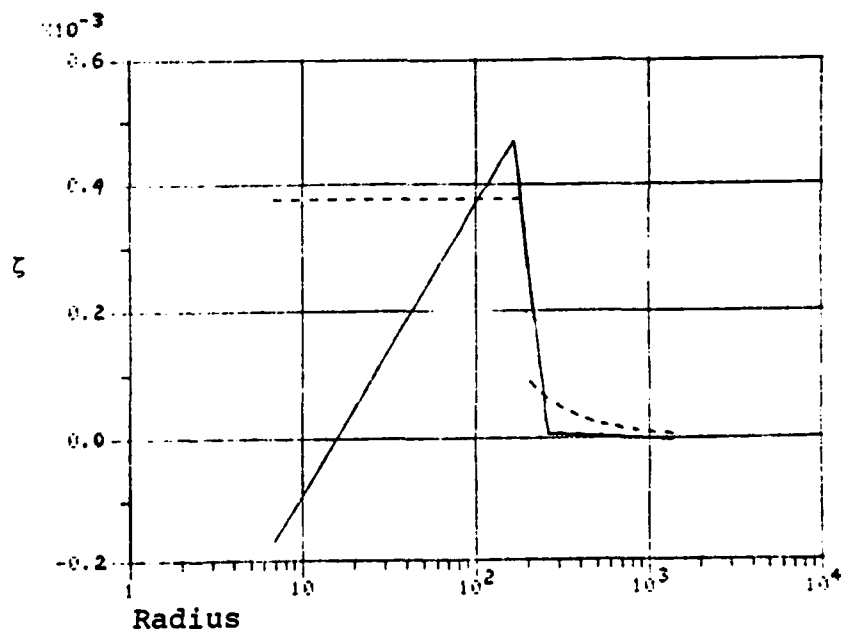
Figure 6.5b: Vorticity profile of
Dallas Tornado at 1000'.

93
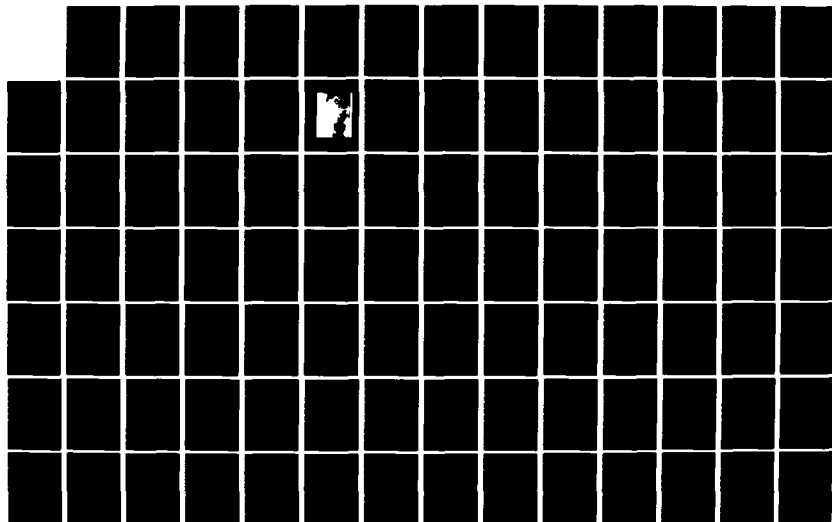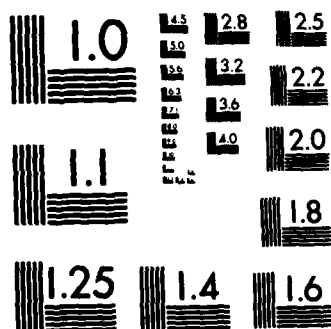
MICROCOPY RESOLUTION TEST CHART
NATIONAL BUREAU OF STANDARDS-1963-A
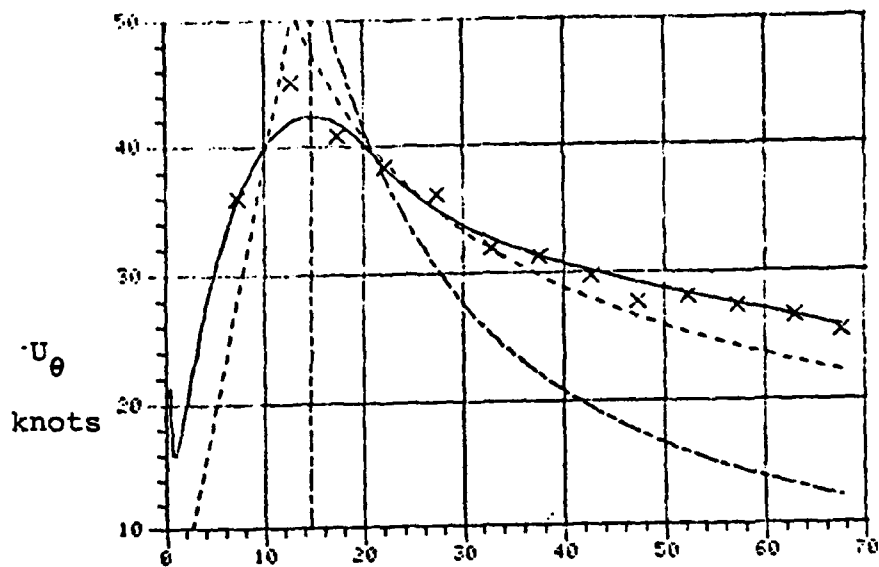
Radius→ n. mi.
Figure 6.6a:Hurricane Daisy, 25 August, 1958, tangential velocity profile. Key as in 6.1. (4)
RMS=1.315, RMSL=5.639, RMSK=12.86
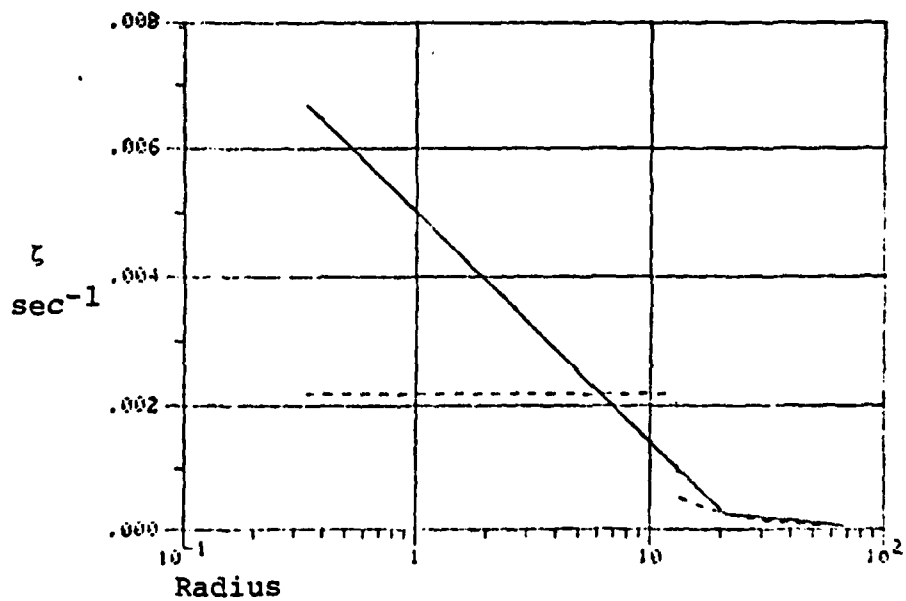
Radius
Figure 6.6b: Vorticity profile for Hurricane Daisy, 25 Aug.
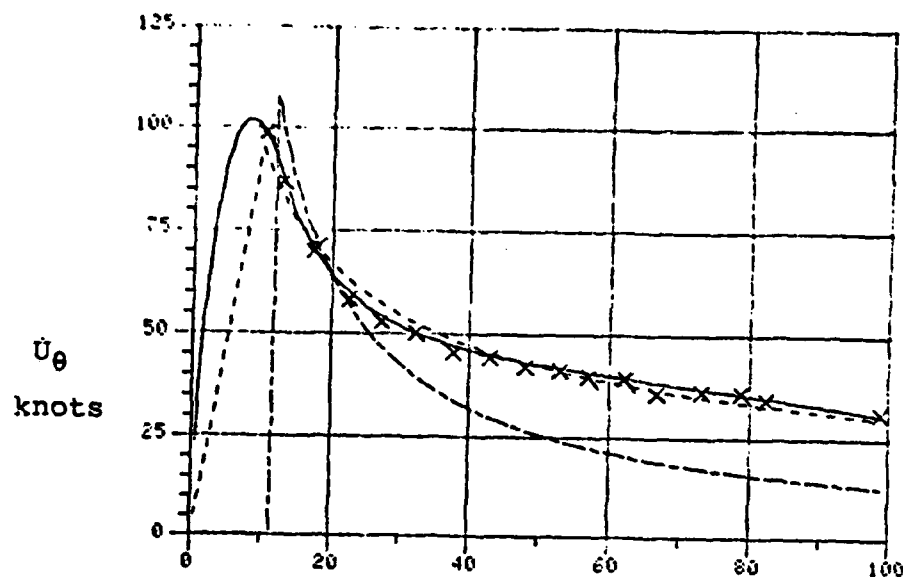
Radius→ n. mi.

Figure 6.7a: Hurricane Daisy, 27 August,
1958 tangential velocity profile. Key as
in 6.1. (4)

RMS-1.316, RMSL=3.645, RMSK=10.74
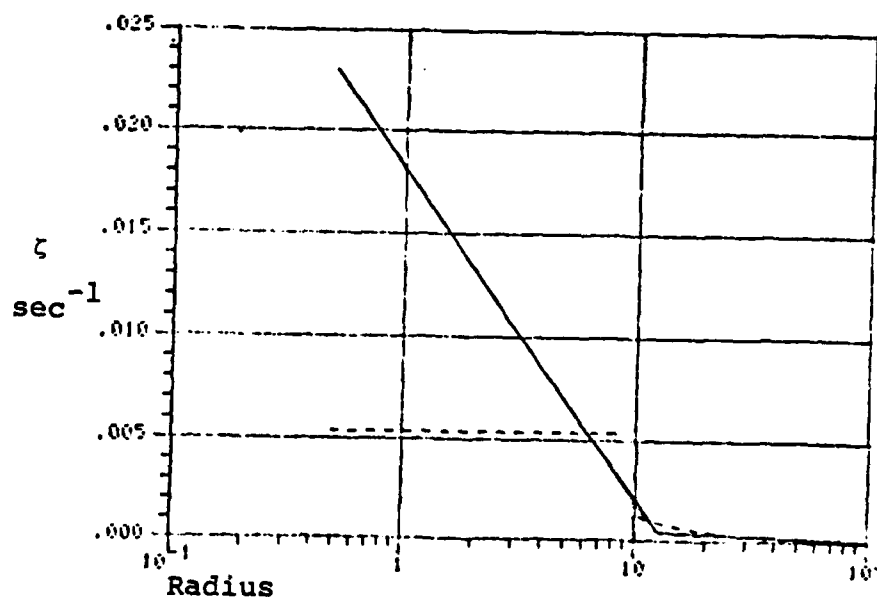
Radius

Figure 6.7b: Vorticity profile for Daisy,
27 August, 1958.
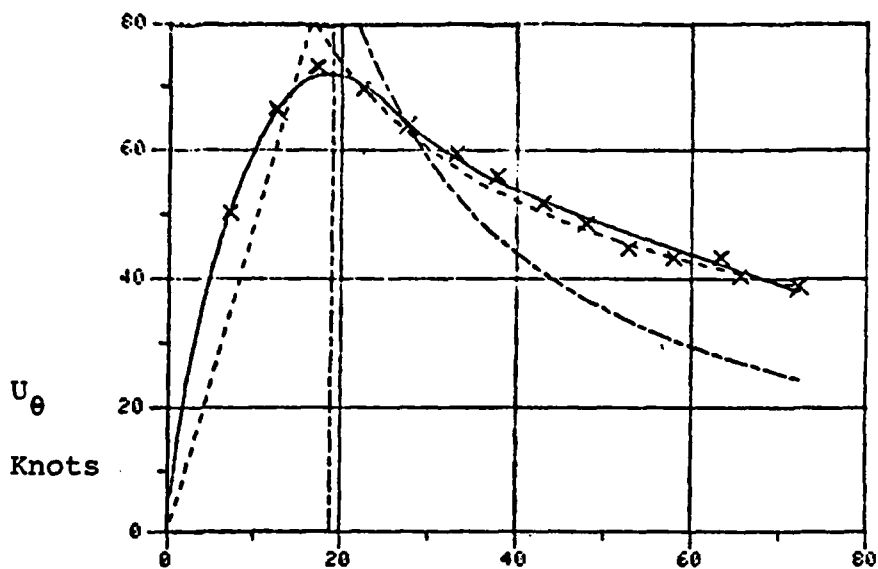
Figure 6.8a: Hurricane Daisy, 28 August, 1958, tangential velocity profile. Key as in 6.1. (5)
RMS=1.18, RMSL=2.888, RMSK=15.98
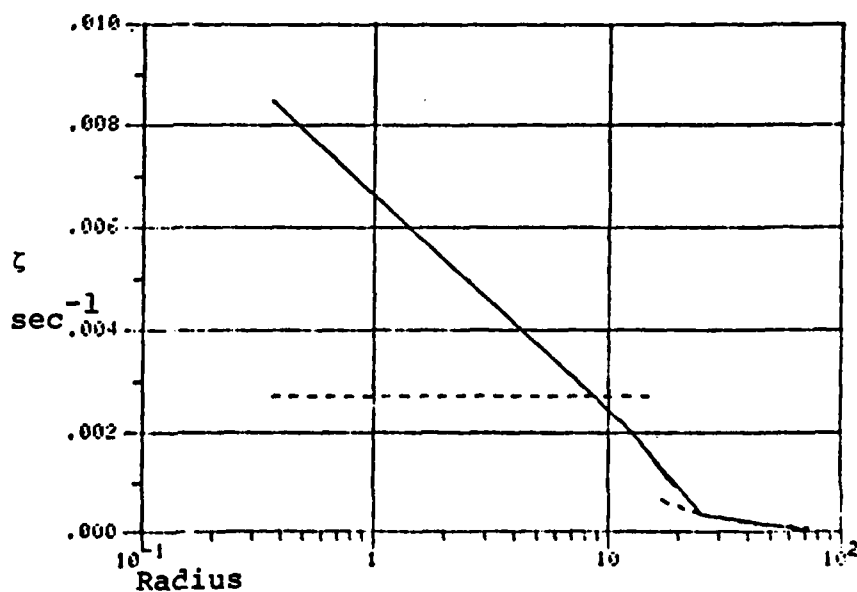
Figure 6.8b: Vorticity profile for Hurricane Daisy, 28 August, 1958.

96
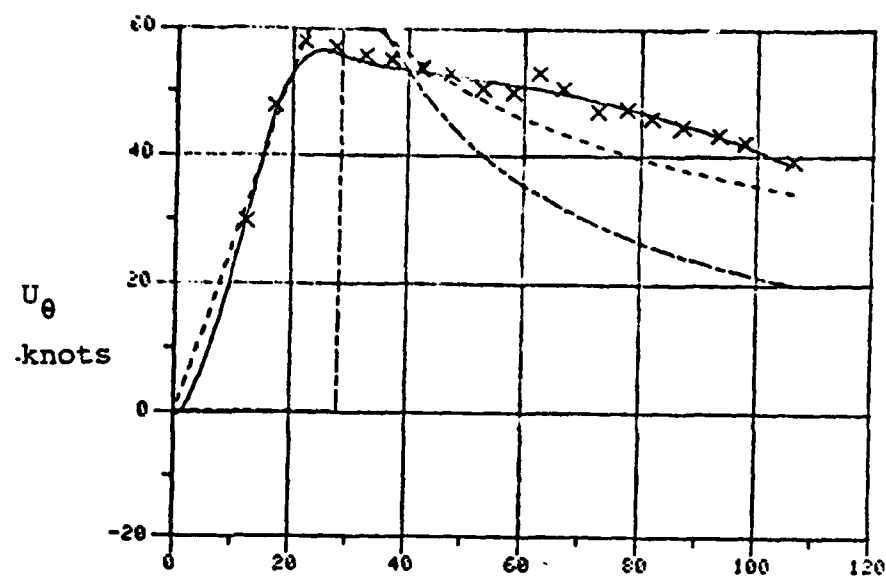
Figure 6.9a: Hurricane Cleo, tangential velocity profile. Key as in 6.1 (5)

RMS=1.403, $MSL=6.01, RMSK=16.03
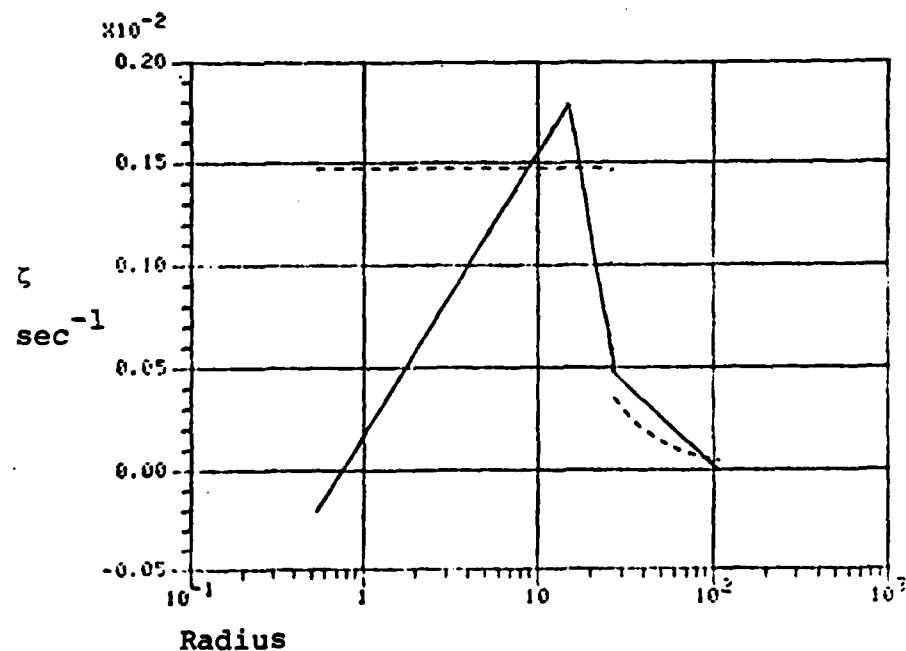
Figure 6.9b; Vorticity profile of Hurricane Cleo,

these models. There are two hurricanes, Daisy and Carrie which
comprise more than one data set. We will deal with the less
troublesome Daisy first, and reserve Carrie for later.

Hurricane Daisy, Figure 6.6, on the 25th of August 1958 at
5500' fits Riehl's outer vortex with a slope of -0.36 rather than
the -0.5 theoretically predicted. The rms for the zero Laplacian
vortex (zLv) of the proposed paradigm with n minus four degrees
of freedom was 1.316 kn. With n minus three degrees of freedom
the Riehl vortex has an rms of 3.645 kn and the Rankine of 10.74
kn. The rms of the zero Laplacian vortex model is small enough
to verge on the suspect, and may be attributed virtually to
measurement error.

Two days later at 13,000' on the 27th, Figure 6.7, with n
minus four degrees of freedom the zLv-rms is only 1.18 kn,
Riehl's rms 2.88 kn and Rankine's 15.98 kn. The boundary between
the inner and outer regime has shifted inward from 20 n. mi. to
12 with a corresponding sharp jump in the slope of the vorticity
distribution reflected in the C_2's and enhanced tangential
velocity maximum. Both the Riehl and Rankine vortex model fits
are calculated with n minus three degrees of freedom apiece. On
the 28th of August, Figure 6.8, the slope of the vorticity in the
inner regime relaxes again with a corresponding decrease in
maximum velocity. Riehl's model does quite well in the outer
vortex but loses considerable ground in the inner vortex
resulting in an almost 3 to 1 lead in rms for the zLv with n-5
degrees of freedom. The Rankine model again runs a poor third
with an rms of 12.86 kn.

Hurricanes Cleo, Helene, Donna and Hannah (Figures 6.9, 6.10,
6.11, 6.12) (Riehl, 1963)

These four are grouped together because they are three part
(mature) vortices with a fixed lower bound for the vorticity of
the core. All are characterized by a relatively large and

98

negative slope to the outer vorticity distribution compared to the positive slope in the boundary layer vortices. Cleo, Figure 6.9, gave Riehl the most problems in this group. The data between 20 and 70 n. mi. were best fit with a -0.2 slope rather than a -0.5 slope. This is reflected in the overall rms for Riehl of 6.01 kn and the relatively steep slope for the vorticity in the outer regime. As usual, the Rankine rms is poorest at 16.03 kn. The zlv-rms ranges from 1.403 to 2.412 kn which may be attributed both to instrument error and analysis uncertainty.

Hurricanes Helene, Figure 6.10, and Donna, Figure 6.11, are distinguished by having outliers skewered by the zLv. In Riehl's original fit the outliers did not fare quite so well. The zLv-rms is 2.412 kn for Helene reflecting that the data is a composit from missions at three low and mid-tropospheric pressure altitudes, Hurricane Donna, taken at 8200 feet has a zLv-rms of 2.125 kn, whereas the Riehl model has 5.01 kn as an rms. Like Helene, Donna's zLv skewers the outlier and has a pronounced negative slope in the outer regime vorticity.

Hurricane Hannah, Figure 6.12, of 20 October, 1959 completes this group. Its zLv-rms is 1.544 kn compared to Riehl's 4.02 and the Rankine 12.88. As with the others the outer vortex has a pronounced negative slope in the vorticity. In summary these four hurricanes are classic examples of the mature vortex with similar vorticity fields but substantially different velocity fields. Donna and Cleo display a change in curvature in the velocity field in the outer vortex. Cleo gave the Riehl model the most trouble. The velocity fields in the outer regimes of the four hurricanes varies from remaining nearly at maximum wind speed for Cleo and Hannah to falling off rapidly as in hurricanes Helene and Donna. The Rankine vortex has an rms between 12.88 and 16.03 kn for this group. The zLv rms ranges from 1.403 to 2.412 kn, an error which may be attributed to instrument error and analysis uncertainty.
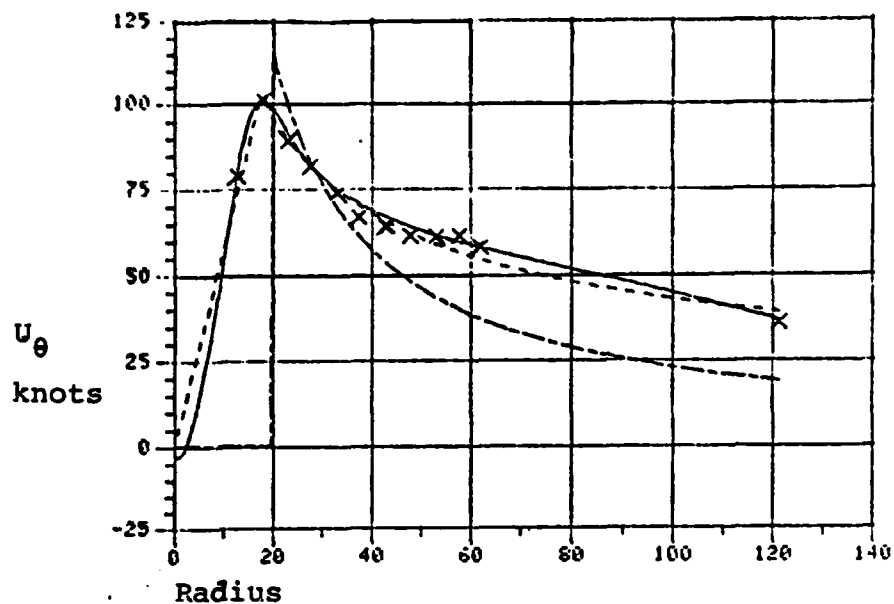
Figure 6.10a: Hurricane Helene tangential velocity profile. Key as in 6.1 (5)
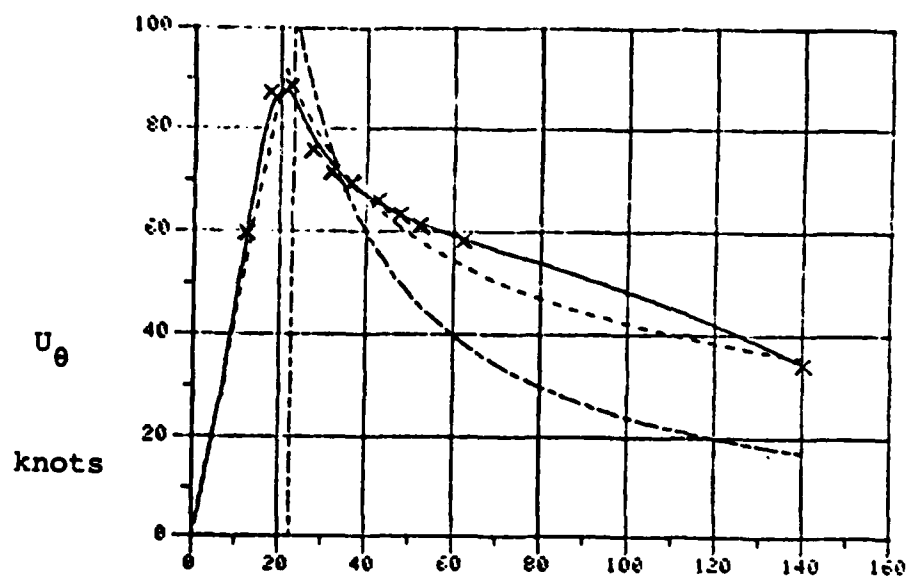RMS=2.412, RMSL=3.349,RMSK=14.99
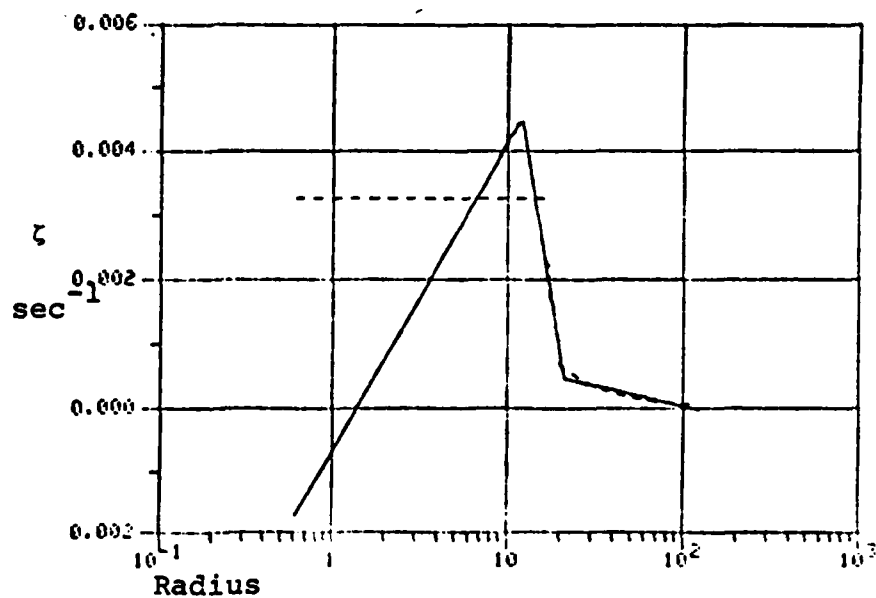
Figure 6.10b: Vorticity profile for Hurricane Helene.

Radius→ n. mi.
Figure 6.11a: Hurricane Donna tangential
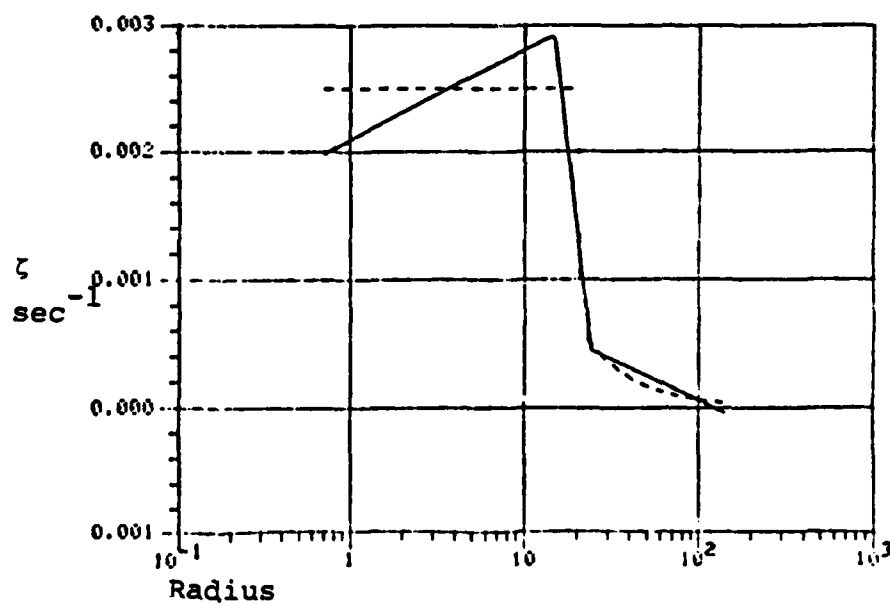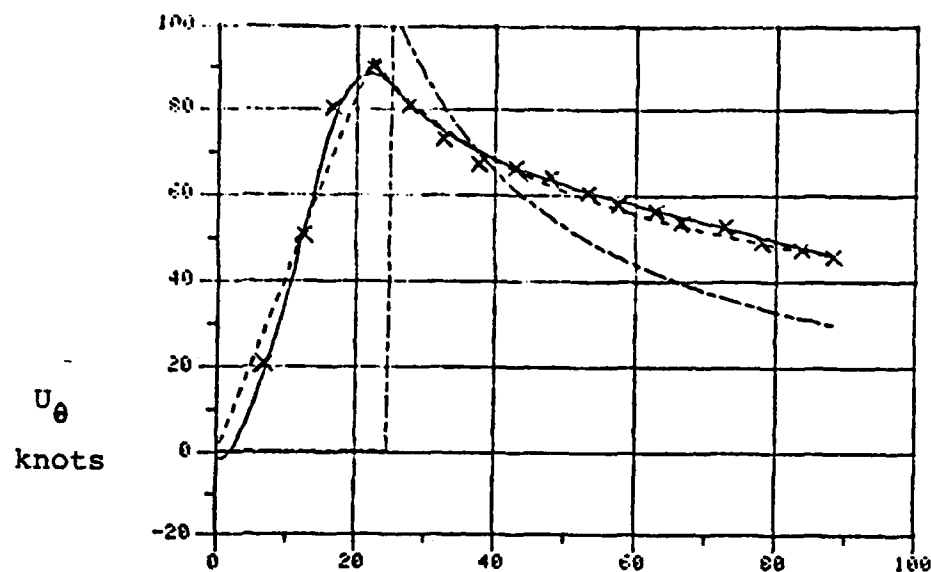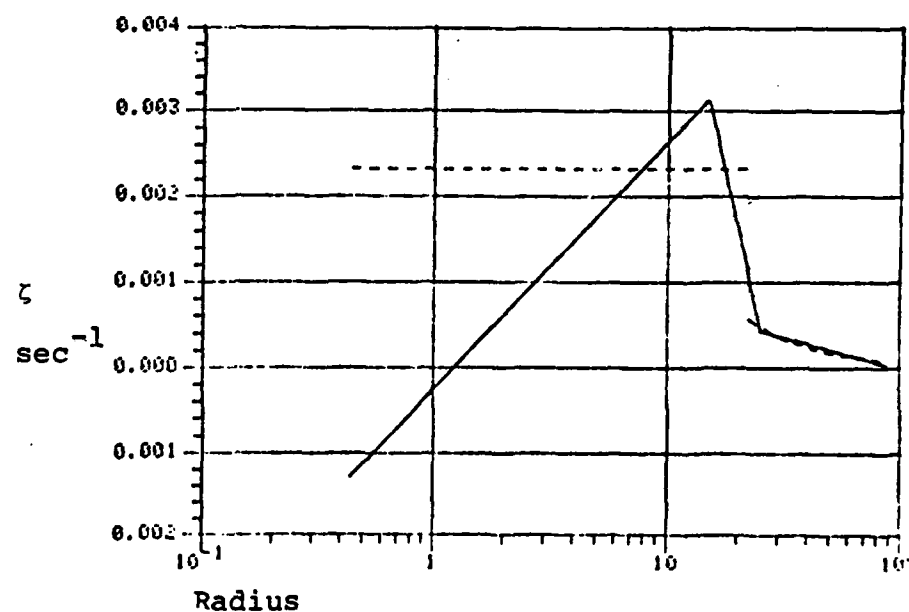velocity profile. Key as in 6.1 (5)
RMS=2.125, RMSL=5.010, RMSK=14.29

Radius

Figure 6.11b: Vorticity profile for
hurricane Donna.

Radius→ n. mi.

Figure 6.12a: Hurricane Hannah tangential velocity profile. Key as in 6.1. (5)
RMS=1.544, RMSL=4.020, RMSK=12.88

Radius

Figure 6.12b: Vorticity profile for Hurricane Hannah.

Hurricane Carrie (Figures 6.13, 6.14) (Riehl, 1963)

Hurricane Carrie: 15 September, 1957, at 14,200 feet, Figure 6.13. 17 September 1957 at 11,000 feet, Figure 6.14.

This data set is of special interest for several reasons. On 15 September, Carrie demonstrates two velocity maxima with a 3.64 kn root mean square error for the zLv. The zLv gives no indication of picking up the dual maxima, although it can and does in other cases, e.g., the stellar velocities in M31. The reason for this may be that as Riehl says "The B-47 data are rather weak and do not cover the hurricane well." (Riehl, 1953).

The sinusoidal variation may be attributable to contributions to the velocity field from the spiral asymmetries in the vorticity field. The poor coverage precludes these variations from being subjected to azimuthal averaging since, presumably, all of the clover leafs were not completed, accounting for the weak B-47 data. The zLv is still better than Riehl's model by 2:1 and the Rankine model by 4:1 with a rms of 8.25 and 18.27 kn apiece.

This error diminishes somewhat over two days for all of the models. The zLv rms is reduced to 2.593 kn, Riehl's to 4.2 and Rankine's to 7.144 kn.

Both days are well represented by a three part vortex similar to the structure found in the group of four comprised of Cleo, Helene, Donna and Hannah. The difference is in the migration of the regime boundaries outward over the period two days with a concurrent disappearance of the inner velocity maximum. The vorticity slope in the outer regime is still strong and negative indicating a healthy creation of negative divergence by the advective term in the divergence equation.* At the maximum wind, this term is -2×10^{-2} sec^{-2}. This value

---

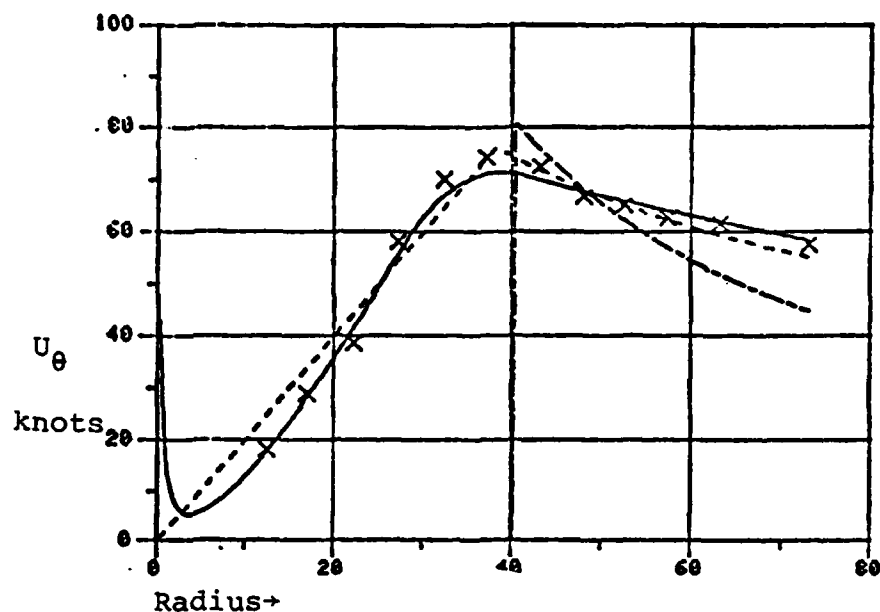*This term is given by $U_\theta \frac{\partial \zeta}{\partial r} = 2\dot{\theta}C_2$

Figure 6.13a: Hurricane Carrie, 15 Sept.,
1957 tangential wind profile. Key as
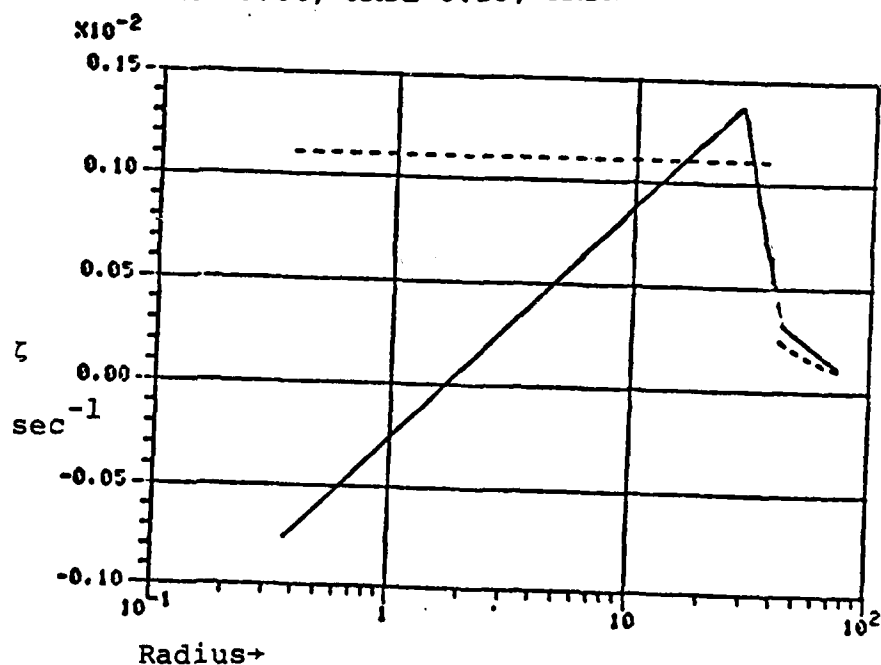in 6.1. (6)

RMS=3.64, RMSL=8.25, RMSK=18.27

Figure 6.13b: Vorticity profile for
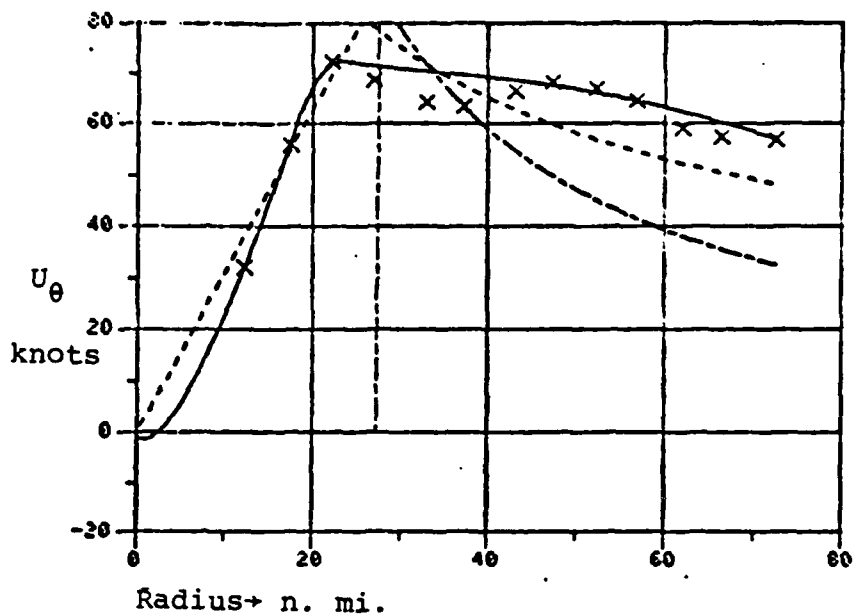Hurricane Carrie, 15 Sept.,
1957.

Radius→ n. mi.

Figure 6.14a: Hurricane Carrie, 17 Sept.,
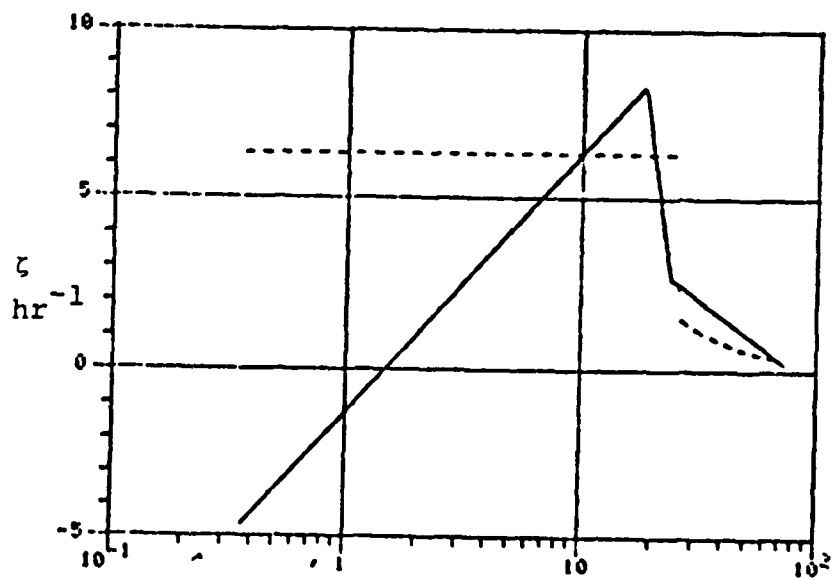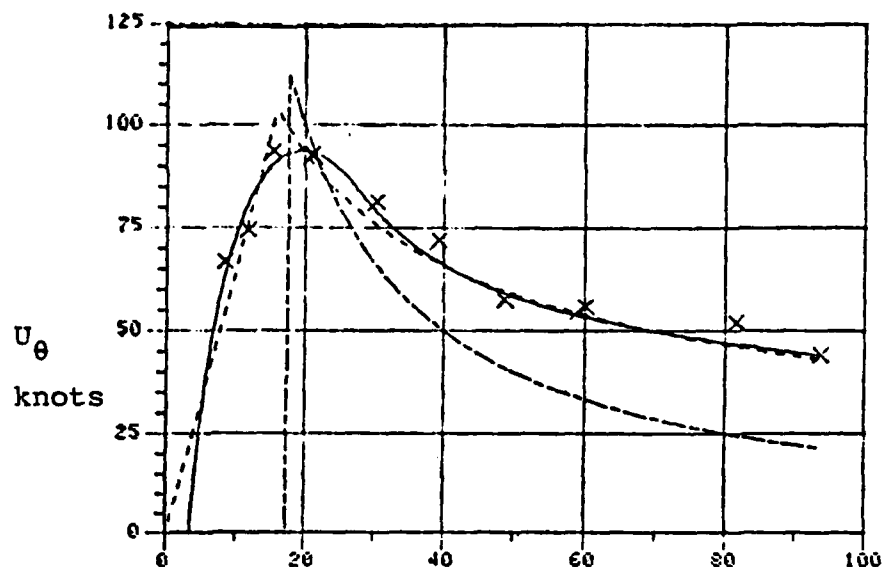1957 tangential wind profile.Key as in 6.1.
(5)

RMS=2.593, RMSL=4.2, RMSK=7.144

Radius→

Figure 6.14b: Vorticity profile for
Carrie, 17 Sept.,1957.

reduces to $-6. \times 10^{-4}$ sec^{-2} in the outermost regime. The creation of divergence in the eye is 3×10^{-3} sec^{-2} at 18 n mi.

Hurricane Camille (Figures 6.15, 6.16) (Bradbury, 1971)

Departing for the moment from the data of the NHRL clover leafs we now turn to the movement of cb's in hurricane Camille analyzed by Bradbury(1971). Figure 6.15. With n minus four degrees of freedom this hurricane had a zLv-rms of 4.735 kn, Riehl's of 6.737 kn and the Rankine at 20.56 kn. It would be difficult to obtain movement of a cb from PPI's with less error that 5 kn, so that the error may be attributed predominantly to instrument or measurement error. Moreover, the cb's need not be of uniform height so that as a measure of the vertically integrated momentum field the vertical integration limits may introduce error by their variation.

This is universally true for all of the vortices. A greater error in measurement, produces a greater rms; a more accurate measurement provides more fidelity to a truly azimuthally averaged state.

Figure 6.15a: Hurricane Camille tangential velocity profile. Key as in 6.1.(4)
RMS=4.735, RMSL=6.737, RMSK=20.56

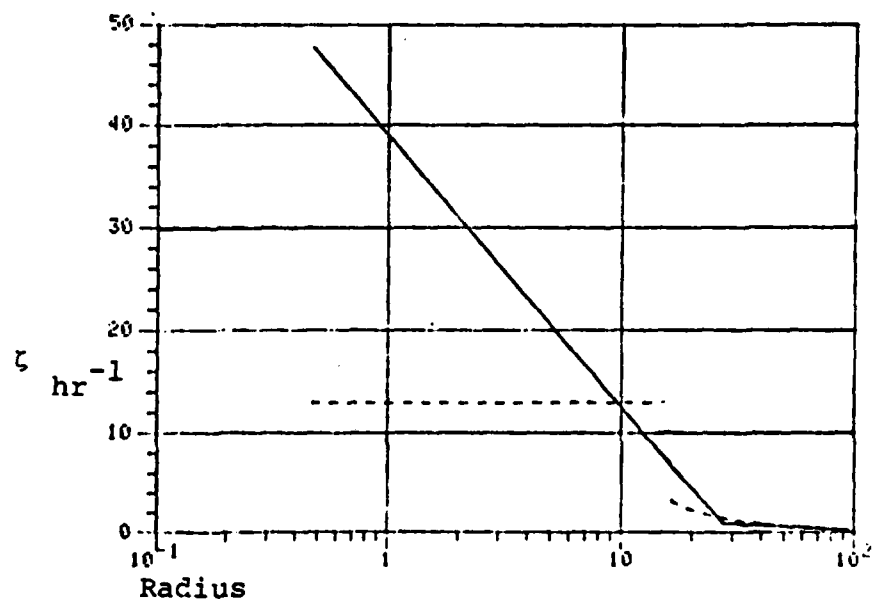Figure 6.15b: Vorticity profile for Hurricane Camille.

Figure 6.16 a

BILOXI KEESLER AFB
PRESSURE READINGS IN HURRICANE CAMILLE

Figure 6.16b
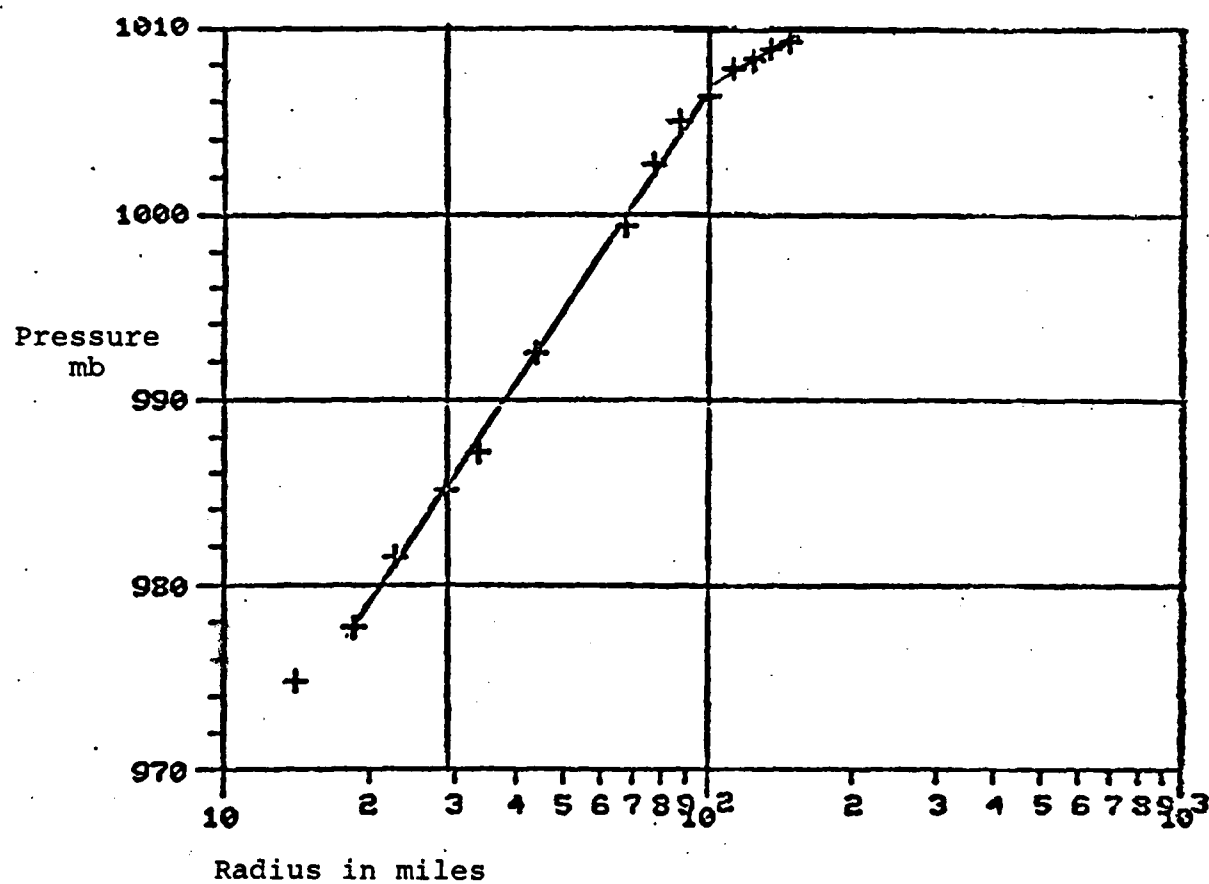
BAROGRAM GULFPORT
  PRESSURE READINGS OF HURRICANE CAMILLE

Figure 6.16c
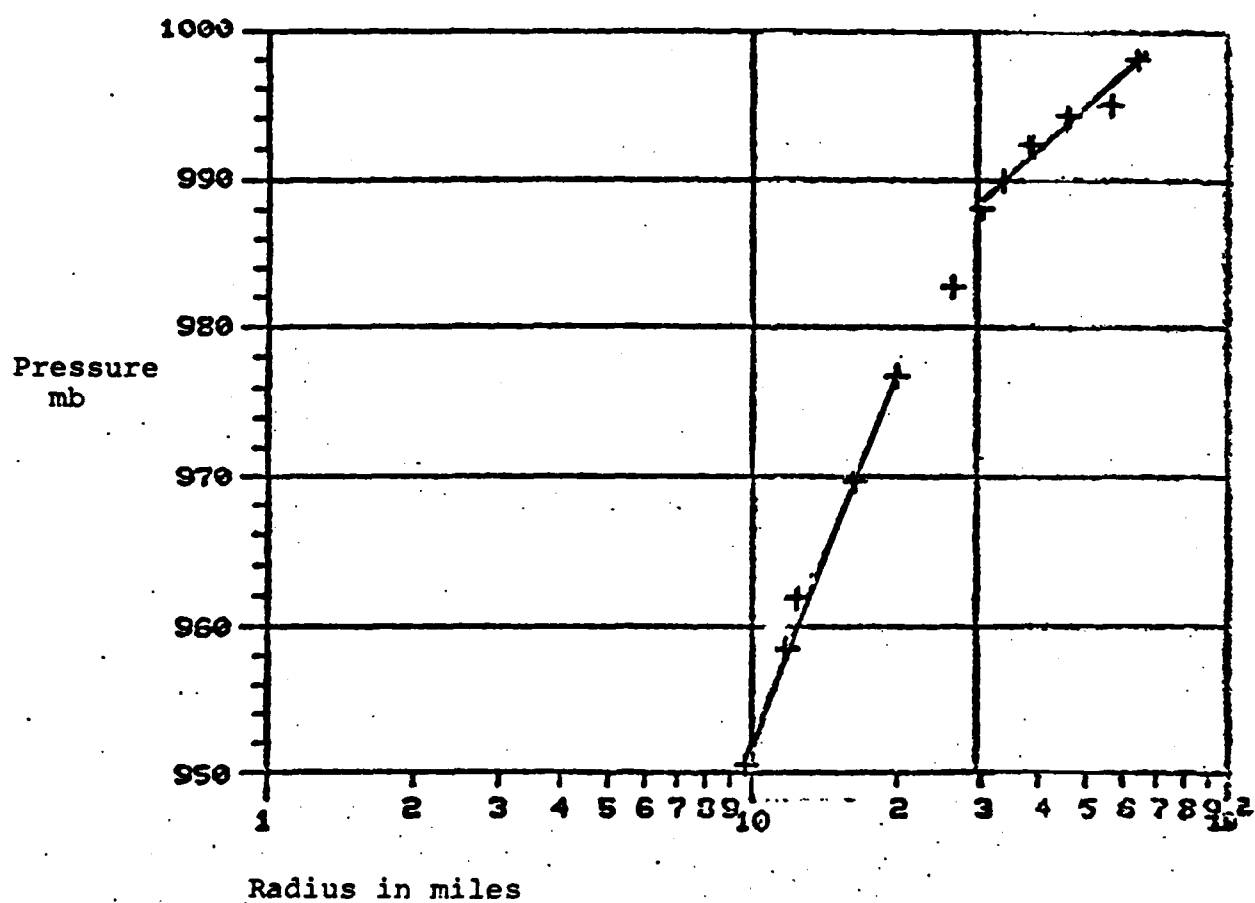MISS TEST FAC WEATHER STATION
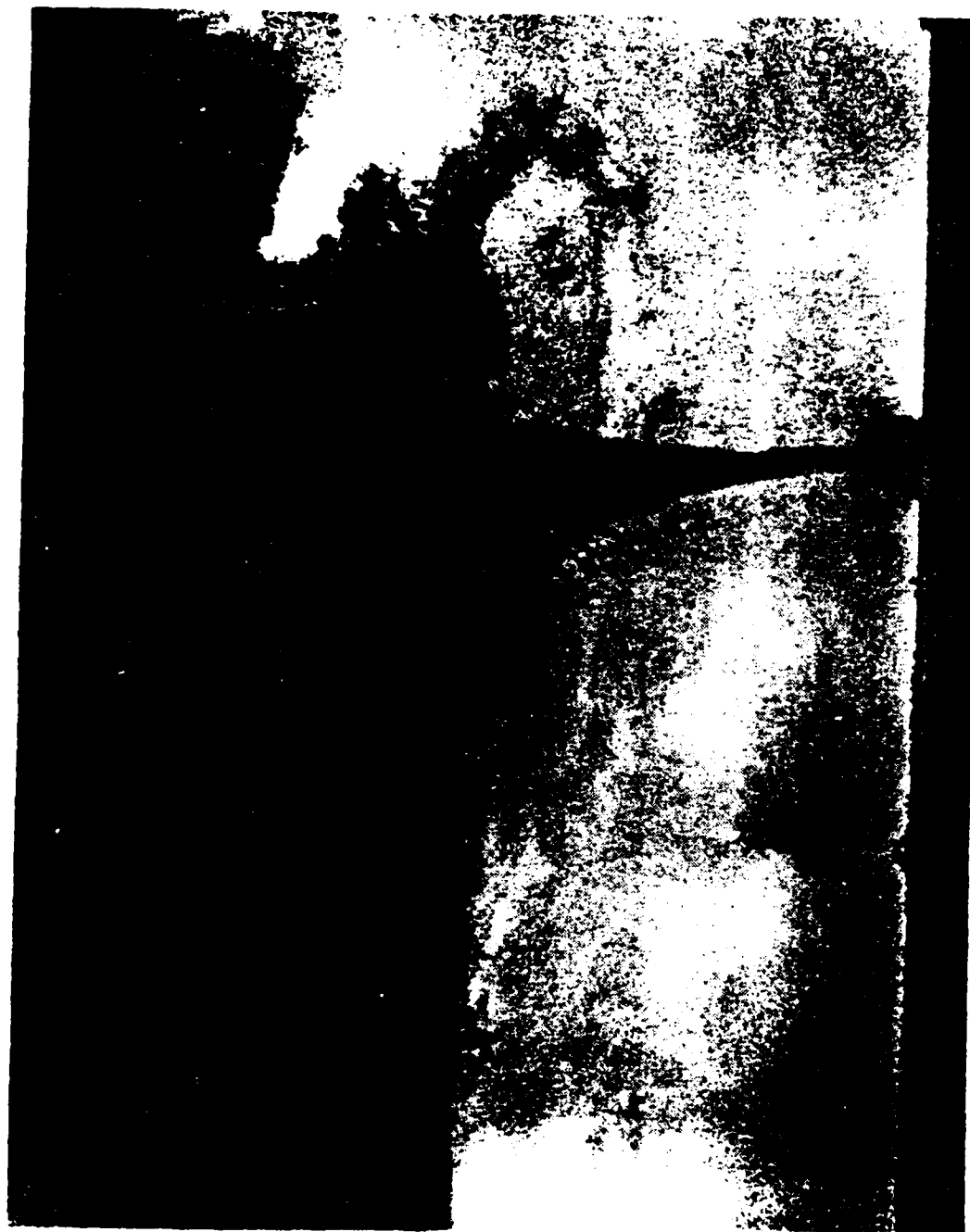PRESSURE READINGS OF HURRICANE CAMILLE



Pressure mb

Radius in miles

Fig. 6.17 Tornado, photographed near Dallas, Texas, on April 2, 1957. (Photo: Bill Burkett)

The logarithmic distribution of pressure in the vortex model has a corresponding value in pressure distribution measurements of Camille shown in Figures 6-16a, b and c. Each of these figures demonstrates a pressure distribution piecewise linear in the logarithm of the radius. Figures 6.16a and 6.16c show a break at about 28 n. mi which also appears in Figure 6.15 in the vorticity distribution. The log distribution is compatible with the funnel shape of tornadoes Figure 6.17 and waterspouts (and draining bathtubs). In bath tubs standing spiral waves on the surface of the water may occur. This indicates that measurements of such waves may be taken in the laboratory, even as measurements of the wind were taken in a Dines vortex cage. As in the case of the latter, such measurements would provide information to establish conformity with the third law. All of these laws may be checked or simulated in the hurricane to establish either their presence or compatibility with Newton's laws.

Andromeda Nebula in M31 (Figure 6.1€) (Rubin and Ford, 1970)

This data set is a radical departure (Figure 6.18) from the data of atmospheric vortices. There are two distinct velocity maxima separated by a minimum. The data are not azimuthally averaged, coming from both the NE and SW quadrants of the galaxy. There are data from the separate emission lines, N_{II}, and H_α, and there is an inherent error of 10 km sec^{-1}. The three part vortex model fits this data with an rms of 26.7 km sec^{-1}. The inner minimum is not captured well possibly due to the scatter in the other parts of the vortex attributable to failure to azimuthally average. It should be pointed out here that one basic code was used to analyze all of the vortex data, and that the code for the double vortex produced in M31 is identical to the code for the Dallas tornado, logical
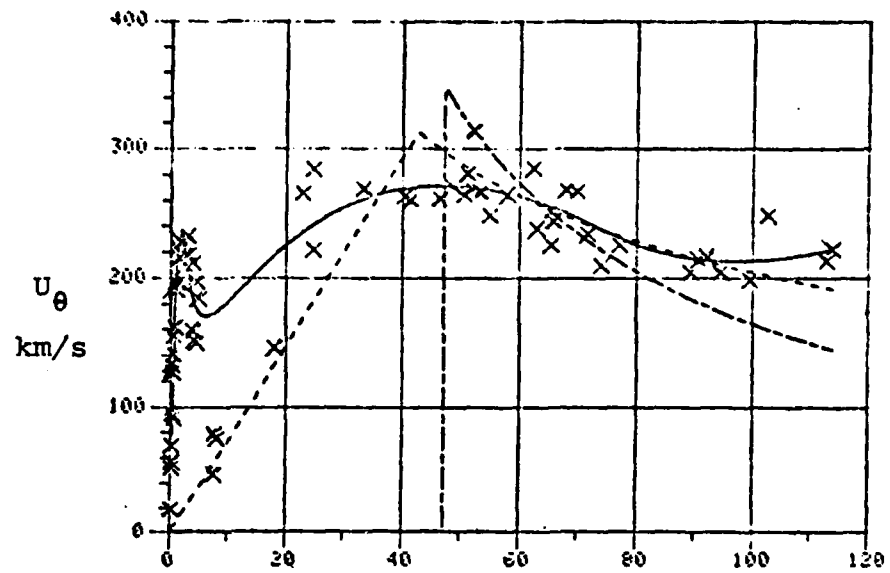
Radius→ kpc
Figure 6.18a: Stellar velocities in M31.
Tangential velocity profile. Key as in
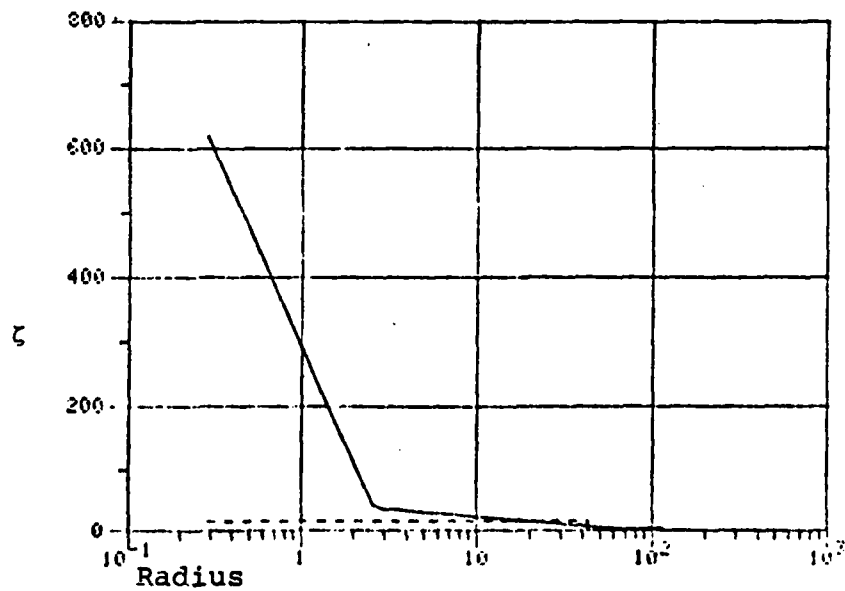6.1. (6)

RMS=26.7

Figure 6.18b; Vorticity profile of
M31 in Andromeda.

113

paths and all. The changes for the other vortex models are
really contingent on the absence or presence of data.

Conclusion

In this chapter we have examined the application of part of
the first law proposed as part of the new paradigm. As Kuhn
says, (p. 46) "A new theory is always announced together with
applications to some concrete range of natural phenomena, without
them it would not be even a candidate for acceptance."
Applications of the theory of piecewise, continuous vorticity
linear in the logarithm of the radius is another way of
expressing the azimuthally averaged part of the first law, i.e.

$$\frac{1}{r^2} \frac{\partial^2}{\partial \ln r^2} \zeta = 0, \infty \qquad (6.5)$$

The data was analyzed for the zero Laplacian vortex models, and
the competing Riehl and Rankine models. In some cases the Riehl
model (hurricanes) was superior to the Rankine model. In other
non hurricane cases (with the exception of M31) the Rankine was
superior to the Riehl model. In no case did either of these
models show superior fit to the zLv. No case was unexplainable
by the zLv. Riehl's model failed for fully one third of the
cases he selected, hurricanes Cleo, Daisy - 25 August and Carrie
- 15 September. Riehl's model failed for all other non hurricane
cases as well. On the other hand, where the Riehl vortex model
did well the Rankine vortex failed even worse than the Riehl
vortex in non hurricane models. There would be little
justification for utilizing the Rankine vortex to simulate a
hurricane's wind field.

The zLv, However, operates successfully in all cases and
under the severest of restrictions. This is true despite the
fact that the zLv is extraordinarily sensitive to boundary
conditions. The slightest displacement of either regime boundary
or value produces wild variations in the velocity profile. The

114

major term in the velocity profile for both the inner and outer regimes in the mature vortex is one comprised entirely of boundary conditions shared with a regime interior to it. These values become incorporated in the hyperbolic terms in the velocity profiles, the C_3's. In the four hurricanes fit by the mature vortex, the wide variation in the velocity profile arises out of minor displacements of the regime values and boundaries, even though the vorticity distributions are remarkably similar.

The velocity maxima are directly related to the slopes of the vorticity segments. The slightest deviation in any of the above also assures the wildest of errors in the velocity profiles. Both Riehl and Rankine's model suffer from zero order discontinuities in the vorticity field producing first order discontinuities in the velocity field. This zero order discontinuity decouples one vortex segment from the another dynamically at a point where the critical wind maximum is presented. This leaves us two vortex models with wind maxima of dubious dynamic validity. The Rankine maximum is universally too high for the data, except for the boundary layer tornado, and the Riehl maxima are too low for non-hurricane cases. Riehl's model is based on bulk aerodynamic considerations of the surface wind field. Rankine's is a combined spiral vortex model with dynamic inconsistencies (Nicholson, 1972) making its application to actual vortices difficult. The zLv gives promise of dynamic insights. The divergence equation

$$\frac{\partial \delta}{\partial t} = -\underset{\sim}{k} \cdot \underset{\sim}{U} \times \nabla_2 \zeta + \ldots + \nu \nabla_2^2 \delta \tag{6.6}$$

indicates that for a positive vorticity gradient divergence is created. For a negative vorticity gradient convergence is created. The former obtains in the core regimes of the four hurricanes and in three of the four boundary layer vortices. Divergence is further created in the outer part of the boundary layer vortices. In the case of the waterspout and low level

tornadoes the convergence sandwich between two rings of divergence is appropriate for the dual toroidal circulation ascribed by some authors to severe low level vortices.

Since the radial velocity may be constructed in the same way as the tangential, from a piecewise, continuous distribution of divergence, linear in the logarithm of the radius, inspection of the divergence and vorticity equations indicates that specification of the distribution of tangential, radial (and from mass conservation the vertical) velocity field, and the fields of divergence, vorticity and pressure goes a long way toward determining the distribution of the terms in the divergence and vorticity equations given below

$$
\begin{matrix} & (1) & (2) & (3) & (4) \end{matrix}
$$

$$
\frac{\partial \delta}{\partial t} = -\underset{\sim}{k} \cdot \underset{\sim}{U} \times \nabla_2 \zeta - w \frac{\partial \delta}{\partial z} - \nabla \alpha \cdot \nabla p - \nabla^2 (\underset{\sim}{U} \cdot \underset{\sim}{U}/2)
$$

$$
\begin{matrix} (5) & (6) & (7) & (8) \end{matrix}
$$

$$
+ \zeta(\zeta + f) - \nabla w \cdot \frac{\partial \underset{\sim}{U}}{\partial z} - \alpha \nabla^2 p + \frac{\partial}{\partial z} \nu_z \frac{\partial \delta}{\partial z}
$$

$$
\begin{matrix} (9) \end{matrix}
$$

$$
+ \nu \nabla^2 \delta \qquad \text{[Divergence Equation]}
$$

and

$$
\frac{\partial \zeta}{\partial t} = - \underset{\sim}{U} \cdot \nabla_2 \zeta - w \frac{\partial \zeta}{\partial z} - \underset{\sim}{k} \cdot \nabla_2 \alpha \times \nabla p - \delta \zeta
$$

$$
- \underset{\sim}{k} \cdot \nabla w \times \frac{\partial \underset{\sim}{U}}{\partial z} + \frac{\partial}{\partial z} \nu_z \frac{\partial \zeta}{\partial z} + \nu \nabla_2^2 \zeta \qquad \text{[Vorticity equation]}
$$

where $\underset{\sim}{U}$ is lateral velocity δ, divergence, ζ, vorticity; w, vertical velocity; α, specific volume; p, pressure; ν, eddy viscosity and f, Coriolis parameter.

With the exception of the terms containing specific volume, α, all of the other terms are comprised of values of velocity $\underset{\sim}{U}$ and their horizontal divergence (δ), vertical component vorticity (ζ), pressure (p), and vertical velocity w derivable from the conservation of mass. The new laws do not

116

usurp Newton's laws. They merely help govern the distribution of the terms in Newton's Laws. Since the laws specify the various fields as solutions to Laplace's equation, the fields themselves are expressible in terms of boundary conditions.

Finally, it is important to note that the only restriction on the zLv models is the availability of data. None of the models fits the data so poorly that the rms may not be attributed to either instrument error or uncertainty from analysis technique (e.g. Dallas tornado), or limitations in obtaining azimuthally averaged values for asymmetric phenomena (e.g. M31).

The range and kind of data is vast, utilizing anemometers and velometers, photogrammetry, spectroscopy, aircraft sorties and radar. The data availability is limited only by the ingenuity of the individual investigator, and in the case of the Dallas tornado, the courage of the observor. Not only are the fits the result of piecewise continuous vorticity fields, but the kinds of models which fit the kinds of data share common characteristics, e.g., boundary layer vortices, the four hurricanes, hurricane Carrie, etc..

The choice of an extra core or inner regime is based on data availability, certitude of vortex center and data quality. The poorer the data, the more degrees of freedom needed to get a satisfactory fit. Hence the tornado data, ingenious but crude in comparison to the hurricane data, loses six degrees of freedom and is fit by an even vortex. The center of the tornado is, at best, an educated guess. The choice of a lower boundary in the core is possible due to a large number of data points, but necessary because of measurement uncertainty, non synoptic observations and uncertainty concerning the center of the tornado. The lack of azimuthal averaging or smoothing in M31 requires similar procedures.

Theoretical Difficulties

Mathematically speaking, the azimuthally averaged vorticity, ζ , is identical to the shearing deformation, β . The azimuthal component is summed rather than subtracted from the radial component

$$\zeta = \frac{1}{r} \frac{\partial}{\partial r} rU_\theta - \frac{1}{r} \frac{\partial}{\partial \theta} U_r; \quad \beta = \frac{1}{r} \frac{\partial}{\partial r} rU_r + \frac{1}{r} \frac{\partial}{\partial \theta} U_r.$$

Johnson (personal communication) has indicated that the azimuthally averaged vorticity distribution may be derived from angular momentum considerations. This is not possible, however, for asymmetric spiral versions of the law. It is possible that in this instance Newton's Laws and the proposed laws overlap, even as Einstein's laws of relativity overlap with Newton's laws for low speeds. The possibility and importance of further overlap and the question of shearing deformation vs. vorticity in an azimuthally averaged vortex remain further parts of the puzzle which those who follow may choose to address.

Further Conclusions

Thus, these data corroborate the model of a piecewise continuous vortex satisfying the symmetric version of the first proposed law. In Chapter VIII Conclusions and Proposals for further research suggestions for corroberation of the asymmetric (spiral) versions of the 2nd law will be advanced.

The following chapter outlines the laws governing the behavior of multiple vortices comprised of distributed fields of divergence and vorticity, the "Interaction" part of "Vortex Structure and Interaction."

CHAPTER VII. TROPICAL CYCLONE MOVEMENT THROUGH LARGE SCALE VORTICITY AND DIVERGENCE BUDGET CONSIDERATIONS

7.1 INTRODUCTION

This treatise has proposed a field theory which incorporates, among other things, five proposed laws of physics and a new branch of spiral mathematics. Although it is beyond the scope of this paper to provide verification of more than the axially symmetric or azimuthally averaged component of the first law (apart from some scanty data supporting the third law), (a subsequent paper will provide evidence for the second law in asymmetric-spiral coordinates), nevertheless, it may prove to be useful to discuss the interrelation of the laws and their placement in the hierarchy of the field theory. The theory is termed "field" for good reason. The first three laws are expressible in terms of Laplace's equation, while the fourth and fifth relate the interaction of vortices as a consequence of their individual field integrity.

Laplace's equation is truly a field equation since the equation specifies that there are neither maxima nor minima in the variable which satisfy the equation, and that this variable's field is entirely determined by values at the boundary. The theory deals with the manner and consequences of multiple fields linking up and the consequences both for vortex structure and interaction.

The laws are given below:

I. $\qquad \nabla_2^2 \zeta = 0, \infty$

II. $\qquad \nabla_2^2 \delta = 0, \infty$

III. $\qquad \nabla_2^2 p = 0, \infty$

IV. $\qquad \Gamma_o = \sum_{i=1}^{n} \Gamma_{s_i}$

119

$$\text{V.} \qquad Q_o = \sum_{i=1}^{n} Q_{s_i}$$

where ζ, δ, and p are vertical component vorticity, horizontal divergence and pressure, respectively and Γ and Q stand for the circulation and sink functions. The subscript 'o' and 's' stand for orbital and spin, respectively and ∇^2_2 is the two dimensional Laplacian. The first three laws specify that the vorticity, divergence and pressure, either satisfy Laplace's equation or that their Laplacians are undefined. The undefined part occurs at the boundary of the field. By L'Hospital's rule the divergence of the gradient of the scalars in question approaches zero as a limit as we approach the field boundary from either field common to the boundary.

By Helmholz's theorem, fluid flow may be divided into rotational and divergent components. The first law states that the limit of the spin per unit area, the vorticity, has no maxima or minima in the field, i.e. satisfies Laplace's equation. This has multiple ramifications which will be treated below. Since the rotational limit has no maxima or minima, it would seem unusual for nature to single out only that part of the flow. Consequently, the limit of the sink function, the divergence, is postulated as having no maxima or minima either, giving the second law. Since Laplace's equation represents the divergence of the gradient of field entities, and the entities in this case represent lateral frictional stresses, then Laws I and II may be considered as saying that the divergence of the tensors represented by the gradients of these stresses operating on annular surfaces is zero. Again, it would be curious if the lateral frictional force operating upon an annular surface providing a sink for kinetic energy (or even a source) were the only lateral component body force operating on an annular surface so that the divergence of the resulting tensor were zero.

120

This leads us to the third law, which sets the Laplacian of pressure to be zero. Thus, part of the pressure gradient force is non divergent, whereas the toroidal acceleration is free to provide work to compensate for the energy lost due to lateral frictional forces derivative from vertical shears.

The Laplacians of vorticity, divergence and pressure appear in the prognostic vorticity and divergence equations. The first three laws may not be derived from either of these equations without making numerous and unjustifiable assumptions regarding the other terms. The incorporation of three new laws into understanding of the field distribution of the other component terms of these equations may prove fruitful since by doing so we obtain partial field solutions for the Navier - Stokes equations.

Thus none of the laws are derivable from one another or even other laws. This is a characteristic of laws of physics. There are no more fundamental entities from which these building blocks of nature may be derived. Their place in the general field theory is a consequence of their interrelation. Laws IV and V arise from consideration of the impact of the first three laws on Stoke's and Green's theorems. Since the component vortices in a group or gyre, as it will be termed in Chapter VII, maintain a certain integrity in conformity with the first three laws, Laws IV and V are the means by which the vortices may satisfy the Stokes' and Green's theorems without violating their structural integrity. The result is application of these theorems in view of the structural integrity of the vortex in order to obtain tangential and radial components of motion around a common center of mass.

Satisfaction of the area integral of vorticity or divergence could be brought about either by an asymmetric mutation of the individual vortices so that they may stay in place and still

satisfy Stokes' and Green's theorems (and coincidentally violate
the first three laws) or they may move in conformity with Laws IV
and V and satisfy both the first three Laws and Stokes' theorem
in IV and Green's in V.

Thus the circulation of a group of vortices about a common
center of mass (orbital circulation) is equal to the sum of the
spin and solid body orbital circulations of each individual
vortex. The radial velocity of the individual vortices may be
obtained in the same manner. These two concepts are further
expanded upon in Chapter VII.

7.1.1 History

The interaction of vortices with their environment and with
other vortices has long been the concern of hurricane
forecasters. As early as 1921 Fujiwhara pointed out the tendency
of two tropical cyclones to rotate one about the other in a
cyclonic fashion but he did not seek either an explanation or a
further application of this phenomenon, later to be called the
"Fujiwhara effect." Riehl (1954) noted the interaction of
subtropical highs with tropical storms but developed the concept
no further. Thus far the only extant non climatological model in
use by the National Hurricane Center is that developed by Sanders
(1968) which is a filtered barotropic model.

7.2 VORTEX INTERACTION

In this series of thought experiments we simulate the
interaction of vortices by application of a three dimensional
mass weighted Stokes' Vorticity Theorem and Green's theorem in
accordance with Laws IV and V.

$$\Gamma_o = \int_{p_o} \int_A (\underset{\sim}{k} \cdot \nabla \times \rho \underset{\sim}{U} \; d \, A \, d \, p) \qquad (7.1)$$

122

where Γ_0 is the orbital or translational circulation, ρJ is
the mass weighted Jacobian in pressure coordinates and A is the
area covered by the region of interest. From Stokes' theorem,
Γ_0 is equal to the sum of all of the circulations within the
volume encompassed by the region A and the pressure surfaces
p and p_0. Thus the translational circulation Γ_t of an
interacting group or gyre is given by the sum of the individual
circulations, or

$$\text{LAW IV} \quad \Gamma_t = \sum_{i=1}^{n} \Gamma_i \; ; \quad \text{LAW V} \quad Q_t = \sum_{i=1}^{n} Q_i^* \qquad (7.2)$$

where Γ_i is the individual circulation of a specific vortex,
and Q_i the individual sink function.

7.2.1 Two Bodied Problem : Anticyclone - Tropical Cyclone

Equation 7.2 for the two bodied interaction of an
anticyclone and tropical cyclone may be set up in the following
manner assuming that each vortex is cylindrical and of the same
vertical extent,

$$\qquad\qquad\qquad\qquad (1) \qquad\quad (2) \qquad\quad (3) \qquad\quad (4)$$

$$\Gamma_t = 2\pi r_t U_t \backsim 2\pi r_A U_A + \pi r_c U_c + \pi r_c^2 U_t/r_t - \pi r_c U_A \qquad (7.3)$$

where the movement of the tropical cyclone is given by the
circulation speed, U_t, and the circulation budget is the sum
for the circulations of the anticyclone, term (1), the
circulation of the tropical cyclone, (2), and the vorticity of
the storm due to this assumed solid body rotation about the

*The essence of Laws IV and V is not that Stokes" or Green's
theorems are satisfied, but that the storms' movement conforms
to these theorems.

123

center of the anticyclone, (3) and term 4 is the bite taken out
of the anticy done by the huricane. The simplifying assumption
that $r_t = r_A$, leads to the solution for the translational speed,
U_t, the speed of the vortex floating in the net circulation to
which it makes a contribution.

$$U_t = U_A(2r_t - r_c) + r_c U_c/(2 r_t - r_c^2/r_t) \qquad (7.4)$$

where U_A is the windspeed at the perimeter of the idealized
anticyclone, r_A, and r_t is the radial distance from the
center of the anticyclone to the cyclone, and r_C is the radius
of the cyclone, and U_C is the wind speed at the perimeter of
the cyclone. For $r_t =$ 500 miles, $r_C =$ 100 miles, $U_C =$ 50
mph and $U_A = -20$ mph, U_t is solved as -13.26 mph. Thus
the cyclone pictured in Figure 7.1 moves slightly slower than 2/3
rds of the speed of the ambient current.

7.2.2 Dual Hurricanes-Fujiwhara Effect

Let us assume identical hurricanes 600 miles apart. The
total area is given by an ellipse with the semiminor axis of 100
miles, the radius of the hurricane and the semimajor axis as 300
miles, half the distance between the storms. The reason for the
ellipse is for computational convenience. This is not too
arbitrary a shape for the group since for a distance over 100
miles from the center of the hurricane the circulation may be
approximated by a constant, independent of distance. Equation
7.2 may be written

$$\Gamma_t = 2\pi \left(\frac{a^2 + b^2}{2} \right)^{1/2} U_t = \pi r_c U_c \qquad (7.5)$$

For $a=100$, $b=300$, $U_c=50$ mph, U_t is solved as 11.18 mph.

124

7.2.3 Hurricane and Large Cyclone

For a large extra-tropical cyclone with the same physical dimensions as the anticyclone, but a wind speed of + 20 mph at the periphery, the solution to (7.4) is + 26.74 mph, the hurricane adding 6.74 mph to its translational velocity instead of subtracting it, to give -13.26 mph.

7.2.4 Dual Anticyclones and A Hurricane

If a hurricane is part of a group in which there are two contiguous anticyclones of equal strength, the hurricane can be expected to follow the cycloidal path of the circulation given in Figure 7.3a. If the whole group is migrating from west to east the path may involve looping, as is illustrated in Figure 7.3b.

If the westernmost anticyclone is significantly weaker than the eastern one such that when considered alone with the hurricane, the net circulation of the two were positive, then the hurricane could be expected to pass between the two of the anticyclones as illustrated in Figure 7.3c. This could occur if the circulation of the lesser anticyclone were not as strong as the circulation of the hurricane. Thus, the magnitudes of the circulations of the vortices would increase going from west to east.

7.2.5 System Tilt With Height

Since the vorticity is mass weighted through a volume the total system may tilt with height. Under these circumstances the hurricane would float in a vertically integrated circulation field, and its path would not correspond neatly to paths considering only surface distributions of the vorticity fields.

7.3 CONCLUSIONS

This model of cyclone movement attempts to investigate tropical cyclone movement in terms of larger scale vorticity considerations of which the tropical cyclone is an integral and contributing part. Obviously far more work must be done in this field, but hopefully this will prove to be an interesting and profitable first step.
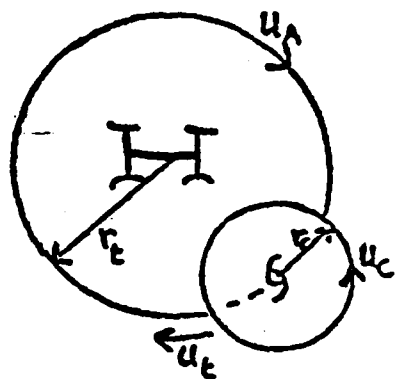
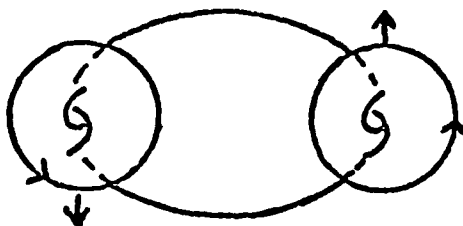Figure 7.1   Plan view of cyclone-anticyclone interaction.

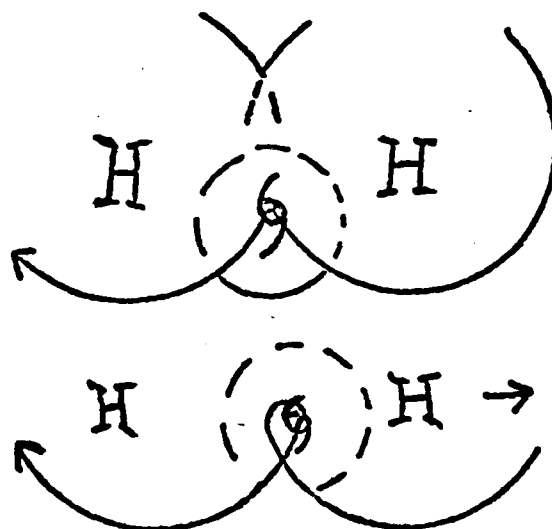Figure 7.2   Plan view for two interacting hurricanes
exhibiting the Fujiwhara effect.

Figure 7.3a,b Upper stationary group illustrating
cycloidal path, lower group translating
illustrating looping.

$$|\Gamma| < |\Gamma| < |\Gamma|$$
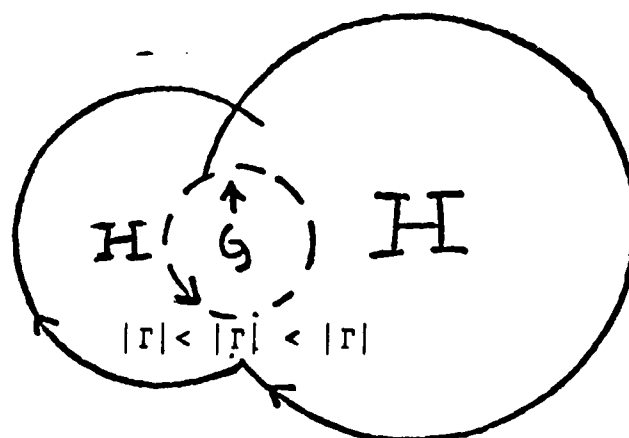
Figure 7.3c.   Plan view of hurricane passing between
two anticyclones of differing circulation
strength.

128

VIII. SUMMARY AND PROPOSALS FOR FURTHER RESEARCH

Summary

In Chapter I we attempted to prepare the reader for an event outside of the ordinary realm of science - the initiation of a scientific revolution - the introduction of a new paradigm incorporating theory, laws and application and inspired by the instrumentation of the space age, the meteorological spin-scan camera of the geosynchronous satellite. In Chapter II three new laws governing vortex structure were presented along with various physical understandings of the first law, its relation to lateral friction, torque and circulation or angular momentum. The second and third laws were added with little further physical explanation.

Chapter III discussed the mathematical application of the proposed laws. The paradox of band movement in extratropical storms, indicative of the flow vs. bands in hurricanes, stationary in defiance of the flow, was examined. The evolution of the concept of piecewise structures in the vortex and a second law governing divergence with solutions in a new coordinate system(s) rounded out application of the laws. The issue of the nature and kinds of logarithmic spirals was next addressed. In Chapter IV steps were then taken relating these spirals to solutions of the laws in the new spiral coordinate systems. The new coordinate systems were examined in order to achieve a better comprehension of the concept of "spiral space."

Examination of the mathematical transformations of shortening, scaling, rotation and stretching followed with application to five* new spiral coordinate systems separable in

---

*Plus a sixth non Euclidean system. There are probably more, but they will be investigated more fully in other papers.

Laplace's, Schroedinger's and the spatial wave equation. These five are more general cases of five extant systems mentioned by Morse and Feschbach detailed in Appendix A. The features of the five new systems with examples of spiral phenomena were looked at next.

Chapter V presents the various combinations of the azimuthally averaged tangential velocity based on a piecewise continuous vorticity field linear in the logarithm of the radius. Also radial velocities corresponding to a piecewise continuous divergence field were presented. The latter clearly provide an outflow component in the eye of the "mature vortex model." Vortices with double maxima, eyes and timelines as log spirals were presented. The simplest model explains the behavior of a marker of Pream in a stirred coffee cup.

In Chapter VI sixteen examples of vortex data covering 21 orders of magnitude are examined and seen to fit the model to within instrument or measurement error. Ramifications of the satisfaction of these laws for Newton's laws are examined at the end of Chapter VI. Chapter VII deals with the volume integration of the sink and circulation values of multiple vortices, and their motions about a common center of mass. Explanations are provided for the Fujiwhara effect, cycloidal paths, recurvature, abrupt path changes and reversal of movement of tropical storms interacting with one another and other vortices.

Appendix A details the expansion of five non-Cartesian coordinate systems separable in Laplace's equation into more general spiral coordinate systems, also separable in three dimensions in Laplace's, Schroedinger's and the spatial wave equations. These five systems include two for application to cylindrical phenomena and two for phenomena on a sphere. The fifth, while of interest, escapes direct meteorological application.

Appendix B has presented a simple two part model of the axially symmetric general circulation. This model incorporates

130

both the zonal wind and meridional transport due to spiral asymmetries superimposed on the zonal vorticity distribution. In this model the Laplacian of absolute vorticity is taken to be zero. As we have seen, the atmosphere at rest also has a vorticity whose Laplacian is zero. This model is applicable to the inner planets and displays Polar easterlies, prevailing westerlies and tropical trades. Enhancement of the cold polar dome of air results in mutations of the wind pattern above with ramifications for ice age behavior. Examination of the data of Kornfield (1969) indicates spherical log spiral asymmetries in the low level divergence field resulting in straight cloud bands flowing from the pole to the equator in Mercator projections, and ordinary log spiral bands in stereographic projections.

Appendix C provides proposed explanations for the general circulation of the outer planets, particularly, Jupiter and Saturn. Full verification awaits analysis of the Voyager data in the context of the field theory as outlined in Appendix C. Appendix C raises important questions concerning the possibility of terrestrial circulation becoming more Jovian, with bands other than the Intertropical Convergence Zone appearing as zonal harmonics.

Proposals For Further Work

The new paradigm is sufficiently open ended that all sorts of new problems may be considered. Not least of these is whether the remaining seven parts of the proposed laws are satisfied and in what instances applicable. Work is being done to analyse IR returns from cloud bands in hurricanes to establish conformity to the spiral component of the second law. Preliminary results are given in Appendix F. This law requires that the bands exhibit logarithmic spiral spacing simultaneously with amplitudes linear in space with extent determined by wave number. Appendix F shows promising preliminary results where this is precisely the case.

131

Following is a partial list of derivative projects under investigation. Sections a, b, and c are proposed numerical model changes.

(a)   Spiral Asymmetries: Asymmetric heating and cooling implicit in the spiral bands of hurricanes allows the solenoidal term in the vorticity equation to be non zero. Incorporation of spiral features of divergence, vorticity and pressure are necessary for realistic simulation of highly asymmetric flow and mass distribution fields.

(b)   Implicit Nesting: Considerations of spiral features and symmetric satisfaction of Laplace's equation focuses attention on the logarithmic features of both the Laplacian and the gradient. Finite difference schemes may make use of logarithmic spacing. This focuses attention on the closely packed features of the eye and cloud wall without missing the overall features of the outer cloud bands. The expanded gridding in the outer vortex may be made more easily to fit into a synoptic scale grid.

(c)   Forecast of regime formation: The velocity profile in hurricanes is particularly sensitive to the value and placement of vorticity. Even more fundamental is the question of the cause of the formation of regimes in the mature vortex. Dose the mature vortex progress through stages, from simple to complex and then mature? If so, what are the roles of enstrophy, and the bulk aerodynamic Richardson number. Can their evolution by used to predict the formation of the inner and core regimes of a hurricane, and possible tornado formation?

(d)   Application to the outer planets: Both the general circulation and the Great Red Spot of Jupiter are considered in Appendix C, which is itself a logical outgrowth of Appendix B, where the general ciruclation of the inner planets is considered. The question of not only ice age circulation but of a possible Jovian type circulation needs to be addressed. Is the Inter Tropical Convergence Zone itself a manifestation of Jovian circulation?

(e)   Application to determination of the wind fields of

132

extratropical storms: The data already present in observing
extratropical storms from satellites needs to be exploited.
The band spacing and winding rate of the frontal bands contribute
information which may be useful in obtaining a vertically integ-
rated wind field in the lower troposphere, including the vertical
as well as lateral wind field. This subject is addressed more
thoroughly in Appendix G.

(f)   Application of toroidal vortices: From plasma
fusion reactors to thermonuclear fireballs, the toroidal vortex
has applications in nuclear physics. Because of the great
efficiency with which the model allows one pulse of fluid to
travel through another, the concept of toroidal vortices needs
to be examined in the context of cloud physics, particularly
the physics of cumulus and cumulonimbus clouds.

(g)   Applications in mathematics: The utility of new
coordinate systems separable in Schroedinger's and the spatial
wave equation needs to be explored. The pechant of nuclear
particles to follow spiral paths may be made more easily
understandable in spiral coordinates.

All of the above are possibilities for further work in the new
paradigm and some are being pursued by the auther. Obviously the
work is more than one individual can do in a lifetime. The
possibilities are limited only by the ingenuity of the
researchers who follow.

BIBLIOGRAPHY

BIBLIOGRAPHY

McGuirk, Jampes P. and Elmar R. Reiter, (1976) " A Vacillation in Atmospheric Energy Parameters," J of At. Sci., Vol 33, November, pp 2079-2093.

Mintz, Y. (1965) Very long-term global integration of the primative equations of atmospheric motion. World Meteoro. Organ., Tech Note No. 66, 141-167.

Nicholson, Francis H., (1976) The Zero Laplacian Vortex in Spherical Coordinates as Applied to a Model of the General Circulation," Preprints Joint DMG/AMS International Conference on Simulation of Large Scale Atmospheric Processes, August 30 - September 4, 1976, Hamburg, F.R.G.

Rossby, C.G. (1947) On the distribution of angular velocity in gaseous envelopes under the influence of large-scale horizontal mixing processes. Bull. Am. Meteorol. Soc. 28, 53-68.

Yeh, T.C., and Chu, P.C. (1958) "Some Fundamental Problems of the General Circulation of the Atmosphere," 159 pp. Inst. Geophys. Meteorol., Academia Sinica, Peking (in Chinese, extended English abstract, pp. 147-156).

BIBLIOGRAPHY

Anthes, Richard Allen, 1970: A Diagnostic Model of the
    Tropical Cyclone in Isentropic Coordinates, _ESSA_
    Technical Memorandum ERLTM-NHRL 89, pp. 147.

Ausman, M., 1959: Some computations of the inflow angle in
    hurricanes near the ocean surface. Dept. Meteor.,
    Univ. Chicago, 19 pp. (Copies available from H. Riehl).

Bradbury, Dorothy L., 1971: The Filling Over Land of Hurri-
    cane Camille, August 17-18, 1969. _SMRP_ Research Paper
    No. 96, Department of Geophysical Sciences, The Universi-
    ty of Chicago.

Einstein: A Centenary Volume, Edited by A.P. French, Harvard
    University Press, Cambridge, Mass. 1979, pp. 331.

Einstein, A., _Ideas and Opinions, The Problem of Space, Ether_
    and Field in Physics, 1954: Dell (pp. 270-283), New York.

Eliasen, E., B. Machenhauer, and E. Rasmussen, 1970: On a
    numerical method for integration of the hydrodynamic
    equations with a spectral representation of the
    horizontal fields, Rept. No. 2, Institut for Teoretisk
    Meteorologi, Kobenhavns Universitet, Denmark, 35 pp.

Fujiwhara, S. 1921: The Natural Tendency towards Symmetry of
    Motion and its Applications as a Principle of Meteor-
    ology, _Quart. Jour. Roy. Meteor.Soc._, 47, pp. 287.

_____ 1923: On the Growth and Decay of Vortical
    Systems., _Quart. J. Roy. Meteor. Soc._, 49, 75-104.

Golden, Joseph H., 1974: The Life Cycle of Florida Keys'
    Waterspouts. I., JAM, vol. 13, No. 6, pp. 676-692.

Haltiner, George J. and R.T. Williams, 1980: Numerical
    Prediction and Dynamic Meteorology, John Wiley and Sons,
    New York.

Hoecker, Walter H. Jr., 1960: Wind Speed and Air Flow Patterns
    in the Dallas Tornado of April 2, 1957, MWR, Vol. 88, No. 5,
    pp. 167-180.

Kornfield, Jack, 1969: A photographic summary of the earth's
    cloud cover for the year 1967, 687-700, JAM vol. 8.

Kuhn, Thomas S., 1970: The Structure of Scientific Revolutions-
    International Encyclopedia of Unified Science, Vol. 2,
    . No. 2, University of Chicago Press, Chicago, pp. 211.

Lanczos, Cornelius, 1970: Space Through the Ages, The Evolution
    of Geometric Ideas from Pythagoras to Hilbert and Einstein,
    Dublin Institute for Advanced Studies, Dublin, Ireland,
    Academic Press, London and New York, 1970, pp. 320.

Morse, Philip M. and Herman Feshbach, 1953: Methods of
    Theoretical Physics, vol. 1 & 2, McGraw-Hill Book Com-
    pany, New York, N.Y., pp. 1978.

Nicholson, Francis H., 1972: A New Vortex Model Based on a
    Zero Laplacian of Vorticity, Ph.D. dissertation, University
    of Wisconsin at Madison, Madison, Wisconsin.

Rankine, W.J., 1888: A Manual of Applied Mechanics, Charles
    Griffin and Co., London, pp. 667.

Riehl, Herbert, 1954: Tropical Meteorology, McGraw-Hill Book Company, Inc., New York, pp. 392.

_____ and J.S. Malkus, 1961: Some aspects of hurricane Daisy, 1958., Tellus, 13, 181-213.

_____, 1963: Some Relations Between Wind and Thermal Structure of Steady State Hurricanes, J. Atmos. Sci., vol. 20, No. 4, pp. 276-287.

Rubin, V.C. and W.K. Ford, Jr., 1970: A Comparison of Dynamical Models of the Andromeda Nebula and the Galaxy, Symposium No. 38. The Spiral Structure of Our Galaxy, ed. W. Becker, Astronomsich-Meteorologische Anstalt, Binningen, Switzerland, and G. Contopolous, University of Thessalonika, Thessaloniki, Greece. D. Riedel Publishing Co., Dordrecht Holland. Springer-Verlag, New York/New York.

Sanders, F. and R.W. Burpee, 1968: Experiments in Barotropic Hurricane Track Forecaszing, JAM 7, 313-323.

Wilkins, E.M., 1962: The Role of Electrical Phenomena Associated with Tornadoes, J. Geophys. Res., 69, pp. 2435-2447.

APPENDIX A

SPIRAL COORDINATE SYSTEMS SEPARABLE

IN LAPLACE'S, SCHROEDINGER'S, AND THE SPATIAL WAVE

EQUATION

1. INTRODUCTION

Various physical phenomena are most easily described in coordinate systems which provide the simplest representation of their activities. Thus, the flight of an arrow is well described in Cartesian coordinates, whereas the flight of an airplane makes more sense in geographical coordinates. The rotation of a tornado is naturally described in cylindrical coordinates, but the general circulation of the earth's atmosphere requires spherical coordinates.

Over and above the facile description of certain processes in one coordinate system or the other, if the coordinate systems are appropriately chosen, they also have properties relevant to the behavior of certain homogeneous second order, linear, partial differential equations. Of particular interest are Laplace's, Schroedinger's and the spatial wave equation. The relevant quality, called separability, renders solutions of these equations simple and rapid.

According to Morse and Feshbach (1953) there are thirteen coordinate systems separable in Laplace's equation in three dimensions. After discarding the rather esoteric toroidal and bispherical coordinate systems, the remaining eleven are also separable in the spatial wave and Schroedinger's equation. Ten of these coordinate systems are degenerate forms of the very general eleventh, the ellipsoidal coordinate system. Of these eleven, it appears that six are also a degenerate type of another kind of coordinate system, a system with spiral characteristics.* This subset of systems has the characteristic of maintaining separation upon rotation or linear recombination of two of the axes about the third (after appropriate factoring). The non-spiral Cartesian coordinate system may also be rotated, but it neither undergoes factoring nor does it then exhibit spiral characteristics.

*The sixth is an imaginary version of the spherical log spiral coordinates. By using Lambert's sphere of radius $i = \sqrt{-1}$, sin becomes sinh and tan, tanh so that we have the non-Euclidean circular hyperboloid as a degenerate form of the more general $\exp\{(\ln \tanh(\theta/2) + i\phi)e^{i\alpha}\}$. There are probably others, but they are beyond the current scope of this work.

2. CIRCULAR CYLINDRICAL COORDINATES

A somewhat more complicated case than the Cartesian coordinate system involves the circular cylindrical coordinate system. The Laplacian is given in this system by

$$\nabla^2 = \frac{1}{r} \frac{\partial}{\partial r} \, r \, \frac{\partial}{\partial r} + \frac{1}{r^2} \frac{\partial^2}{\partial \theta^2} + \frac{\partial^2}{\partial z^2} \tag{1}$$

By multiplying the first right hand term of (1) by r/r we may recombine and rewrite (1) as

$$\nabla^2 = \frac{1}{r^2} \left(\frac{\partial^2}{\partial \ln r^2} + \frac{\partial^2}{\partial \theta^2} \right) + \frac{\partial^2}{\partial z^2} \tag{2}$$

Thus r^{-2} is the factor and the semilog variants of this coordinate system must be rotated about the vertical or z axis.

Semilog coordinates may be rotated to create logarithmic spiral coordinates by the transformation

$$S_r = \ln r \, \cos\alpha + \theta \, \sin\alpha \tag{3}$$

$$S_\theta = \theta \, \cos\alpha - \ln r \, \sin\alpha \tag{4}$$

where S_r and S_θ are the new logarithmic spiral coordinates illustrated in Figure 1, $\ln r$ and θ are the original semilog coordinates, and α is the angle of rotation.

Equations (3) and (4) may be inverted to obtain $\ln r$ and θ in terms of S_r and S_θ, so

$$\ln r = S_r \, \cos\alpha - S_\theta \, \sin\alpha \tag{5}$$

$$\theta = S_\theta \, \cos\alpha + S_r \, \sin\alpha \tag{6}$$
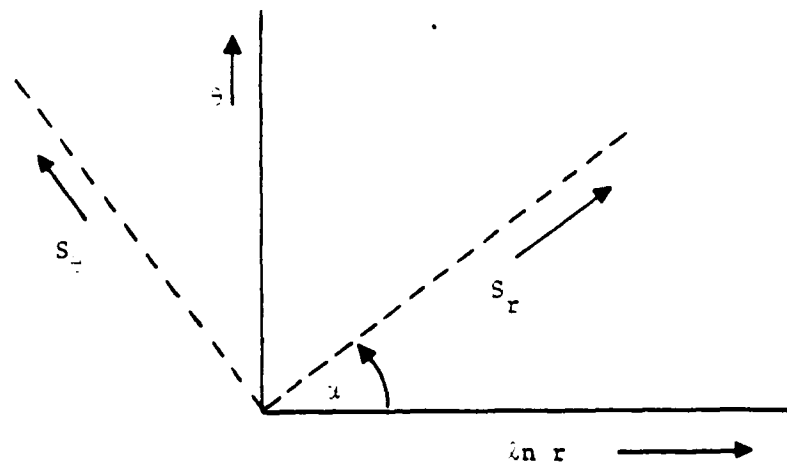
Figure 1. Rotation of Semilog Coordinates $\ln r$, θ To Produce Spiral Coordinates S_r and S_θ

leading to a reexpression of (1) as

$$\nabla^2 = e^{2(S_\theta \sin\alpha - S_r \cos\alpha)}\left(\frac{\partial^2}{\partial S_r^2} + \frac{\partial^2}{\partial S_\theta^2}\right) + \frac{\partial^2}{\partial z^2} \tag{7}$$

thus reexpressing the Laplacian entirely in log spiral coordinates.

3. SPHERICAL COORDINATES

A similar procedure is possible for spherical coordinates with Laplacian

$$\nabla^2 = \frac{1}{r^2 \sin\phi} \frac{\partial}{\partial\phi} \sin\phi \frac{\partial}{\partial\phi} + \frac{1}{r^2 \sin^2\phi} \frac{\partial^2}{\partial\theta^2} + \frac{\partial^2}{\partial r^2} \tag{8}$$

By using the same technique on (8) as was used on (1), multiplying the
first r.h.s. of (8) by $\sin\phi/\sin\phi$, we obtain

$$\nabla^2 \equiv \frac{1}{r^2 \sin^2 \phi} \left(\sin\phi \frac{\partial}{\partial\phi} \sin\phi \frac{\partial}{\partial\phi} + \frac{\partial^2}{\partial\lambda^2}\right) + \frac{\partial^2}{\partial r^2} \quad . \tag{9}$$

Rewriting $\sin\phi\frac{\partial}{\partial\phi}$ as $\frac{1}{\csc\phi}\frac{\partial}{\partial\phi}$ or $\frac{\partial}{\partial\ln(\tan(\phi/2))}$ we obtain

$$\nabla^2 \equiv \frac{1}{r^2 \sin^2 \phi} \left(\frac{\partial^2}{\partial(\ln(\tan\phi/2))^2} + \frac{\partial^2}{\partial\lambda^2}\right) + \frac{\partial^2}{\partial r^2} \tag{10}$$

Subjecting (10) to the same sort of rotation about the r axis, we may
express $\ln(\tan(\phi/2))$ in terms of S_ϕ and S_r. Then, since $\ln(\tan(\phi/2))$
$= S_\phi \cos\alpha - S_\lambda \sin\alpha$, we may express ϕ as

$$\phi = 2 \tan^{-1}(\exp(S_\phi\cos\alpha - S_\lambda\sin\alpha))$$

and $r^{-2} \sin^{-2}\phi$ as

$$r^{-2} \sin^{-2} (2\tan^{-1}(\exp(S_\phi\cos\alpha - S_\lambda\sin\alpha))) \ ,$$

so that (10) may be rewritten entirely in spiral spherical coordinates as

$$\nabla^2 \equiv \frac{1}{r^2} \sin^{-2}(2\tan^{-1}(\exp(S_\phi\cos\alpha - S_\lambda\sin\alpha)))$$

$$\left(\frac{\partial^2}{\partial S_\phi^2} + \frac{\partial^2}{\partial S_\lambda^2}\right) + \frac{\partial^2}{\partial r^2} \quad . \tag{11}$$

4. ELLIPTICAL CYLINDRICAL, CONIC AND PARABOLIC CYLINDRICAL COORDINATES

The other coordinate systems are less familiar, but no less interesting.
They are two cylindrical coordinates: elliptic and parabolic, and conic
coordinates, formed by the traces of elliptic cones on spheres. The conic
coordinates are the spherical representation of elliptic cylindrical, just
as the spherical coordinates are the spherical representation of the circular
cylindrical coordinates.

Unlike the preceding systems, none of these three requires factoring in order to establish a quasi-Cartesian framework for a spiral Laplacian. The three Laplacians may be written immediately as

$$\nabla^2 \equiv \frac{1}{d^2} (\cosh^2 \mu - \cos^2 \phi) \left(\frac{\partial^2}{\partial \mu^2} + \frac{\partial^2}{\partial \phi^2} \right) + \frac{\partial^2}{\partial z^2} \tag{12}$$

for the elliptic cyclindrical system,

$$\nabla^2 \equiv \frac{1}{\xi_1^2 + \xi_2^2} \left(\frac{\partial^2}{\partial \xi_1^2} + \frac{\partial^2}{\partial \xi_2^2} \right) + \frac{\partial^2}{\partial z^2} \tag{13}$$

for the parabolic cylindrical system, and

$$\nabla^2 \equiv \frac{1}{\alpha^2 \, cn^2(\lambda,\alpha) + \beta^2 \, sn^2(\mu,\beta)} \left(\frac{\partial^2}{\partial \lambda^2} + \frac{\partial^2}{\partial \mu^2} \right) + \frac{\partial^2}{\partial r^2} \tag{14}$$

for the conic coordinate system.

In the case of (12- 14) we may rotate the complex space by the versor, $e^{i\alpha}$ to get the spiral forms $S_\mu + i\, S_\phi$ for $(\mu + i\phi)e^{i\alpha}$, $S_{\xi_1} + i\, S_{\xi_2}$ for $(\xi_1 + i\, \xi_2)e^{i\alpha}$, and $S_\lambda + i\, S_\mu$ for $(\lambda + i\mu)e^{i\alpha}$.

The parameters $\mu + i\phi$, $\xi_1 + i\, \xi_2$ and $\lambda + i\mu$ may be expressed individually as functions of their spiral equivalents in the same pattern as (5) and (6). We have

$$\mu = S_\mu \cos\alpha - S_\phi \sin\alpha$$

$$\phi = S_\phi \cos\alpha + S_\mu \sin\alpha$$

so (12) may be rewritten as

$$\nabla^2 \equiv \frac{1}{d^2(\cosh^2(S_\mu \cos\alpha - S_\phi \sin\alpha) - \cos^2(S_\phi \cos + S_\mu \sin\alpha))}$$

$$\left(\frac{\partial^2}{\partial S\mu^2} + \frac{\partial^2}{\partial S_\phi^2}\right) + \frac{\partial^2}{\partial z^2} \quad , \tag{15}$$

and (13) may be rewritten as

$$\nabla^2 \equiv \frac{1}{\left(S_{\xi_1}^2 + S_{\xi_2}^2\right)}\left(\frac{\partial^2}{\partial S_{\xi_1}^2} + \frac{\partial^2}{\partial S_{\xi_2}^2}\right) + \frac{\partial^2}{\partial z^2} \tag{16}$$

since

$$\xi_1 = S_{\xi_1}\cos\alpha - S_{\xi_2}\sin\alpha$$

$$\xi_2 = S_{\xi_2}\cos\alpha + S_{\xi_2}\sin\alpha$$

and (14) as

$$\nabla^2 = \frac{1}{\alpha^2 \, cn^2((S_\lambda\cos\alpha - S_\mu\sin\alpha),\alpha) + \beta^2 \, cn^2((S_\mu\cos\alpha + S_\lambda\sin\alpha),\beta)}$$

$$\left(\frac{\partial^2}{\partial S_\lambda^2} + \frac{\partial^2}{\partial S_\mu^2}\right) + \frac{\partial^2}{\partial r^2} \tag{17}$$

since

$$\lambda = S_\lambda\cos\alpha - S_\mu\sin\alpha$$

$$\mu = S_\mu\cos\alpha + S_\lambda\sin\alpha \quad .$$

5. CONCLUSION

The three-dimensional Laplacians for the five coordinate system mentioned above may all be rewritten entirely in terms of their rotated spiral equivalents. Thus, there exist solutions in spiral coordinates for the three forms of the homogenous, second order linear equations

$$\nabla^2 \psi + k^2 \psi = 0, \quad k^2 = 0.$$

The analysis above also applies when $k^2 \neq 0$, permitting Helmholtz and Schroedinger equations to be included in the application.

6. REFERENCES

Morse, P. and H. Feshback, _Methods of Theoretical Physics_, Vol. 1, McGraw-Hill Book Company, New York, 1953, p. 997.

APPENDIX   B

THE GENERAL CIRCULATION OF EARTH AND THE INNER

PLANETS

THE ZERO LAPLACIAN VORTEX IN
SPHERICAL COORDINATES AS
APPLIED TO A MODEL OF THE
GENERAL CIRCULATION

by

Francis H. Nicholson, Ph.D.
February 1979

ABSTRACT

The general circulation is parameterized in
terms of a vorticity distribution which satisfies LaPlace's
equation both in symmetric and asymmetric modes. The
correlation of the extent of polar easterlies and the
strength of the westerlies and possible disappearence
of the trades during an ice age are considered. Com-
parison is made between the Mintz-Arakawa 2-level
model and the observed data for the southern hemisphere.
The parameterization provides a simple yet coherent way
of describing in two dimensions atmospheric flow above
the boundary layer.

1.0   Introduction

In this paper a simple analytical expression for horizontal planetary flow is presented. The expression, presented in spherical coordinates, has the property that the Laplacian of the vorticity derived from the flow is zero. Examples will be given and discussed. First the model is developed with a zero wave number, and then a non-zero wave number is introduced.

2.0   Description of the Model

The model shown in Figure 1 is divided into two sections, the northern, or circumpolar regime and the southern or tropical regime. Since the Laplacian of vorticity may be zero both if the vorticity is constant and also if it varies in a prescribed manner, the absolute vorticity will be considered as constant in the polar regime and as zero at the equator, increasing with latitude to the value of the constant vorticity in the polar regime at the boundary of that regime so that the vorticity distribution is continuous. In addition, the velocity distribution is also continuous.

This approach has a partial precedent in the work of Rossby (1947) who suggested "that the broad scale features poleward of the latitude of maximum wind could be accounted for on the basis of a north-south mixing of

absolute vorticity." (Rossby, C. G., 1947) This mixing
is implicit in the assumption that the Laplacian of the
absolute vorticity is zero, which is to say that turbulent
mixing, conceivably by extratropical cyclones and anti-
cyclones, distributes the absolute vorticity in such a
manner that turbulent mixing causes neither vorticity con-
vergence or divergence.

3.0 Derivation of the Analytical Expression for the Zonal Model

The expression for the zero Laplacian of vorticity
in spherical coordinates is given by

$$\nabla^2 \zeta = \frac{1}{r^2} \cos\phi \frac{\partial}{\partial\phi}\left(\cos\phi \frac{\partial\zeta}{\partial\phi}\right) = 0 \qquad (1)$$

where $\zeta = -\frac{1}{r}\cos\phi \frac{\partial}{\partial\phi}\left(\cos\phi\ U_\lambda\right)$ \qquad (2)

where U_λ is the zonal velocity.

3.1 The Tropical Regime

Multiplying by $r^2\cos\phi$ and letting $\iota = \frac{\partial\zeta}{\partial\phi}$ we
obtain upon integrating the resulting expression between
$\phi = 0$ and ϕ, $\cos\phi\ \iota - \iota_0 = 0$ where

$$\iota_0 = \frac{\partial\zeta}{\partial\phi}\Big|_{\phi = 0} \quad \text{or} \quad \iota = \iota_0 \sec\phi \qquad (3)$$

Further integration yields

$$\int_{\phi=0}^{\phi} (\partial\zeta/\partial\phi)\,d\phi = \iota_o \int_{\phi=0}^{\phi} \sec\phi\,d\phi \qquad (4)$$

$$\zeta - \zeta_o = \iota_o \ell n\,\tan(\frac{\pi}{4} + \frac{\phi}{2}) \qquad (5)$$

where $\zeta_o = 0$. After substituting (2) into (5) and multiplying by $-(r\cos\phi)$ to obtain

$$\int_{\phi=0}^{\phi} \frac{\partial}{\partial\phi}\cos\phi\, U_\lambda d\phi = -\int_{\phi=0}^{\phi} r\iota_o \cos\phi\, \ell n\,\tan(\frac{\pi}{4} + \frac{\phi}{2})d\phi \qquad (6)$$

The right hand side may be integrated by parts

$$\int udv = uv - \int vdu \quad \text{where } u = \ell n\,\tan(\frac{\pi}{4} + \frac{\phi}{2}),$$

$du = \sec\phi d\phi$, $dv = \cos\phi d\phi$ and $v = \sin\phi$.

Thus $\cos\phi\, U_\lambda - U_{\lambda_o} = -r\iota_o(\sin\phi\, \ell n\,\tan(\frac{\pi}{4} + \frac{\phi}{2}) + \ell n\,\cos\phi)$

where the right hand expressions are zero at $\phi=0$. By rearranging and subtracting $r\Omega\cos\phi$ we obtain the relative velocity,

$$U_{\lambda_r} = U_{\lambda_o} \sec\phi - r\iota_o\sec\phi\{\sin\phi\, \ell n\,\tan(\frac{\pi}{4} + \frac{\phi}{2}) + $$

$$\ell n\,\cos\phi\} - r\Omega\cos\phi \qquad (7)$$

3.2 The Polar Regime

Where the vorticity is constant, ζ_N, from (2)

$$\zeta_N = -\frac{1}{r}\cos\phi\,\frac{\partial}{\partial\phi}\cos\phi\,U_\lambda$$

then by multiplying both sides by $-(r\cos\phi)$ and integrating we obtain

$$\int_{\pi/2}^{\phi}\frac{\partial}{\partial\phi}\cos\phi\,U_\lambda d\phi = \zeta_N\int_{\phi}^{\pi/2} r\cos\phi\,d\phi \qquad (8)$$

$$\cos\phi\,U_\lambda = r\zeta_N\sin\phi\big|_{\phi}^{\pi/2} \quad \text{or}$$

$$U_{\lambda_r} = r\zeta_N(\sec\phi - \tan\phi_N) - r\Omega\cos\phi \qquad (9)$$

where $U_{\lambda_r} = 0$ at $\phi = \phi_N$ then

$$\zeta_N = \Omega\cos\phi_N/(\sec\phi_N - \tan\phi_N) = \Omega\cos^2\phi/(1-\sin\phi_N)$$

Thus ζ_N may be expressed in terms of the latitude of zero relative velocity. Also ι_o may be solved for by substituting ζ_N for ζ and ϕ_i (the latitude of the boundary separating the two regimes) for ϕ in (5).

Since not only the vorticity but the velocity is
continuous between the two regimes, U_{λ_o} may be determined
by equating the right hand side of (7) and the right hand
side of (9), substituting ϕ_i for ϕ. By adding $r\Omega\cos\phi$ to
both sides and multiplying both sides by $\cos\phi_i$ we obtain

$$U_{\lambda_o} = r\zeta_N(1-\sin\phi_i) + r_{l_o}(\sin\phi_i \ln \tan(\frac{\pi}{4} + \frac{\phi_i}{2_i}) + $$

$$\ln \cos\phi_i) \tag{11}$$

Thus from a knowledge of where U_{λ_r} is zero in the polar
regime, and the boundary between the two regimes we may
specify the total zonal circulation.

4.0 Illustrations of Various Possible Circulations

In the illustrations given below the two variables
are the latitude of the zero relative velocity in the polar
regime, indicated by the numerator in the accompanying
fraction, and the latitude which delineates the boundary
between the polar and tropical regimes. The lower the
numerator, the more intense the circumpolar vortex. The
lower the denominator, the greater the extent of the
circumpolar vortex.

Figure 2 illustrates a circulation with the relative zonal wind at 60 degrees north as being zero, and the boundary of the two regimes at 55 degrees north. The trade winds are well developed with a maximum of about 16 m/s. The westerlies begin at 26 north, reaching a maximum of 14 m/s at 45 north, and ceasing at 60 north. The polar easterlies reach a maximum at 74 north of 6 m/s.

In figure 3 the latitude of zero relative velocity is shifted north by 5 degrees reducing the extent and magnitude of both the trades and the polar easterlies. The westerlies, however, have intensified, extending their sway as far south as 15 degrees north and as far north as 65 degrees north. Obviously, the latitude of the zero relative velocity in the polar regime is also the northern boundary of the westerlies.

By virtually eliminating the circumpolar vortex and the polar easterlies and shrinking the polar regime to 58.5 north we increase the magnitude of the westerlies to about 26 m/s and displace their maximum north. The trades also increase in magnitude and extend their realm north to 21 degrees north. This is shown on the next page in Figure 4.
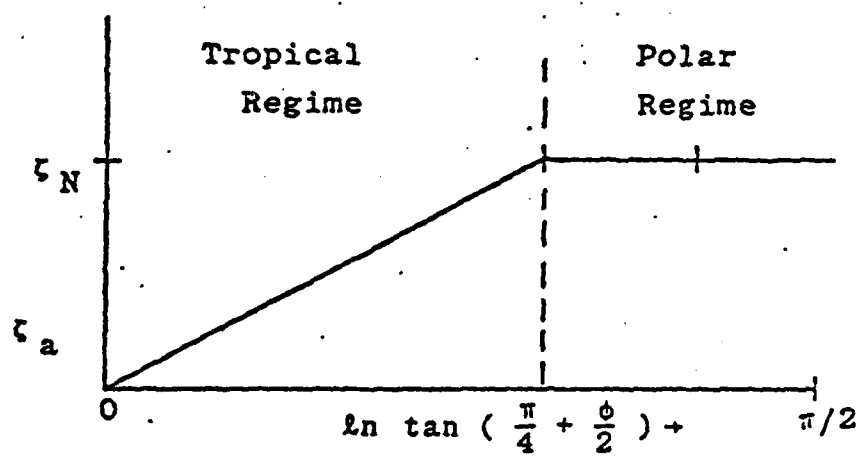
Figure 1.   Absolute Vorticity as a Function
of Latitude

Figure 3. Circulation model 65/55.

Figure 2. Circulation model 60/55.

B-9

MISS TEST FAC WEATHER STATION
 PRESSURE READINGS OF HURRICANE CAMILLE

B-10
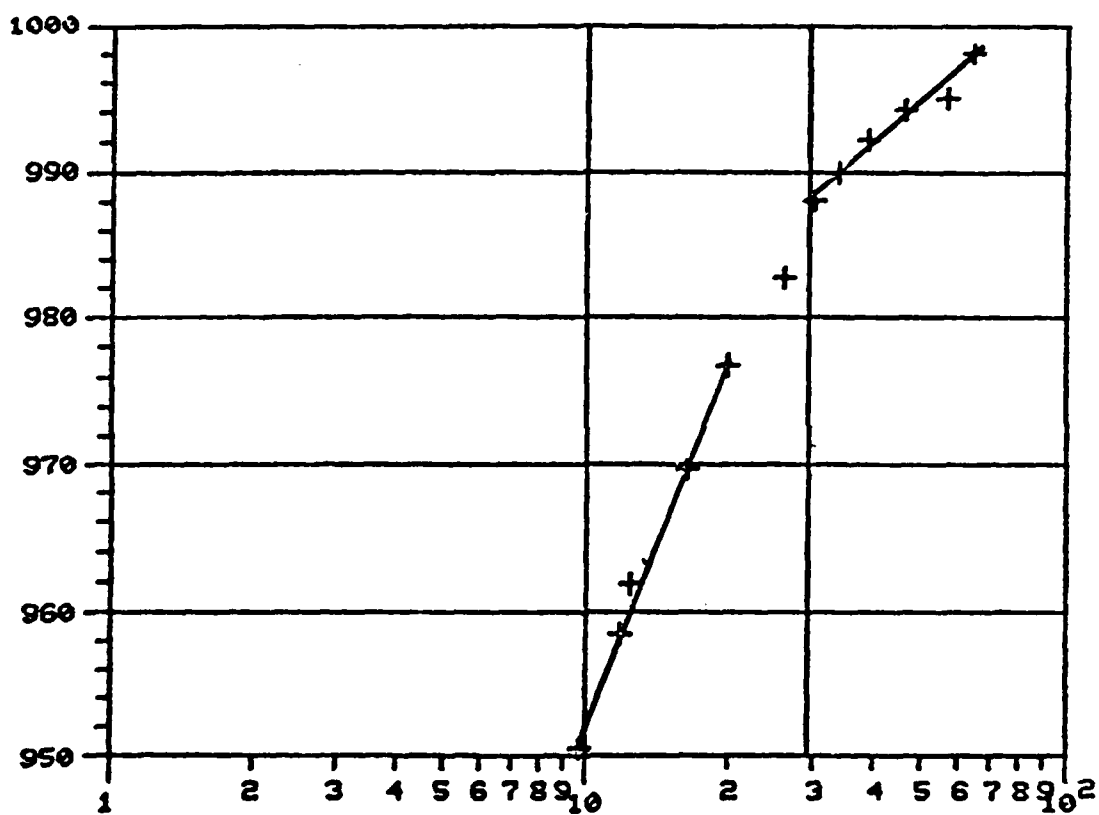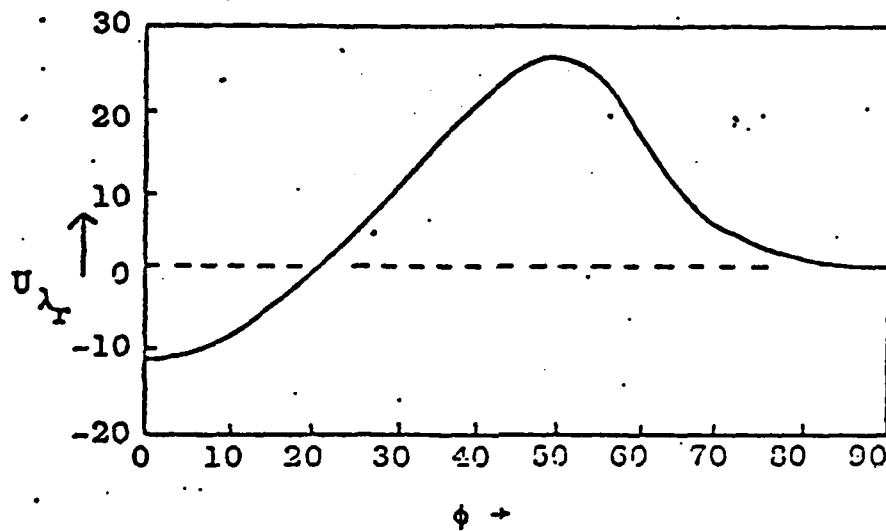
Figure 4.   Circulation
           model 89/58.5.

The next two illustrations indicate possible
various stages in the advance of an ice age. In Figure 5
the northern limit of the westerlies is at 50 degrees
north, and is coincident with the limit of the polar regime.
There are weak westerlies, very weak trades, but strong
and extensive polar easterlies. As the polar easterlies
deepen and become more extensive, with both the limit of
the polar regime and of the westelies at 45 north, the
trades disappear altogether, to be replaced by strong
westerlies with a slight maximum at 25 north of 19 m/s.
If this were indeed the case then north of 45 degrees the
winds would virtually all be from the east, cold and dry.
Such a situation would be devastating for western Europe
which depends upon winds from the Atlantic to bring both
warmth and moisture. South of 45 degrees the winds would
blow from the west, reversing patterns of the present,
perhaps bringing more moisture to the Sahara and even
altering the patterns of the monsoon in India and southeast
Asia. Undoubtedly the flow of the oceanic currents would
also be disrupted, first by the lowering of sea level which
must of necessity accompany an ice age and then by the
significant shift in the driving torque due to the south-
ward shift of the westerlies, the disappearance of the
trades and the intensification and greater extent of the
polar easterlies.

Comparison to Actual Data and Numerical Simulation

     The General Circulation Model of Nicholson (1976) based on the Zero Laplacian Vortex in spherical coordinates simulates the southern hemisphere's axially symmetric atmospheric circulation in January 1973 for the levels at 800 and 400 mb in a manner comparable to the Mintz-Arakawa two level model, as can be seen by the comparisons in Figure 7. Obviously further development of the model is warranted to assess the model's capabilities to simulate asymmetries in the general circulation.
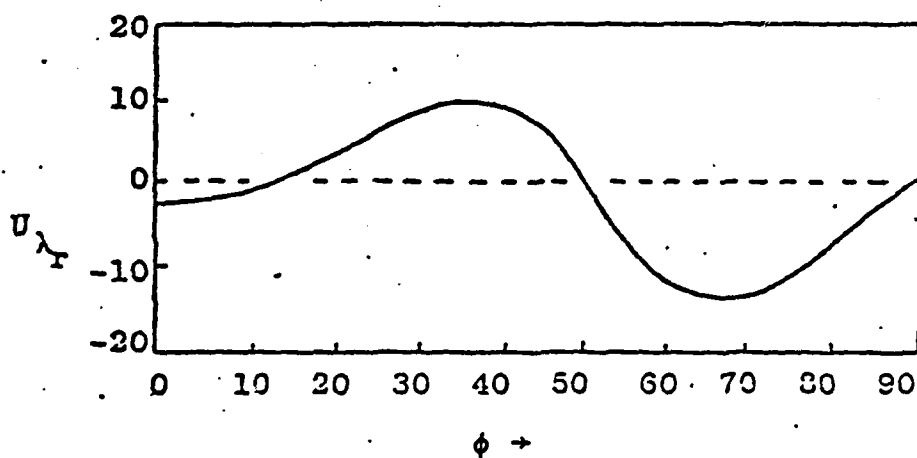
Figure 5.   Circulation
model 50/50.
(Begin Ice Age)
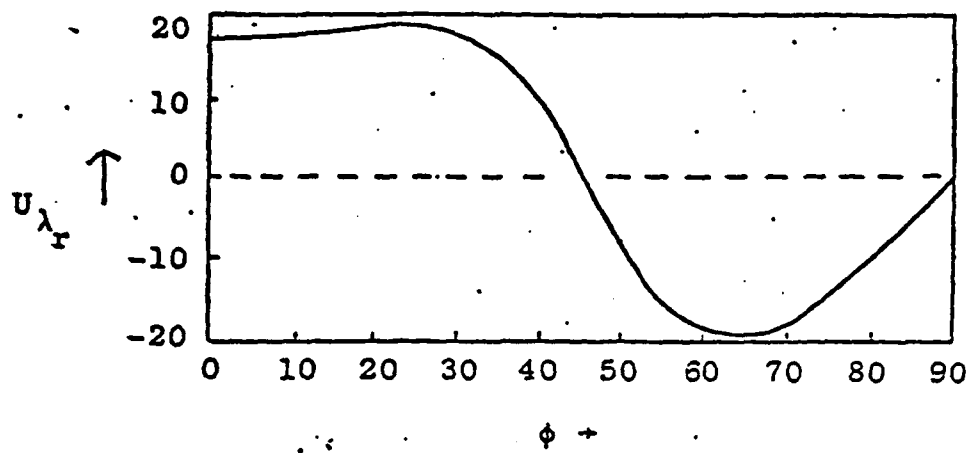
Figure 6. Circulation model
45/45. (Ice Age)
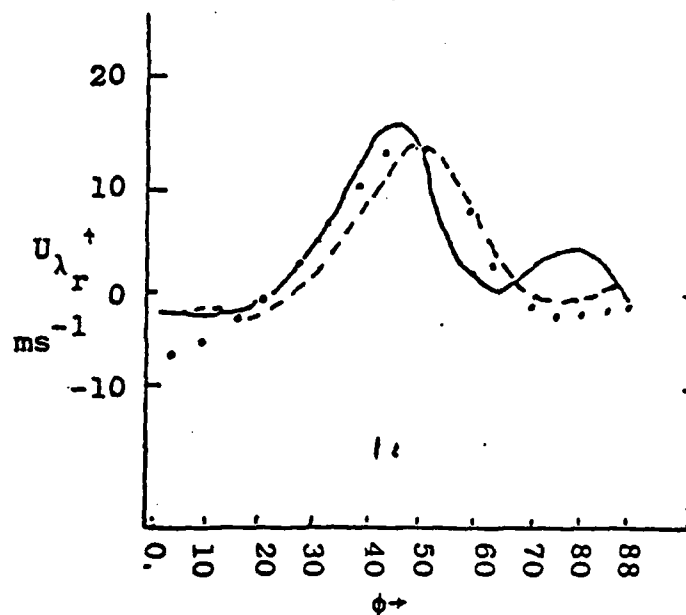
Figure 7a. January Circulation at 800 mb

- - - - - = Observed Data

. . . . . . = Zero Laplacian Vortex

————————— = Mintz-Arakawa 2-Level Model
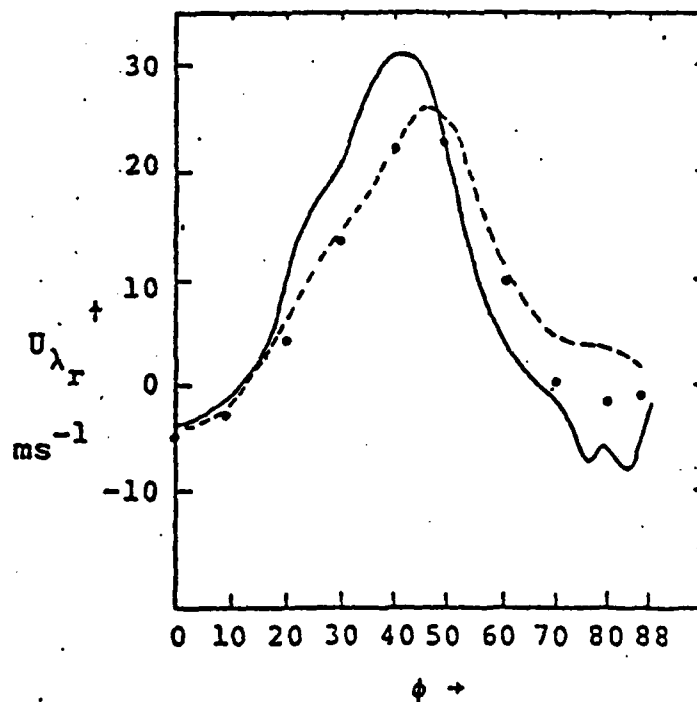
Figure 7b. January Circulation at 400 mb.

- - - - - - - - = Observed Data

. . . . = Zero Laplacian Model

————————— = Mintz-Arakawa 2-Level Model

B-16

5.0 The Asymmetric Portion of the Zero Laplacian Vortex

The general circulation model may be made more realistic by relaxing the constraint of axial symmetry. Preliminary analyses from the ATS and NOAA satellites as well as the knowledge that planetary waves have a tilting axis from south to northeast (Palmen and Newton, 1969) suggests the following analysis. This is done by first considering the mathematical form of spiral asymmetries..

5.1 The Spherical Laplacian

For an asymmetric case the spherical Laplacian of the scalar ψ is given in geographic coordinates by

$$\nabla^2 \psi = \frac{1}{r^2} \cos\phi \, \frac{\partial}{\partial\phi} \left(\cos\phi \, \frac{\partial\psi}{\partial\phi} \right) + \frac{1}{r^2} \cos^2\phi \, \frac{\partial^2\psi}{\partial\lambda^2} \qquad (12)$$

where λ signifies longitude and ϕ latitude and r is the radius of the earth. Equation (12) may also be condensed into the form given below.

$$\nabla^2 \psi = \frac{1}{r^2} \cos^2\phi \left[\frac{\partial^2\psi}{\partial\ln^2(\tan\frac{\phi}{2}+\frac{\pi}{4})} + \frac{\partial^2\psi}{\partial\lambda^2} \right] . \qquad (13)$$

A coordinate system can be constructed using λ as the ordinate and $\ln \tan (\phi/2 + \pi/4)$ as the abscissa.

B-17

In this coordinate system, a curve of
a special mathematical nature plots as a straight line.

This curve is a "spherical" logarithmic spiral and appears
as a straight line on a Mercator projection.

The cylindrical log spiral is described by the
equation

$$\ln \frac{r}{r_o} = \pm \, a(\theta - \theta_o) \tag{14}$$

where here r is the radius, and θ the azimuthal angle. The
analogous expression for the spherical log spiral is given
by

$$\ln \left\{ \tan \left(\frac{\pi}{4} + \frac{\phi}{2} \right) \Big/ \tan \left(\frac{\pi}{4} + \frac{\phi_o}{2} \right) \right\} =$$

$$\pm \, a \, (\lambda - \lambda_o) \tag{15}$$

where ϕ is the latitude and λ longitude. Any curve which
is a straight line in the $\ln \tan (\pi/4 + \phi/2)$, λ
coordinate system is by definition a spherical log spiral,
including meridians and lines of longitude. By a simple
rotation of axes, we may express functions in terms of the
othogonal spherical spiral coordinate system. When two
axes are rotated through the angle α ($\alpha < 45^\circ$) the new
coordinates may be described in terms of the old by the
following relations

$$S_\phi = \ln \tan \left(\frac{\pi}{4} + \frac{\phi}{2}\right) \cos\alpha + \lambda \sin\alpha \qquad (16$$

$$S_\lambda = \cos\alpha - \ln \tan \left(\frac{\pi}{4} + \frac{\phi}{2}\right) \sin\alpha \qquad (17)$$

where S_ϕ is most nearly parallel to meridians and S_λ most
nearly parallel to longitude lines. Consequently the
Laplacian may be rewritten

$$\nabla_H^2 \psi = \frac{1}{r^2} \cos^2\phi \left[\frac{\partial^2 \psi}{\partial S_\phi^2} + \frac{\partial^2 \psi}{\partial S_\lambda^2} \right] . \qquad (18)$$

assuming an asymmetry which may as·easily be the height of
a pressure surface, a divergence pattern or a vorticity
pattern.

$$(20)$$

In spherical spiral coordinates, μ, ν the function $f(z)$
is represented by

B-19

$$f(\bar{z}) = f_0(\bar{z}) + \gamma_0 \ln \tan\left(\frac{\mu}{2} + \frac{\pi}{4}\right)$$

Symmetric

$$\sum_{n=1}^{\infty} \gamma_0(n) \exp\{ \langle \nu + i\ln \tan \frac{\mu}{2})e^{i\alpha} \} \qquad (21)$$

Asymmetric

The transformation from spherical to geographic coordinates may be made by substituting ν for λ and $(\pi/2 + \phi)$ for μ.

A slight modification of the two regime symmetric model to include a third, equatorial regime, may also provide a rationale for the existence of the Intertropical Convergence Zone, explaining both its location and possible seasonal fluctuations.*

*See Appendix C for further explanation of the ITCZ in terms of zonal harmonics in the divergence field.

5.2 Climatic Implications

A possible result of an extension of the circum-polar vortex would be the accentuation of the difference in temperature between the continents and the oceans. According to Yeh and Chu (1958) the effects of heat sources cooperate with those induced by mountain chains to maintain mean troughs near the east coasts of Asia and North America in winter. These two contributions differ over Asia however so that a weakening or strengthening of the influence of the heat sources due to oceans could result in a significant difference over Asia. The wintertime Siberian high would not exist at all were it not for the influence of the long west-east mountain chain across southern Eurasia. Mintz (1965) found that with the simulated absence of the mountains baroclinic disturbances occured between the air warmed by the Indian Ocean and the air over Siberia which is cooled by radiation. The net result was a transport of heat into Siberia from the Indian Ocean.

6.0 Conclusion

This paper has presented a model of the general circulation based on the spherical Zero Laplacian Vortex. The long atmospheric waves may be handled by a Fourier series with spiral coordinates defining the argument of the series. This provides a simple non dispersive wave with an axis tilted so as to satisfy angular momentum exchange considerations. Both meridional and zonal atmospheric motions may thus be simulated.

The limiting parameters which govern these hypothetical circulations should be investigated more thoroughly in a numerical model using the filtered equations in their full extent using satellite albedo data for input into the vorticity and divergence fields. The interaction with the oceans, how the currents may have altered under these different wind regimes derived from satellite cloud motions thus affect adjacent continents would provide some interesting insights.

With an analytical model of the atmospheric circulation it may be possible to analyze short term atmospheric trends. Man's modification of the sea air interface may show up as a primary factor in these trends by changing the forcing functions in the wave equation.

Among these trends are the displacement of storm tracks which may increase rainfall and even flood some areas while bringing droughts to others.

With this parameteritation as a start, it may be possible to achieve greater understanding some of the paleo-climates and their radical changes which led to the possible extinction of numerous prehistoric fauna. Further research along this line may also reveal how close man may be to radically altering his own climate.

Evidence of asymmetric spiral divergence fields appearing in the climate may be found in Kornfield (1969) where cloud bands appaer as straight lines in Mercator projections and log spiral bands in stereographic projections. The bands are time averages over weeks and months. Any phenomenon which is a straight band in a Mercator projection is also a spherical log spiral with the pole as its center. The same is true of a stereographic projection. Any phenomenon in such a projection is also a spherical log spiral if it shows up as an ordinary log spiral in this projection. Kornfield's cloud averages appear as both.

APPENDIX C

ON THE GENERAL CIRCULATION AND BANDING OF THE

ATMOSPHERES OF JUPITER AND THE OUTER PLANETS

by

Francis H. Nicholson, Ph.D.

I. Introduction.

The transit of the Voyager spacecrafts past Jupiter and
Saturn provided an unequaled closeup view of the features
of the Jovian and Saturnian atmospheres. The spacecraft
obtained explicit details of their banded structure as well
as movement of atmospheric features revealing the zonal
general circulation. Thus far, there has been no theory
extant which simply and concisely explains the atmospheric
banding or general circulations, let alone the structure
of the elliptically-shaped storms appearing between the
bands, major among which is the Great Red Spot, itself
characterized by spiral bands.

Nicholson (1983), in a report to the Office of Naval
Research, proposed a new General Field Theory for Vortex
Structure and Interaction. This field theory advances five
new laws of physics and a new branch of mathematics. The
laws are field laws and as such describe the structure of
the vortex and the behavior of vortex interaction. The
number and kind of phenomena to which the field theory has
been applied are extensive. These phenomena include
waterspouts, tornadic winds and funnels, hurricanes, extra-
tropical storms, the general circulation of Earth and
spiral features around the Venusian poles, and now the
atmospheric banding and circulation of Jupiter and Saturn,
and quite possibly Uranus and Neptune. The field theory
further provides models of the circulation of the Great Red
Spot, nuclear fireballs, smoke rings, and circulation and
pressure distribution of toroidal plasmas in nuclear fusion
reactors. Moreover, the movement of stars and the structure
of spiral arms in spiral galaxies, the winding of spiral
fronts of extratropical storms, the hook echoes of tornados,
and the flow field in laboratory Dines vortex cages are all
modelled.

An attempt to duplicate the full field theory will not be
made here; only that part of the theory relevant to the
atmospheres of Jupiter and Saturn will be discussed.

II. The First Two Field Laws of Vortex Structure.

Of the five laws proposed to govern vortex structure and
interaction, the first two are described by solution of
the two-dimensional Laplace's equation applied to the
divergence and vorticity fields in the general circulation.
The two dimensions constitute the surface of the sphere.
The divergence, δ, occurs within that surface. The vorticity,
ζ, is normal to it. Therefore,

$$\nabla_2^2 \begin{bmatrix} \zeta \\ \delta \end{bmatrix} = 0, \infty \tag{1}$$

(the Laplacian is either zero or undefined) where $\zeta = k \cdot \nabla_2 \times U$,
and $\delta = \nabla_2 \cdot U$. U is the velocity and k is the unit vector
normal to the spherical surface containing the two dimensions
of interest.

Let us assume that the bands on Jupiter and Saturn represent
alternating upwelling and downwelling accounting in turn for
the different band colors due to different physical phases
and/or chemical composition for the rising, as opposed to
sinking, gases of the planetary atmospheres. Then the bands
would represent solutions to the divergence field. The spec-
ific solutions are indicated by band spacing which corresponds
to the placement of nodes in the solution to the divergence
field.

The conventional solutions to Laplace's equation on a sphere
are called spherical harmonics. Bands such as are observed
on the outer planets varying solely with latitude are further
termed zonal harmonics and are discussed below.

III. Zonal Harmonic Solutions to the First Two Laws.

Laplace's equation for scalar psi (ψ) in spherical coordinates is given by

$$\frac{1}{r^2}\frac{\partial}{\partial r}\left[r^2\frac{\partial\psi}{\partial r}\right] + \frac{1}{r^2\sin^2\theta}\frac{\partial}{\partial\theta}\left[\sin\theta\frac{\partial\psi}{\partial\theta}\right] + \frac{1}{r^2\sin^2\theta}\frac{\partial^2\psi}{\partial\phi^2} = 0. \quad (2)$$

This equation separates as follows:

$$\psi = R(r)\,\Theta(\theta)\,\Phi(\phi), \quad (3)$$

$$\frac{d^2\Phi}{d\phi^2} + m^2\Phi = 0, \quad (4)$$

$$\frac{1}{\sin\theta}\frac{d}{d\theta}\left[\sin\theta\frac{d\Theta}{d\theta}\right] + \left[n(n+1) - \frac{m^2}{\sin^2\theta}\right]\Theta = 0, \quad (5)$$

$$\frac{1}{r^2}\frac{d}{dr}\left[r^2\frac{dR}{dr}\right] - \frac{n(n+1)}{r^2}R = 0. \quad (6)$$

Solutions of the second equation are the Legendre functions

$$P_n^m(\cos\theta) = \sin^m\theta\ T_{n-m}^m(\cos\theta). \quad (7)$$

The functions where $m = 0$ are called zonal harmonics. Since these functions depend only on θ, the nodal lines divide the sphere into zones.

Letting $x = \cos\theta$, the general solution to the second equation in the case where $n = 0, 1, 2, 3, \ldots$ is given by

$$y = c_1 P_n(x) + c_2 Q_n(x)$$

where $P_n(x)$ are Legendre polynomials and $Q_n(x)$ are Legendre functions of the second kind which are unbounded at ± 1.

Not only are two different Legendre polynomials orthogonal
in the interval $-1 < x < 1$, but if $f(x)$ satisfies the Dirich-
let conditions, then at every point of continuity of $f(x)$
in the interval $-1 < x < 1$ there will exist a Legendre series
expansion having the form

$$f(x) = A_0 P_0(x) + A_1 P_1(x) + A_2 P_2(x) + \ldots$$

$$= \sum_{k=0}^{\infty} A_k P_k(x) \tag{8}$$

where $A_k = \dfrac{2k+1}{2} \int f(x) P_k(x)\, dx$. $\tag{9}$

This being the case, then, any solution of Laplace's eq-
uation for the divergence and vorticity fields may be
expressed as a Legendre series, and any solution of the
general circulation must be a spherically integrated
Legendre series since

$$\zeta = \frac{1}{r \sin \theta} \frac{\partial}{\partial \theta} \sin \theta\, U_\phi = \sum_{k=1}^{\infty} A_k P_k(\cos 2\theta), \tag{10}$$

so that

$$U_\phi = \frac{1}{\sin \theta}\, r \int_0^\theta \sin \theta \sum_{k=0}^{\infty} A_k P_k(\cos 2\theta)\, d\theta, \tag{11}$$

where A_k are the series coefficients; $P_k(\cos 2\theta)$ are
the Legendre polynomials, and U_ϕ is the zonal velocity.

IV. Analysis of Legendre Coefficients.

Haltiner and Williams, in chapter 6 of their text, Numerical
Prediction and Dynamic Meteorology, discuss in some depth the
problem of integrating Legendre polynomials over a sphere to
obtain the series coefficients discussed above in (9). In
particular, application of the spectral method to the barotropic
vorticity equation is discussed using the Galerkin method.

Specifically, the Legendre integrals in latitude are
evaluated by Gaussian quadrature following Eliasen et
al. (1970). If the integrand is denoted by Q(x), we may
have the following expression for the non-linear terms:

$$F_{m,n} = \frac{1}{2} \sum_{k=1}^{K} G_k^{(K)} Q(x_k) \tag{12}$$

Haltiner and Williams say, "The summation is carried over
K values of x_k where the x_k's are roots of the Legendre
polynomial $P_{0,k}$ and $G_k^{(K)}$ are the corresponding Gauss
coefficients. The formula is exact for any polynomial of
degree smaller than or equal to 2K-1. Thus, apart from
roundoff errors, no approximation is introduced by computing
the integral when a sufficiently high value of K is used."

V. Application.

Since numerical methods exist for determining the basis
functions describing the divergence and vorticity fields,
the task remaining is to apply these methods to the data
at hand.

Since neither vorticity nor divergence may be measured
directly, it is necessary to utilize measurements of planetary
albedo and circulation. The albedo measurements in the
terrestrial atmosphere are closely correlated with low-level
divergence fields which induce cloudiness through phase change
of water vapor due to updrafts and consequent cooling. Similar
phase changes in methane (CH_4) and ammonia (NH_3) on Jupiter
and Saturn may arise out of pseudoadiabatic cooling due to
upwelling.

Determination of the appropriate Legendre polynomials by
Gaussian quadrature to fit the albedo maps of both planets
should give an indication of the underlying divergence field

and the zonal harmonics satisfying Laplace's equation.

The vorticity may easily be determined by finite differencing
of the circulation data after weighting by the sine of the
colatitude. The procedure given above may be employed to
obtain the zonal harmonics for the vorticity fields.

The findings may then be compared and the spectral energy of
the vorticity and divergence fields may be assessed. Peaks
or concentration in the spectra indicate fidelity to the two
proposed physical laws. Preliminary investigations are
examined below.

VI. Preliminary Findings.

Preliminary examinations of Legendre series' integrated over
the surface of a sphere to obtain the corresponding planetary
circulations demonstrate patterns and potential for spectral
grouping. These groupings suggest applicability as solutions
to Laplace's equation expressed in the proposed physical laws
mentioned above.

Major aspects of patterns in both the Jovian and Saturnian
circulations have been synthesized by the addition of a minimal
number of polynomials in the Legendre series. Given a set of
reasonable assumptions, to be described shortly, description of
the circulations of the two planets appears likely. The first
of these assumptions, which is supported by data, is that the
circulation described by integration of a polynomial in $\cos \theta$
over 2θ radians is similar in its general features to one
described by integration of the same polynomial in $\cos 2\theta$ over
θ radians, or

$$U_\phi = \frac{1}{\sin \theta} r \int_0^{2\theta} P_n (\cos \theta) \, d\cos \theta \approx \frac{1}{\sin \theta} r \int_0^{\theta} P_n (\cos 2\theta) \, d\cos \theta \quad (13)$$

This is an important assumption since the left-hand side of (13)

may be integrated directly by inspection to a polynomial of
one degree higher, while the right side of (13) may not.
This assumption is important in estimating the circulation
of Jupiter.

The second assumption, derivative from the first, is that if
a short series of Legendre polynomials may be found approx-
imating a planetary circulation (as in the case of Saturn),
then another short series probably exists which in integrated
form also represents the planetary circulation. The actual
series, of course, must be found by Gaussian quadrature upon
the properly prepared data itself, following Eliason et al.
(1970). In the first case, an exact rather than numerical
integration, while only an approximation to the series of
interest, is rapid and avoids roundoff errors. Integration
of the right-hand side of (13) by the trapezoidal method
leads to a cumulative error large enough to cause wild
fluctuations after the integration of the polynomial and
division by the sine of the colatitude past $\pi/2$ radians.

Since the integration must show symmetry, the approximation
and exact integration of the left-hand side of (13) is
preferable, replacing the range $0 - 2\theta$ with $0 - \theta$ in the graph
of the results. Comparisons of numerical integration of
circulations for several series and their exact approximations
are given in figure 1. It can be seen that the assumption is
both meritorious and utilitarian. The left-hand side of (13)
may be expressed as

$$U_\phi = \frac{1}{\sin\theta} r \int_0^{2\theta} P_n(\cos\theta)\, d\cos\theta = r P'_{n+1}(\cos\theta) \qquad (14)$$

where P'_{n+1} is not a Legendre polynomial but rather a simple
polynomial of one degree higher than P_n.

The second assumption states that if a series of Legendre

polynomials exists which well-describes the general circulation, there also exists an integrated series of lower degree describing the same general circulation. Or, if the general circulation may be well-described by a short series, then so too may the corresponding vorticity field. The second assumption is merely an alteration of (14), i.e.,

$$U_\phi = \frac{1}{\sin\theta} r \sum_{n=1}^{\infty} \int_0^\theta P_{n-1}(\cos 2\theta)\, d\cos\theta = r\sum_{n=1}^{\infty} P_n(\cos 2\theta) \quad (15)$$

In the first assumption applicable to the circulation of Jupiter shown in Figure 2, the integration of the series

$$\frac{1}{\sin\theta} \int_0^{2\theta} \{P_{10}(\cos\theta) - P_9(\cos\theta)\}\, d\cos\theta$$

is substituted for

$$\frac{1}{\sin\theta} \int_0^\theta \{P_{10}(\cos 2\theta) - P_9(\cos 2\theta)\}\, d\cos\theta$$

and is shown in figure 3.

The general features are well-represented, particularly the outlying foothills leading up to a topographic feature characterized by an inflection point reminiscent of the integrated series

$$U_\phi = \frac{1}{\sin\theta} \int_0^{2\theta} \{P_4(\cos\theta) - P_3(\cos\theta)\}\, d\cos\theta \quad (16)$$

shown in figure 4.

Obviously, the final assessment must come from an analysis of the data itself by Gaussian quadrature, where any set of data will be representable by a Legendre series. Hopefully, this series will be confined to a handful of polynomials, as is indicated by the synthesis of $P_{10} - P_9$ and $P_4 - P_3$.

The circulation of Saturn shown in fig. 5 is simulated in fig. 6 by the series $P_{10}(\cos 2\theta) - 0.8P_9(\cos 2\theta) - 0.2P_1(\cos 2\theta)$ shown in figures 7, 8 and 9, respectively. By the second assumption, also only verifiable by analysis of the data by Gaussian quadrature, there exists a series of polynomials which satisfies the vorticity field of Saturn. The actual polynomials are probably closer to $P_8 - P_7$, which would account for fewer wave numbers in the circulation spectrum, while retaining the central Everest among the lesser foothills.

It should be pointed out that even solid rotation with a vorticity of $2\Omega \cos \theta$, the Coriolis parameter of the vorticity of a solid rotation sphere, is itself a Legendre polynomial of the first kind, $P_1(\cos \theta) = \cos \theta$.

Again, both Jupiter and Saturn have circulations bearing striking similarities to the difference of the two close Legendre polynomials including central plateaus ($P_4 - P_3$), central peaks ($P_{10} - P_9$) and attendant foothills increasing in amplitude from the poles toward the equator.

In any event, the determination of the Legendre polynomials representing the vorticity field derived from the Saturnian circulation should prove both interesting and rewarding.

VII. The Great Red Spot.

The Great Red Spot is characterized by ellipticity and bands
similar to log spirals but displaying the same elliptic
distortion as the spot itself. From Appendix A it is evident
that this system may be analyzed in either elliptic coordin-
ates or its spherical equivalent, conical coordinates. For
simplicity's sake, we will restrict ourselves to elliptic
cylindrical coordinates. The nodes in this system are
ellipses and confocal hyperbolas. The terrestrial equivalent
of the Great Red Spot is the extra-tropical storm. This storm
is characterized by the logarithmic spiral bands which move
with the flow, becoming more tightly wound in the flow. The
bands are spherical log spirals and as such have harmonics in
the divergence field satisfying Laplace's equation and thus the
second law, $\nabla_2^2 \delta = 0$.

Parallel to the development of the terrestrial extra-tropical
storm where the vorticity is linear in the logarithm of the
tangent of the scaled half-radial angle, i.e.,

$$\zeta = A + B\ln\tan(\mu/\mu_0), \tag{17}$$

the vorticity of the Great Red Spot should be linear with the
hyperbolic radius, μ, shown in figure 10. The spiral bands
therefore would represent divergence fields satisfying the
elliptic Laplacian

$$\nabla_2^2 = \frac{1}{d^2}(\cosh^2\mu - \cos^2\phi)\left(\frac{\partial^2}{\partial\mu^2} + \frac{\partial^2}{\partial\phi^2}\right)\delta \tag{18}$$

where $\pm d$ are the foci, ϕ the elliptical azimuth, and μ the
hyperbolic radius. The divergence field therefore exhibits
harmonics given by the following:

$$\delta = \sum_{n=1}^{\infty} \delta_0(n)e^{n(\mu+i\phi)}e^{i\alpha} \tag{19}$$

where $e^{i\alpha}$ is the versor rotating the bands into elliptic log spirals. Elliptic log spirals are defined as spirals making a constant inflow angle to the intersected ellipses and hyperbolas. Appendix B outlines a procedure for obtaining a Fourier analysis of these bands for the earthly storm in spiral coordinates. The procedure may be modified for elliptic log spiral coordinates or, to be more precise, conical. The resultant spectral analysis should indicate the fidelity of the theory and applicability to this phenomenon by the ratio of signal to unexplained noise.

VIII. Conclusion.

Appendix C contains the application of the general field theory for the terrestrial and possibly Venusian atmospheres. Evidence of validity for the outer planetary circulations lends credibility to assessment of the circulations of the inner planets by the different application of the appropriate laws. The inner planets are characterized by low rotation rates and strong insolation. The outer planets display more rapid rotation and very much lower insolation. The inner planets display significant meridional transport consonant with their rotation rates and radiation balance differential between the poles and the equator. This is manifest in the spiral bands in cloud averages shown by Kornfield (1969) and in the spiral bands around the Venusian poles (Krauss et al., personal communication). The outer planets seem to have predominantly zonal circulations, evidence of which appears in the banding which we hope to explain by zonal harmonics in the planetary divergence field.

The inner planets are referred to as terrestrial planets, and the outer planets as Jovian; there are a number of factors which separate the two types. Of interest here is the distance from the sun, which is small for the terrestrial planets, 0.4 to 1.4 Astronomical Units (AU), and large for the Jovian planets,

C-11

5.2 to 30.1 AU. Bearing in mind that the strength of the
insolation falls away as the square of the radius, then
Jupiter receives less that 1/25th of the unit insolation of
Earth. Saturn, on the other hand, receives less that 1/170th
of the insolation of Venus. The radiation gradient in the
infrared is correspondingly much greater for the terrestrial
that the Jovian planets and requires meridional transports to
achieve balance. Slow rotation rates make this possible.
Jupiter and Saturn, on the other hand, with rotation rates
of the order of ten and eight hours, respectively, and an
almost vanishingly small insolation gradient between the poles
and the equator, have less need and less allowance for merid-
ional transport.

The rotation rate of the terrestrial planets is moderate to
slow, with Earth the fastest, 24 hours to 243 days; for the
Jovian planets, 8 to 16 hours. Moreover, Uranus is tilted so
far in its orbit that its North pole pointed toward the Earth
in 1946.

The exciting possibility raised by assessment of the relevance
of the General Field Theory to the circulations of the Jovian
planets is that there already exists such an application
tailored for the terrestrial planets and included in Appendix
C. Over and above the applications contained in Appendix C,
evidence of spiral bands in the climatological divergence
field are apparent in both terrestrial and Venusian atmospheres.
In Kornfield et al. (1969), the cloud bands appear as straight
bands emanating at an angle from the South pole when displayed
on a Mercator projection. This is the sine qua non for the
bands to be logarithmic spirals on a sphere described in each
of the appendices. The occurrence of such bands was postulated
in 1974 when Appendix C was first written and included among the
abstracts for the conference held in Germany. A solution to
Laplace's equation on a sphere may be given by spiral bands

having a constant inflow angle. Such a spiral is a straight
line on a Mercator projection, or an _ioxodrome_ or ship path
of constant angle with lines of longitude.

Conceivably, the Inter-Tropical Convergence Zone, which seems
to migrate back and forth across the equator in a seasonal
manner, is a convergence zone in a Legendre polynomial for a
field defined in the tropics, whereas the rest of the planet's
circulation is modelled more on the meridional mode given in
Appendix C. Laplace's equation may have different solutions
for different regions, as long as the boundary values are
appropriately matched. Thus, the terrestrial atmosphere may
represent a transition between the other terrestrial planetary
atmospheres and the truly Jovian atmospheres.

If this is the case then it is important to understand whether
there is a trigger mechanism by which the planet may go from
one circulation type to another. Is the Earth's atmosphere
now in a delicate balance between the two types, and could man-
made atmospheric changes tilt it one way or the other? Could
lack of meridional transport initiate another ice age? Is an
ice age indicative of a more general Jovian circulation on Earth?
Bearing in mind that the present climate is an inter-ice age
climate, is it not reasonable that there is a manifestation of
Jovian circulation in the tropics in the presence of the ICTZ?

There are both short- and long-term benefits to this study. A
field theory explaining both the Jovian and terrestrial types
of atmospheres has ramifications in the short run for a poss-
ible explanation for the mechanism of the advance and retreat
of the ice age circulation and the behavior of the atmosphere
at rest, where $\zeta \propto P_1(\cos \theta)$.

In the long run a conceptual structure such as the field theory
can be checked to see if it is scientifically "true." Accord-
ing to Holton (1979), Einstein felt that such "truth" "depends

on how nearly the aim of making a system deal with a large
amount (ideally, cover the totality) of diverse sense exper-
ience has been achieved, and how economical or parsimonious
the introduction of separate basic concepts or axioms into
a system has been.... A really good theory, one that has a
high scientific 'truth' value,   is correct not merely by
virtue of not harboring any logical contradictions, it also
allows a close check on the correspondence between the pred-
ictions of the theory and a large range of possible exper-
imental experiences. He summarized all this in the following
way: 'One comes nearer to the most superior scientific goal,
to embrace a maximum of experimental content through logical
deduction from a minimum of hypotheses.... One must allow
the theoretician his imagination, for there is no other poss-
ible way for reaching the goal. In any case, it is not an
aimless imagination but a search for the logically simplest
possibilities and their consequences.'" (The Problem of Space,
Ether and Field in Physics, in the translation by Seelig)

In the Jovian and Saturnian atmospheres there are data of
inestimable value in assessing the fidelity of the General
Field Theory of Nicholson (1983). These data are the digital
albedos of the two planets complete with navigation, the
circulation of the two planets, and the vorticity and albedos
of the Great Red Spot.

Fits of Legendre polynomials to the albedo and derived vorticity
fields and the cross-correlation and spectral grouping would
provide evidence for the General Field Theory on the planetary
scale. The spiral Fourier analysis in elliptic coordinates and
the assessment of the circulation of the Jovian storm to determine
whether or not vorticity is linearly proportional to the hyper-
bolic distance supplies evidence for such applicability on the
planetary synoptic level. Both instances provide a powerful new
set of tools for understanding the atmospheres of not only the
Jovian planets Jupiter, Saturn, Uranus and Neptune, but ultimately
the terrestrial planets, especially Venus and Earth.
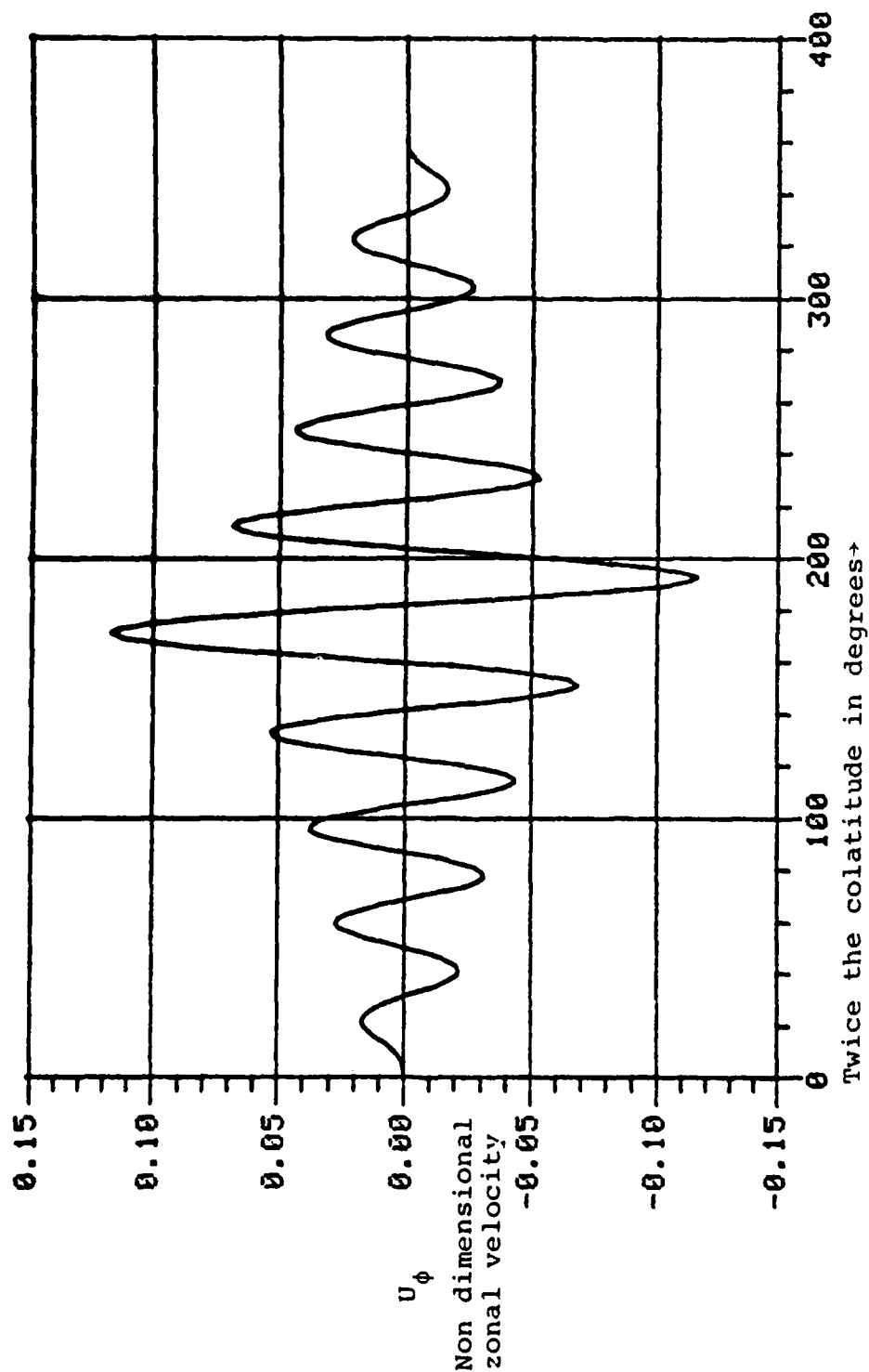
Figure C-1a: Legendre series $P_{10}(\cos\theta) - P_9(\cos\theta)$ integrated over 2π radians and weighted by the sine of the colatitude to simulate a circulation field on a sphere whose vorticity field is described by zonal harmonics given by the Legendre series above.
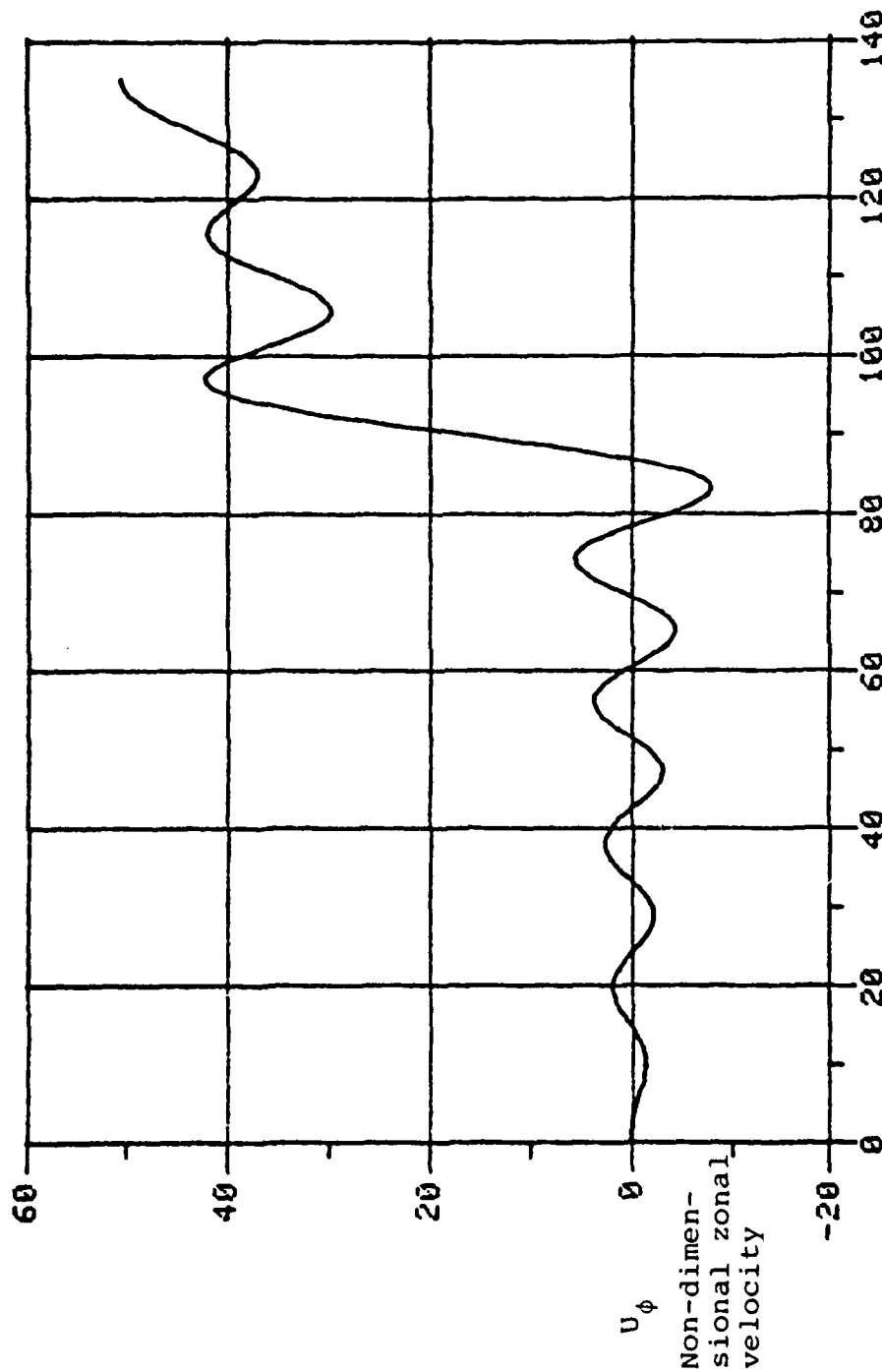
Colatitude in degrees→

Figure C-1b: Series as in C-1a, only in cos 2θ integrated by trapezoidal rule. Range is 0 to 135°. With exception of wild fluctuation due to numerical instability beyond 90° curve is very similar to 1a. Maxima and minima are very nearly coincident (although reversed) and nodes as well. Fluctuation beyond 90 is reason for substitution.

Colatitude in degrees→
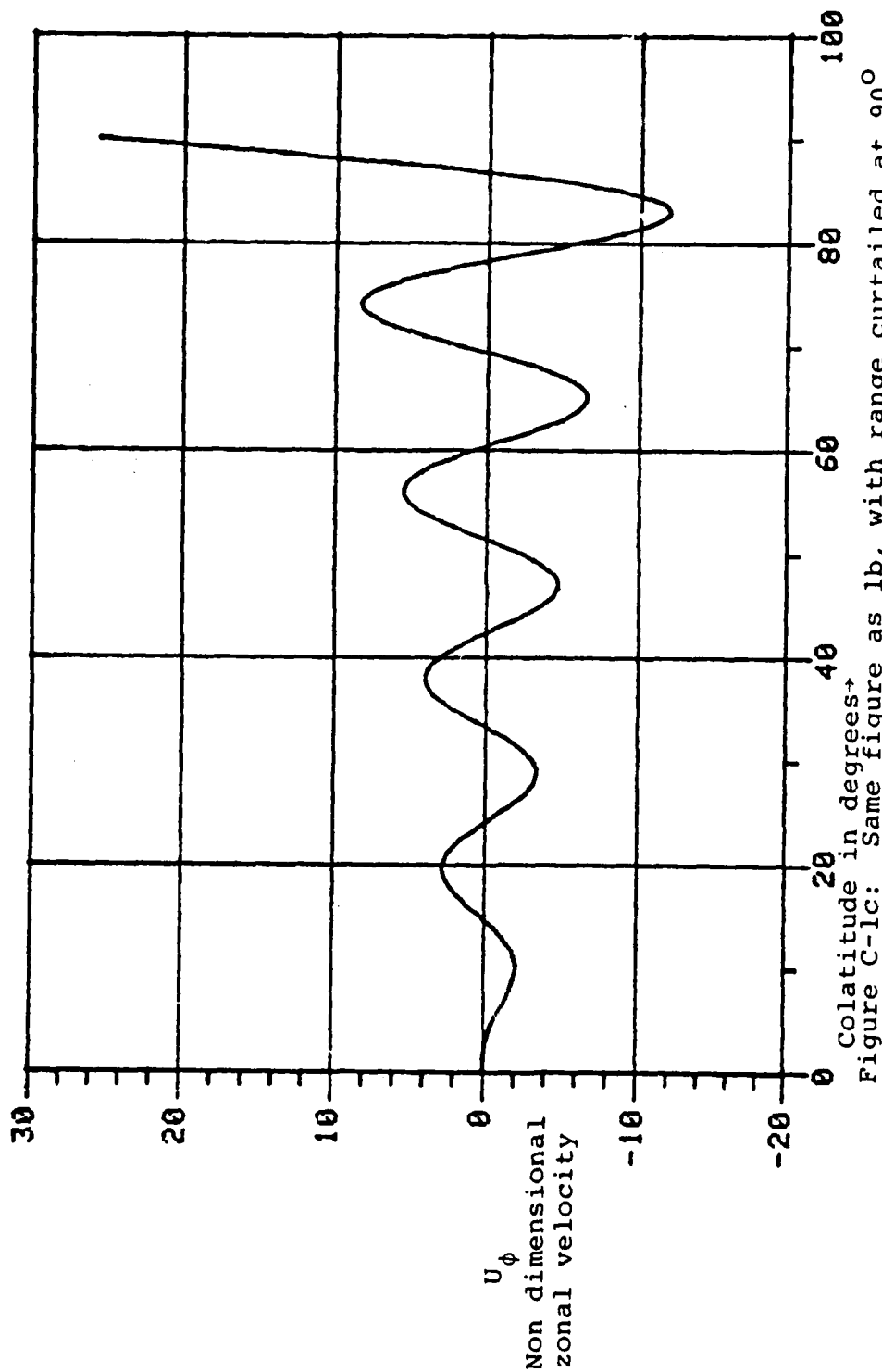
Figure C-1c: Same figure as 1b, with range curtailed at 90°
to demonstrate similarities of actual integration
with approximation given in 1b. Reversal of the
figure would give greater fidelity. Overall features
including increasing amplitude of foothills lead-
ing to central peaks, number and spacing are well
reproduced.

U_ϕ
Non dimensional
zonal velocity

MICROCOPY RESOLUTION TEST CHART
NATIONAL BUREAU OF STANDARDS-1963-A

Colatitude in degrees→
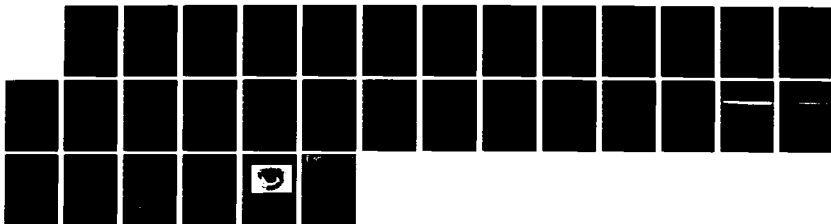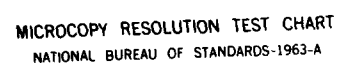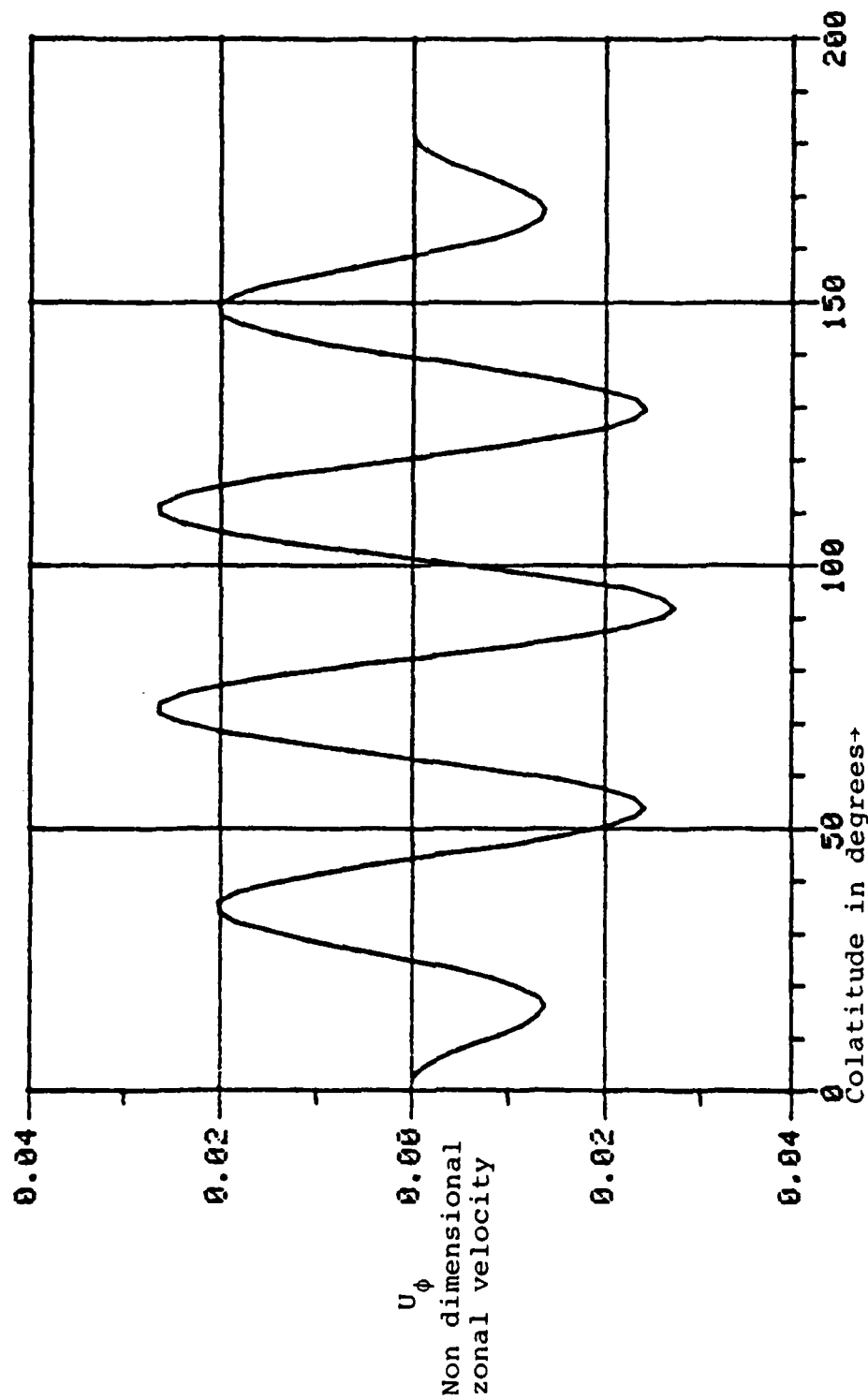
Figure C-1d: Legendre series $P_5(\cos\theta) - P_4(\cos\theta)$ integrated over π radians and weighted by the $\csc\theta$ to simulate planetary circulation with vorticity described by zonal harmonics in above series.

U_ϕ
Non dimensional
zonal velocity
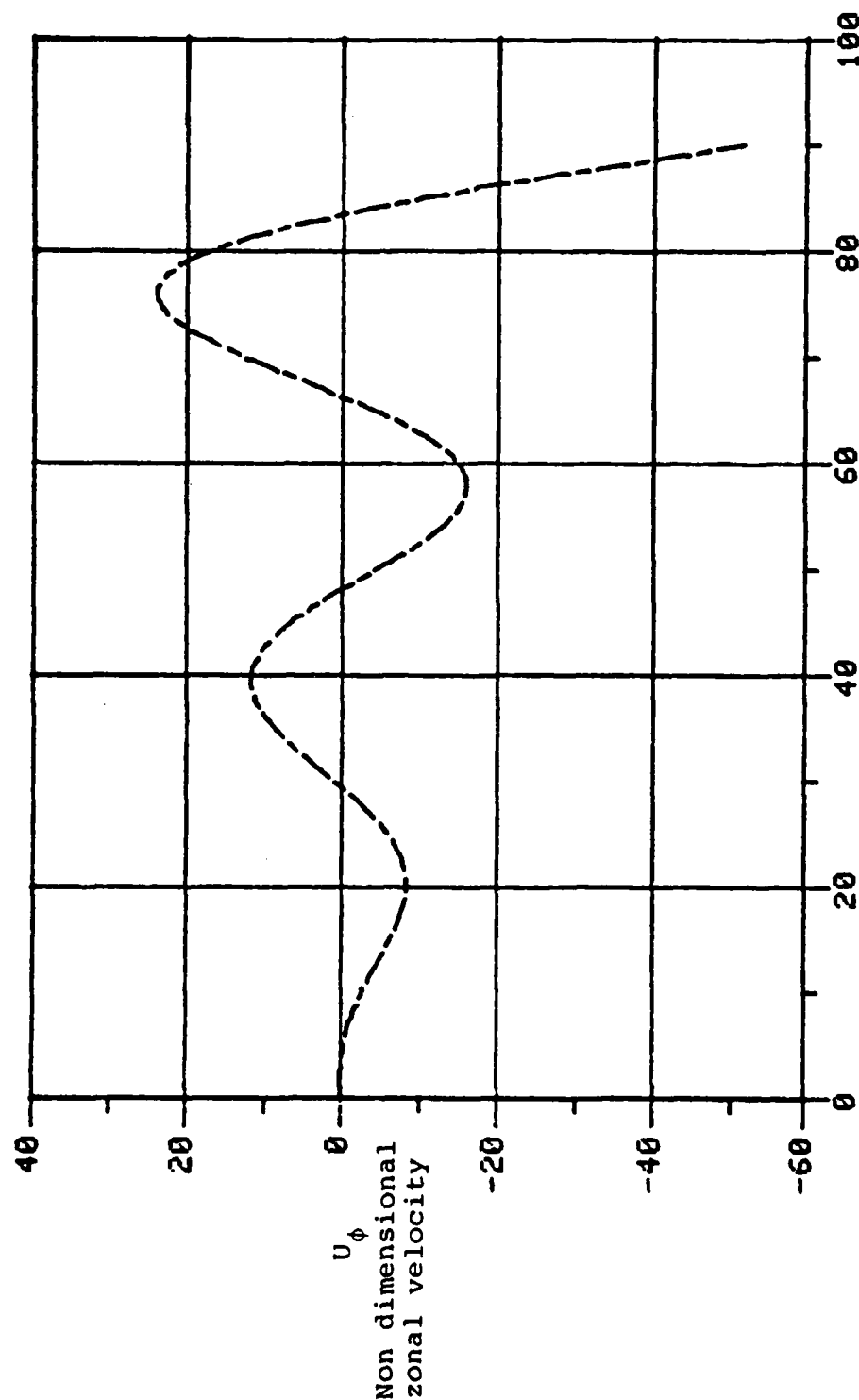
Colatitude in degrees→

Figure C-le: Numerical integration of $P_5(\cos 2\theta) - P_4(\cos 2\theta)$ by trapezoidal rule. Similarity to 1d is evident in number and placement of maxima, minima and nodes, as well as increase in amplitude toward 90°.

U_ϕ

Non dimensional zonal velocity

C-19
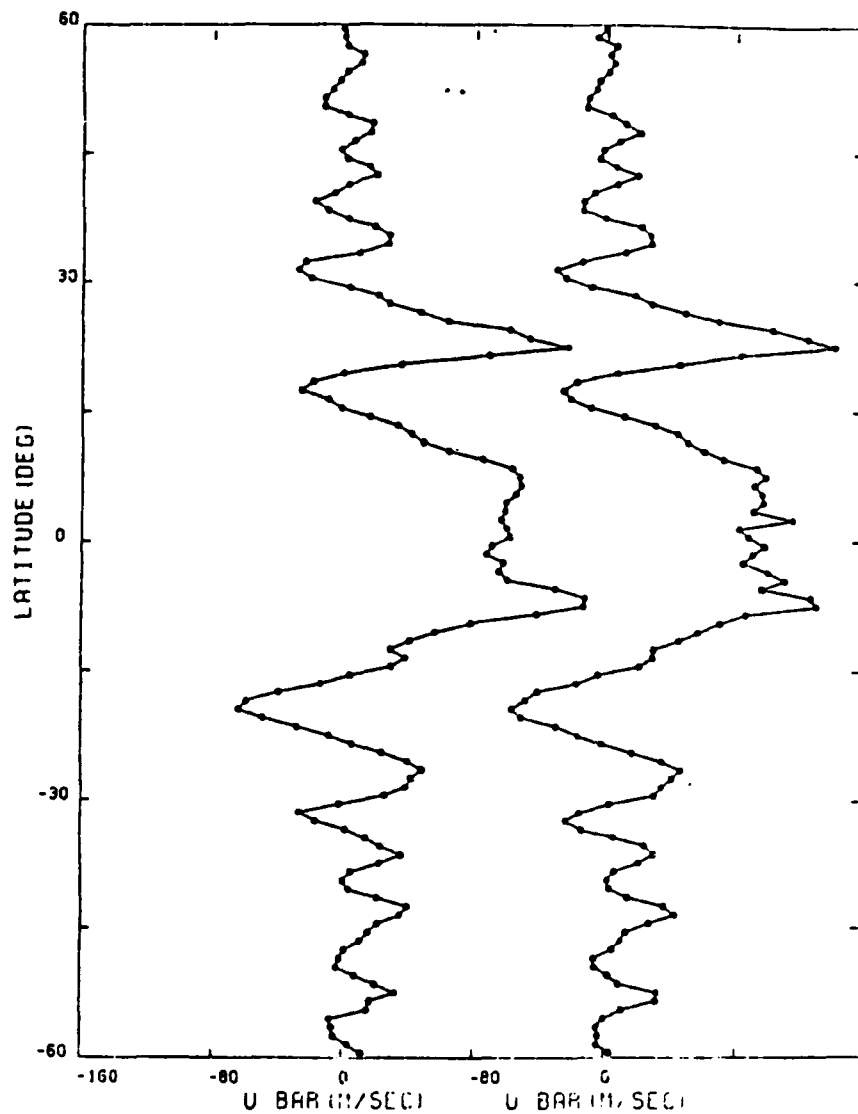
FigureC2. Comparison of zonal velocity $\bar{u}$ in late
February 1979 (Voyager I, left) with that in early
July 1979 (Voyager 2, right). The correlation coef-
ficient is 0.986 for the two curves.
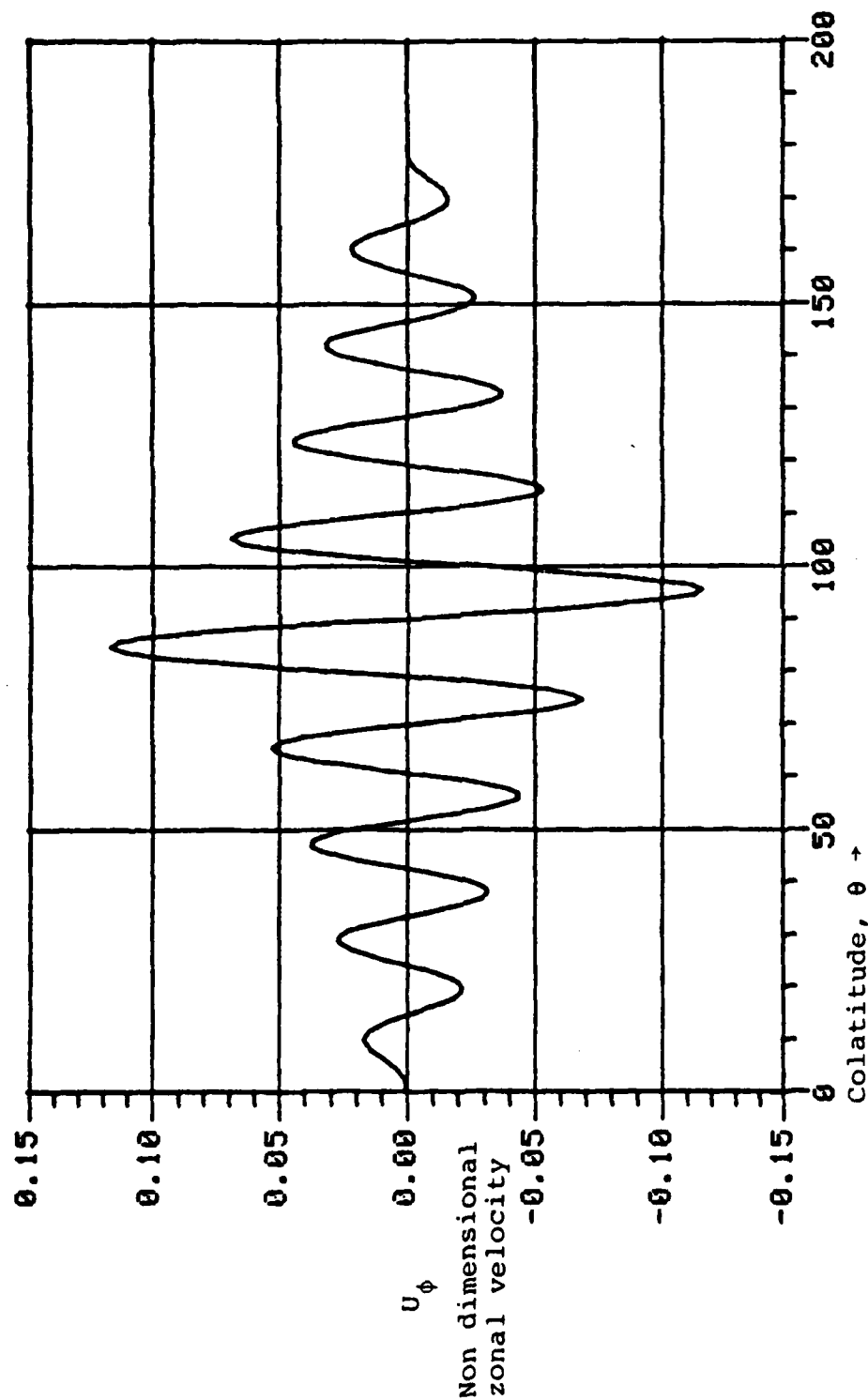
Figure C3. Simulation of main aspects of Jovian zonal circulation by $\csc\theta \int_0^{2\theta} \{P_{10}(\cos\theta) - P_9(\cos\theta)\} d\cos\theta$. Actual Legendre coefficients must be found by appropriate Legendre analysis as described in text. This simulation is for feasibility purposes only.
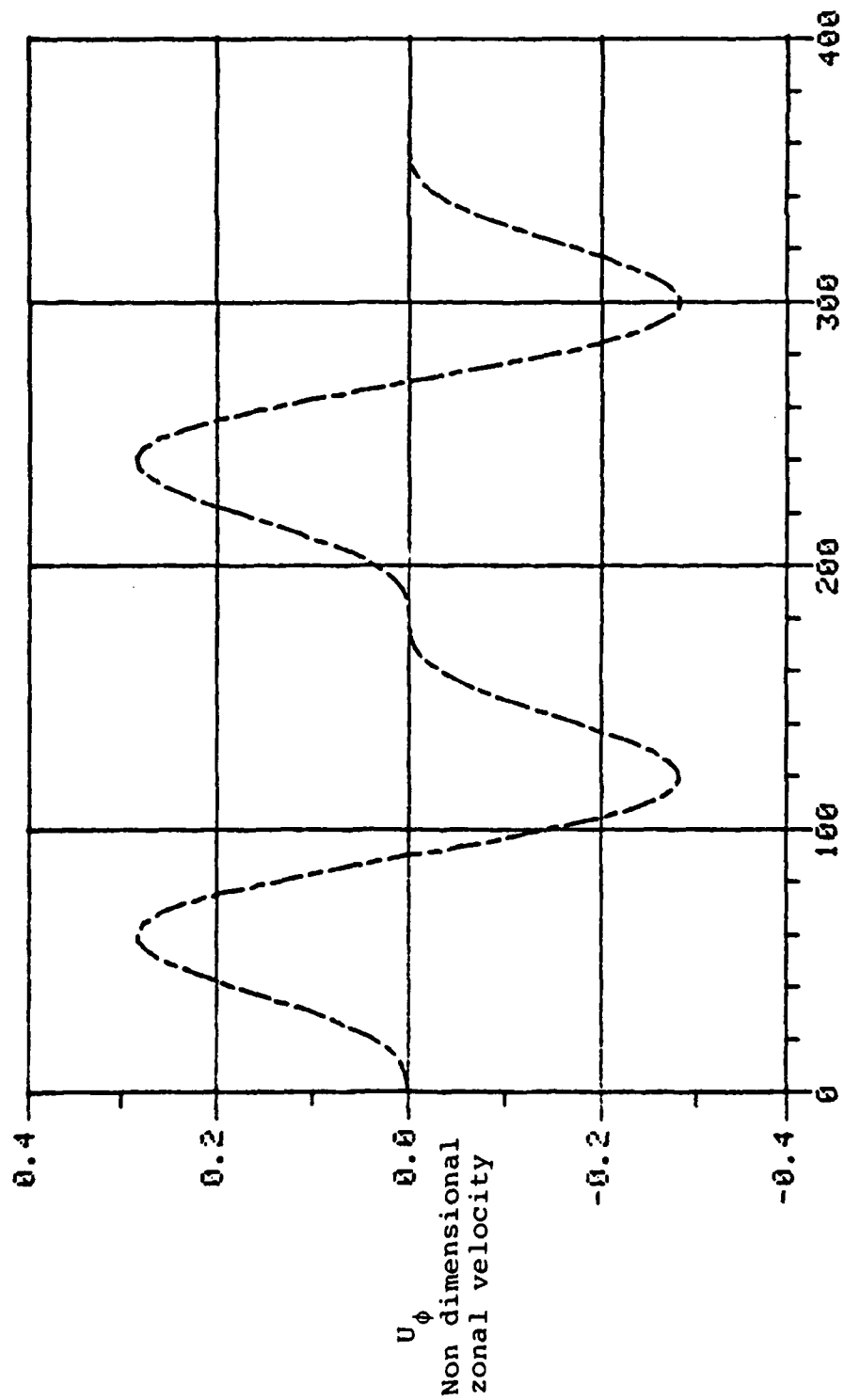
Twice the colatitude →
FigureC4.   Integrated Legendre series $\csc\theta/2\theta\{P_4(\cos\theta) - P_3(\cos\theta)\}d\cos\theta$
to demonstrate inflection point at 180°.

C-22
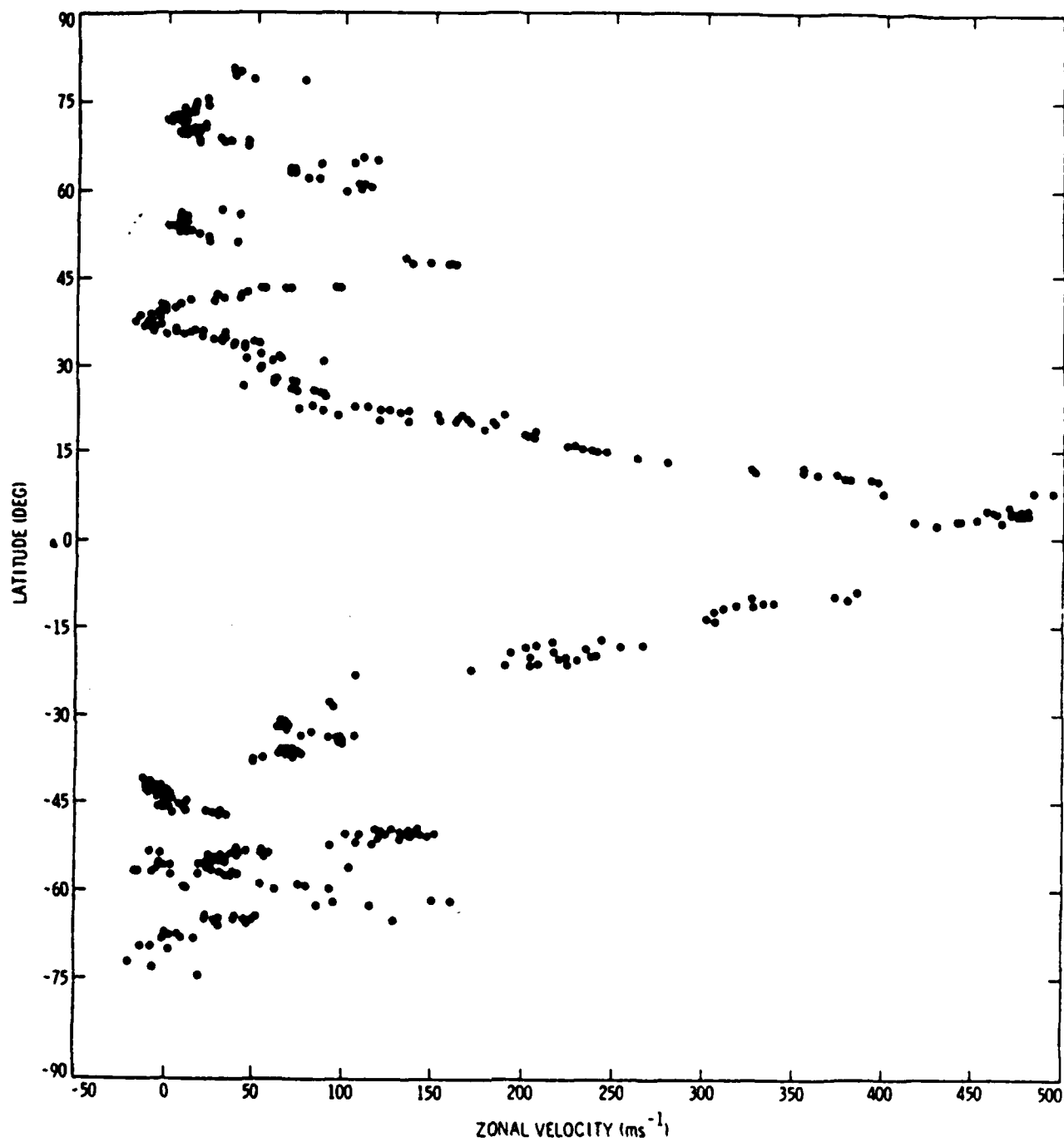
FigureC5. Zonal velocity of Saturn from Voyager flybye, coutesy
           of Andy Collins, Jet Propulsion Laboratory, Pasedena,
           California.

Colatitude, θ →
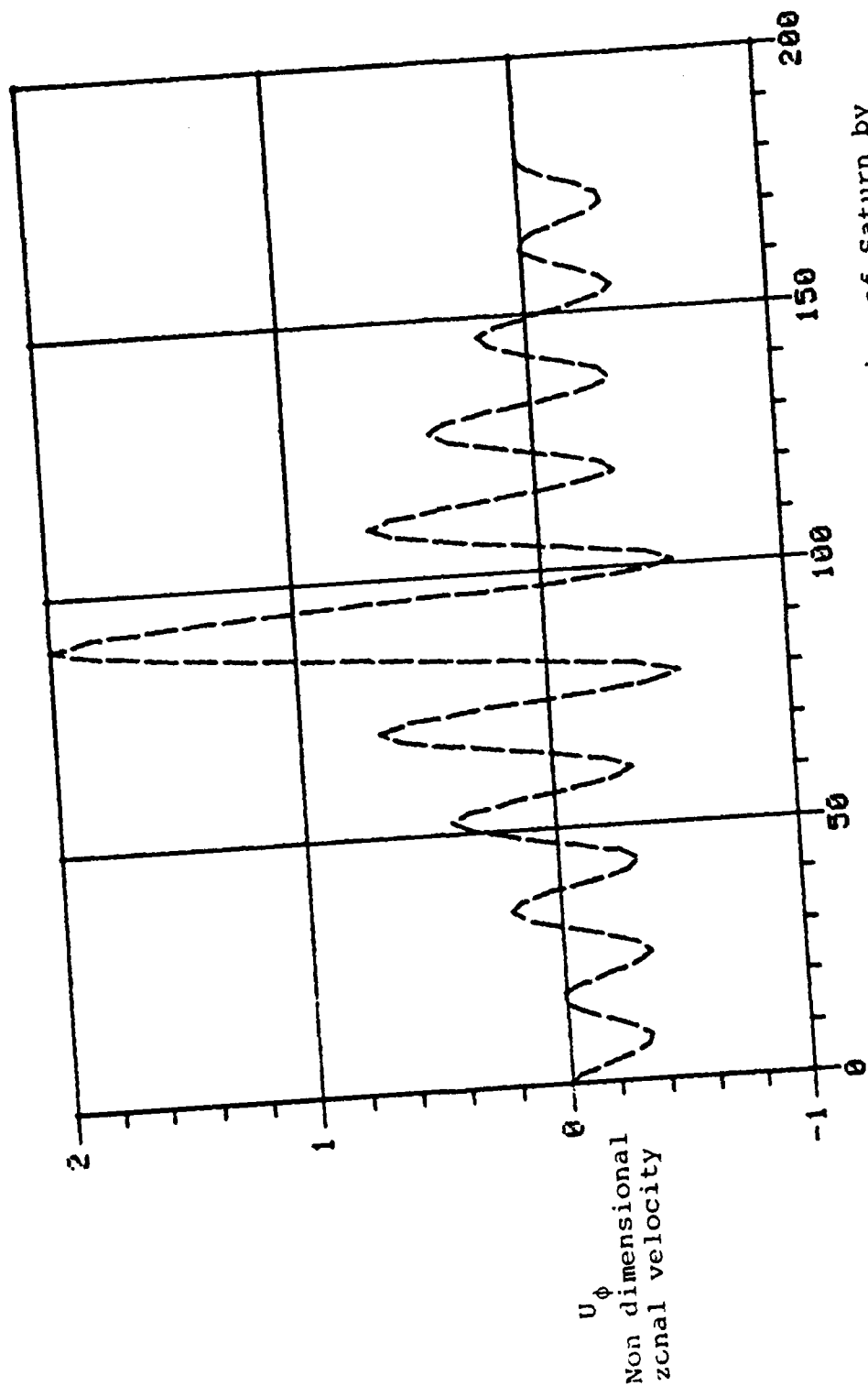
Figure C-6: Simulation of zonal circulation of Saturn by Legendre series $P_{10}(\cos 2\theta) - 0.8P_9(\cos 2\theta) - 0.2 P_1(\cos 2\theta)$. The assumption is that there exists another series integrable to simulate the Saturnian circulation if a Legendre series already exists simulating the circulation in primitive form.

U_ϕ
Non dimensional zonal velocity
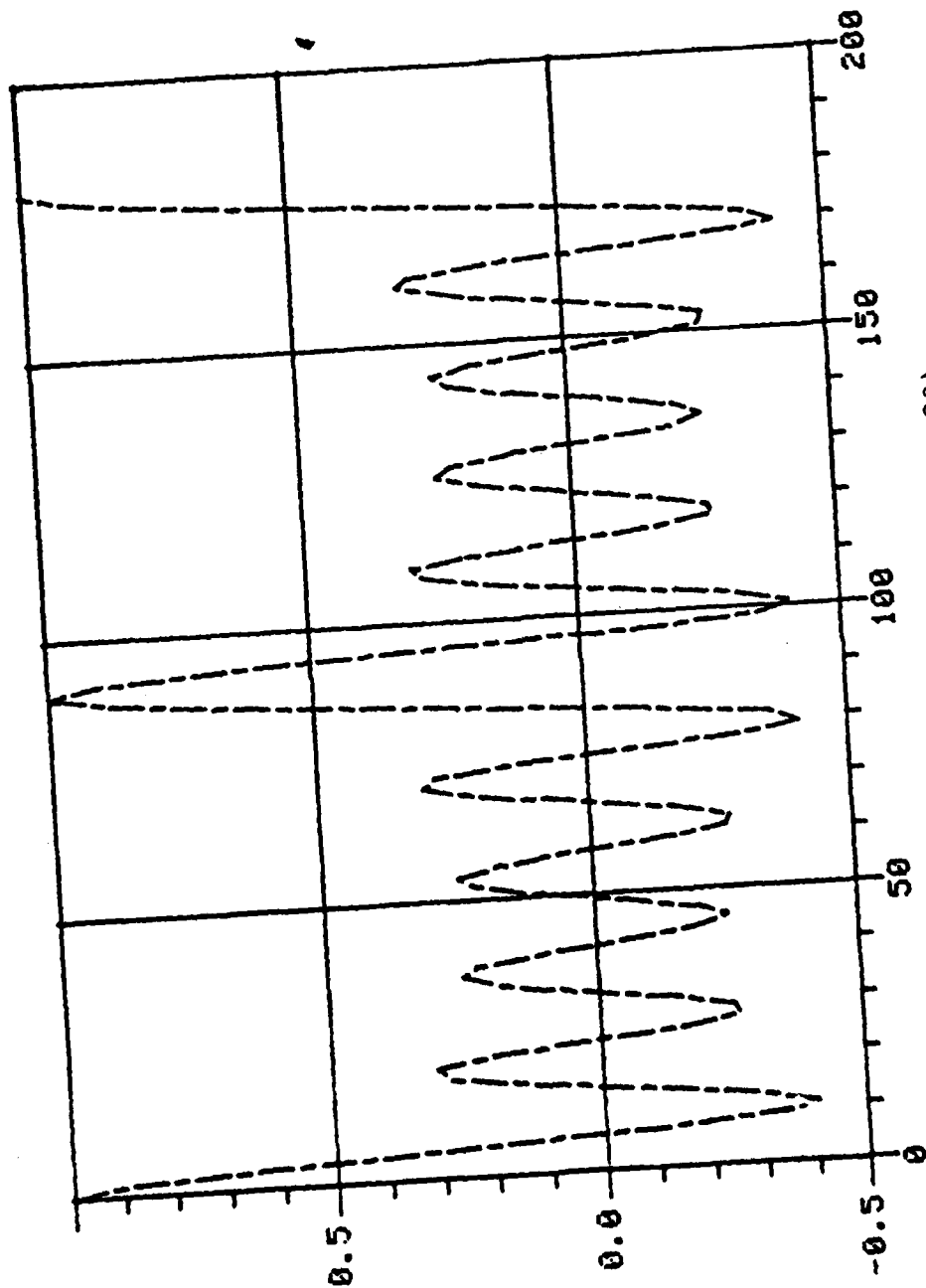
Figure C-7: Legendre polynomial $P_{10}(\cos 2\theta)$.

Figure C-8: Legendre polynomial $P_9(\cos 2\theta)$.

C-26
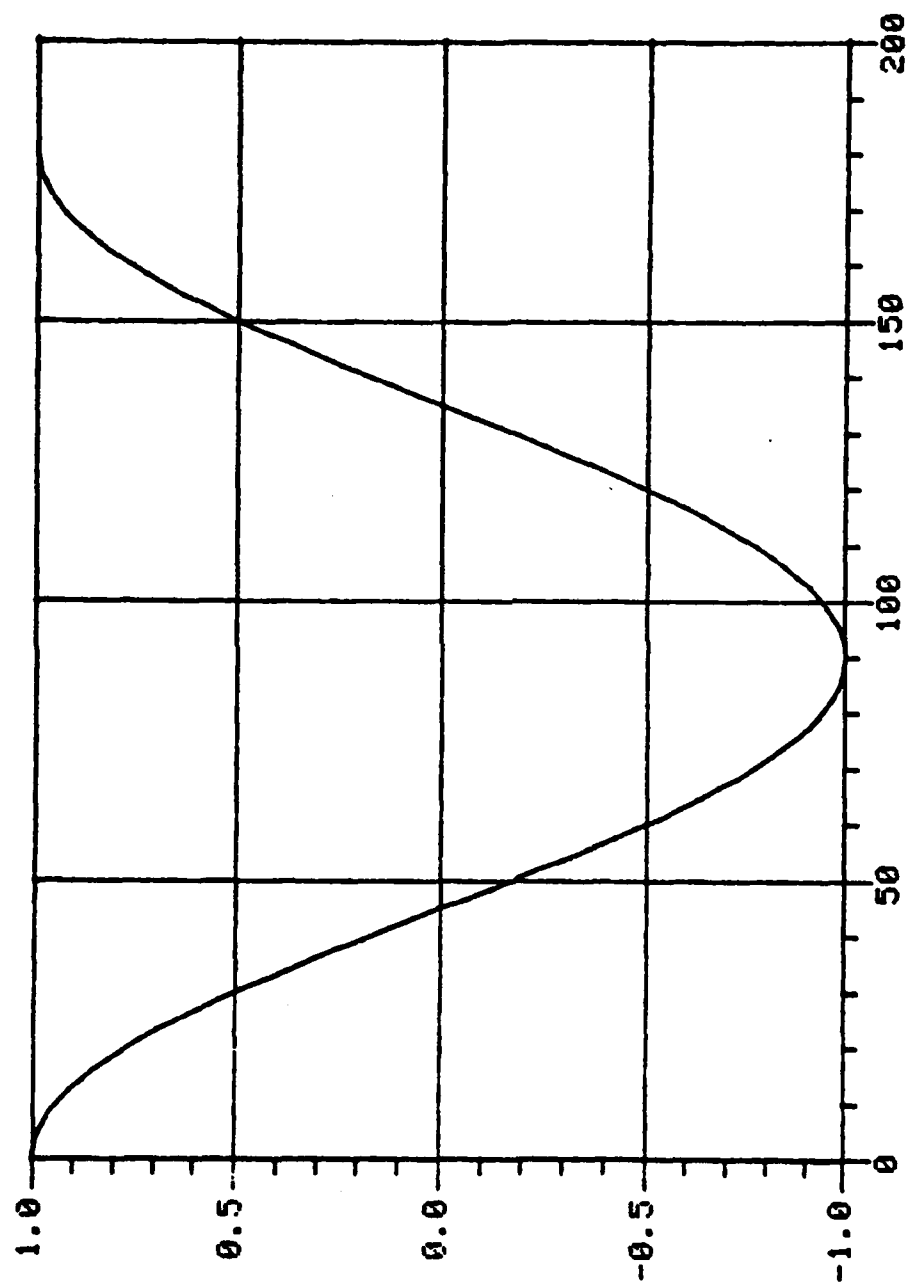
Figure C-9: Legendre polynomial $P_1(\cos 2\theta)$.

Polar Coordinates   **Elliptic Coordinates**
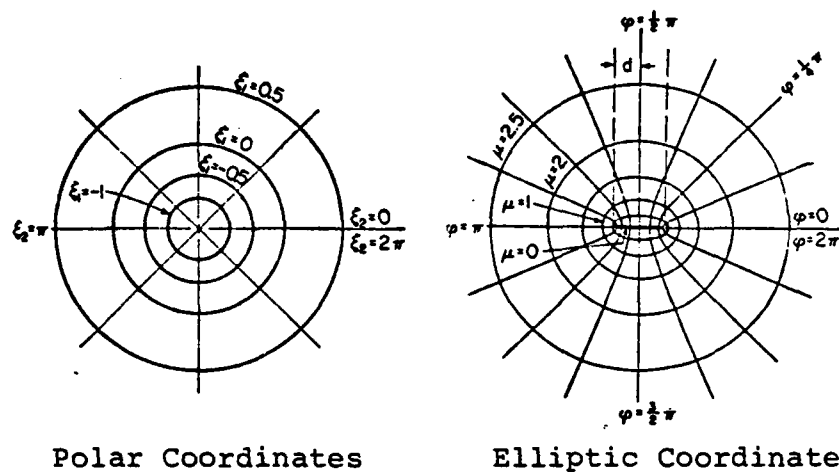
Figure C-10: Comparison of Polar and Elliptic Coordinates.
The isopleths of ξ's represent equal values of $\ln r/r_0$.
The μ's in the elliptic coordinates represent equal
values of the hyperbolic radius. It is by rotation of
ξ,θ coordinates in the first case and μ,ϕ coordinates
in the second case that we obtain the orthogonal log
spiral mutations providing spiral solutions to Laplace's
Equation in both cylindrical variations.

A P P E N D I X   D

ON OPTIMAL DOPPLER RADAR SAMPLING OF

HIGH EXPLOSIVE DETONATIONS

AND

THE CONTAINMENT OF TOROIDAL PLASMAS

by Francis H. Nicholson, Ph. D.

ABSTRACT

A model of the nuclear and high explosive fireball
is proposed in toroidal coordinates where the vorticity
field satisfies Laplace's equation. Recommendations
for ascertaining vortex geometry and subsequent circu-
lation parameters through Doppler and photogrammetric
sampling and their evolution are made.

A model of the contained fusion plasma is pro-
posed in toroidal coordinates where the pressure field
satisfies Laplace's equation. Possibilities of enhan-
cing local pressures through toroidal harmonics to
achieve pressures critical to reaction completion
are considered.

I.   Introduction

Current Model and Code

The modelling of high explosive detonations and, by analogy,
nuclear fireballs currently requires an extensive and complicated
hydrodynamic code based on a physical model of the fireball.
This code incorporates initial shock, buoyancy and the Euler
equations. The code presumes an inviscid fluid and probably
a Hill spherical vortex.

Typically, numerical models of such events simultaneously (or
alternately) solve a series of partial differential equations
by finite difference methods employing a spacial matrix of
points at which values of pressure, temperature, velocity
and sometimes water vapor are specified (and in this case
radioactive debris and byproducts of nuclear fusion) and from
their relations one to another undergo sequential readjustment
in accordance with the governing partial differential equations.

Unfortunately, such a procedure must be initialized and _then_
takes some time to adjust to the shock of initialization. More-
over, the governing equations are defined at a point so that the
evolving field is a function of matrix spacing, simplifying
assumptions, and above all, the physical laws which the equations
purport to represent.

Code Initialization and Data

The code is useless unless initialized. The initialization
depends on data. The ability to procure the data for a high
explosive detonation is limited. Currently, Doppler radar is
the only viable means of obtaining any kind of velocity fields.
Unfortunately, the fields must be obtained by scanning, and
only then provide radial velocities. There is no extant

model available to govern the sampling procedure, let alone to
direct the interpretation of the data for optimal inclusion in
the code. This leaves us in a double bind. On the one hand,
we have a code worthless without initialization. On the other
hand we have a sampling device, but no way to optimize the
sampling in order to achieve proper initialization parameters.
The problem is further complicated by lack of an adequate
physical model governing chaff and/or dust distribution so that
the Doppler radar may operate in the first place. The ultimate
goal of the code is to provide a realistic flow field and per-
haps pressure field simulating the fireball phenomenon and other
sequential vortex phenomena.

II.   The Fireball as a Toroidal Vortex

General Vortex Field Theory

Both a crisis and a resolution are brought about by the discovery
of a new branch of mathematical physics presented in A General
Field Theory for Vortex Structure and Interaction , Nicholson(1983).
The field theory presents, among other things, a toroidal vortex
model based on a proposed law of physics. This law states that
the frictional curl of the fluid parallel to the axial circle of
the torus vanishes (cf Fig. 1), but that the fluid is viscous so
that $\underset{\sim}{F}$, the frictional force, is non zero. Since the frictional
force may be represented as proportional to the Laplacian of the
velocity field, and the order of the operators is immaterial, then
the curl of the Laplacian of the velocity is equivalent to the
Laplacian of the curl of the velocity. Thus the vorticity parallel
to the axial circle of the torus satisfies Laplace's equation.
In mathematical form, then, since

$$\underset{\sim}{F} = \nabla_2 \cdot \nu \nabla_2 \underset{\sim}{U}$$

where ν is the lateral (in the cross sectional circle of the torus)
coefficient of eddy viscosity, then $\underset{\sim}{k} \cdot \nabla_2 \times \underset{\sim}{F} = \nu \nabla_2^2 (\underset{\sim}{k} \cdot \nabla_2 \times \underset{\sim}{U}) = \nabla_2^2 \zeta$,
where ζ is the axial component of vorticity and $\underset{\sim}{k}$ is the unit

vector parallel to the axial circle.

Another way of looking at this is to say that the vorticity grad-
ient is as small as possible under boundary conditions. Laplace's
equation is a field equation. Therefore both the vorticity of
the entire field and the circulation are analytically determined
by boundary conditions. Toroidal coordinates constitute such a
set of boundary conditions since Laplace's equation separates
in three dimensions in these coordinates. Thus the toroidal
nodes may be used to express solutions to this homogeneous,
linear second order partial differential equation.

The toroidal vortex is so structured that it travels through
the enveloping fluid as rapidly as its inviscid counterpart
because the torus actively clears its own path through the am-
bient fluid. Due to the geometry and the requirement of zero
frictional curl the torus propogates with no effective drag.
No slip conditions can be observed on the lateral boundaries
of the rising torus. (cf Fig. 2) By this means the torus both
propogates and retains its structural integrity. Indeed, its
structural integrity is predicated upon its optimal propogation
through the viscous host medium.

Vortex Geometry

Consequently, initialization and evolution of the entire fluid
field is a function of geometry and the field values at the
geometrically determined boundaries. Thus the proper utilization
of a numerical code should be to describe the initial state and
evolution of both the geometry and field boundary values. Point
equations are replaced by field equations. A new branch of phy-
sics describing not only flow but pressure distribution is ini-
tialized and incorporated into a model of the rising fireball.
This model even has physical prototypes such as the smoke-ring
produced by a playful cigarette smoker.

From a negative standpoint, any code which overlooks a relevant
branch of physics (including models, laws, geometry and mathema-
tics) describing vortex evolution is about as relevant as a code
omitting Newton's Laws. The incorporation of the new physics
may not be able to guarentee success, but omission of the physics
is certain to ensure failure.

III.   Scanning the Toroidal Vortex

Toroidal Coordinates

Vertical and lateral Doppler scans, supplemented by photogrammetry,
are called for to determine coordinate geometry and thereby circu-
lation parameters consonent with a vorticity field satisfying
Laplace's equation in toroidal coordinates. First, it would be
useful to review the cross section of a torus given by bipolar
coordinates. Toroidal coordinates are obtained by rotating
bipolar coordinates around the perpendicular bisector of the
line joining the two poles. The coordinate, ξ_0, is the surface
of a torus with axial circle of radius a coth ξ_0 and cross section-
al radius of a csch ξ_0, where

$$\xi = \tanh^{-1}\left(\frac{2\ ax}{a^2 + x^2 + y^2}\right) \quad ; \quad \theta = \tan^{-1}\left(\frac{2\ a\ y}{a^2 - x^2 - y^2}\right)$$

and θ is the angular coordinate ranging from 0 to 2π. The
surface θ_0 is a sphere of radius a csc θ_0 centered at y = a cot θ_0.
Every θ circle goes through the points $\pm$ a,0 in the cross
sectional x-y plane. The complex transformation between the
Cartesian x-y plane and the toroidal (with azimuthal ϕ constant)
ξ-θ "plane" is as follows,

$$z = x + iy; \ w = \xi + i\theta$$
$$z = a \tanh(w/2); \ w = 2 \tanh^{-1}(z/a).$$

It should be pointed out that the circular cross sections are

not concentric with the axial circle. The circles are displaced
outward with increasing size, crowding the ξ surfaces together
interior to the axial circle. Circulation distribution may be
determined by knowledge of the toroidal parameter a coth ξ_0 so
that the circulation Γ is given by

$$\Gamma = 2\pi \ a \ \text{csch} \ \xi \ \bar{U}_\theta, \quad \text{(cf. Fig. 3)}$$

where $\bar{U}_\theta$ is the azimuthal average of the velocity parallel to ξ's.
The axial parameter, a, may be inferred either from a lateral
Doppler scan or photogrammetrically. Of course 'a' can and
probably does change with time, just as a smoke ring expands
prior to ultimate dissolution. $U_\theta (\xi,\theta)$ may be determined by
a vertical scan for certain values of θ. The θ dependence
may be determined photogrammetrically on the surface of the
fireball where ξ is a constant.

Solutions to Laplace's Equation

Typical solutions to Laplace's equation incorporate ξ, θ,
$e^\xi \cos \theta$, $\cosh(n\xi)\sin(n\theta)$, etc.. In toroidal coordinates solu-
tions of Laplace's equation for the radial ξ component occur
as half-order spherical harmonics. Thus, a solution for the
vorticity field would have the form

$$\zeta = \frac{\zeta_0}{\pi} \ \sqrt{2(\cosh \xi - \cos \theta)} \ \sum_{n=0}^{\infty} \left(\frac{Q_{n-\frac{1}{2}}(\cosh \xi_0)}{P_{n-\frac{1}{2}}(\cosh \xi_0)} \ P_{n-\frac{1}{2}}(\cosh \xi) \cos(n\theta) \right.$$

where $Q_{n-\frac{1}{2}}$ and $P_{n-\frac{1}{2}}$

are half order spherical harmonics.

Scanning Problems

If the rate of ascent of the fireball is rapid compared to scan

time of the radar, the radar may be most appropriately used in
a stationary mode scanning the fireball as it passes, then
incrementing up and letting the fireball pass again, etc.. A
vertical scan would probably present a dual bimodal distribution
(cf Fig. 4) due to observations of the velocities at the far
end of the torus. (cf Fig. 5) From the scan angles, if a pseudo-
synoptic flow field can be determined, then the circulation may
be reconstructed. Naturally, the translational component of
the moving torus would have to be subtracted from the observed
circulation, as necessary, in order to reconstruct the circulation
of the torus seen moving with the torus. The whole flow field
may then be reconstructed by adding back in the translational
to the rotational velocities.

IV.   On The Containment of Toroidal Plasmas

The branch of physics featuring five field laws and a complementary
branch of mathematics may prove relevant to the problems of
magneto-hydrodynamic (MHD) stability in a toroidal plasma. The
relevance to the problem of formulating MHD equilibrium would
be simplified by knowledge of pressure distribution in the torus,
and in particular of its toroidal harmonics. A solution to
Laplace's equation of the pressure field specifies that the
pressure gradient be as small as possible, given boundary condi-
tions. The boundary conditions, including harmonic variations,
may conceivably be induced by appropriate design of the contain-
ment vessel and/or the placement of the electromagnets.

The distribution of pressure in a toroidal plasma is a vital
ingredient for determining stability. A critically high pressure
is needed for the fusion reactions to go to completion.

Currently, pressure is parameterized as a function of the magnetic
field strength, B. If the pressure in a plasma in the form of a
toroidal vortex does indeed satisfy the third proposed law, the

consequences would be as follows:

1) The MHD stability occurs as a consequence
of satisfaction of the third law, including the
toroidal harmonics in the pressure field;

2) Numerical codes become greatly simplified
by utilization of an analytic expression
describing pressure distribution, dependent
solely upon boundary values;

3) Critical pressures and temperatures may be
reached in toroidal harmonics which would not
otherwise be possible.

Utility of these proposed laws in a plasma is yet to be demonstra-
ted, but promise is indicated. Manipulation of the boundary
conditions of the plasma to produce toroidal harmonic solutions
of a specified wave number may spell the critical difference in
achieving temperatures and pressures necessary for fusion.

Axial circle
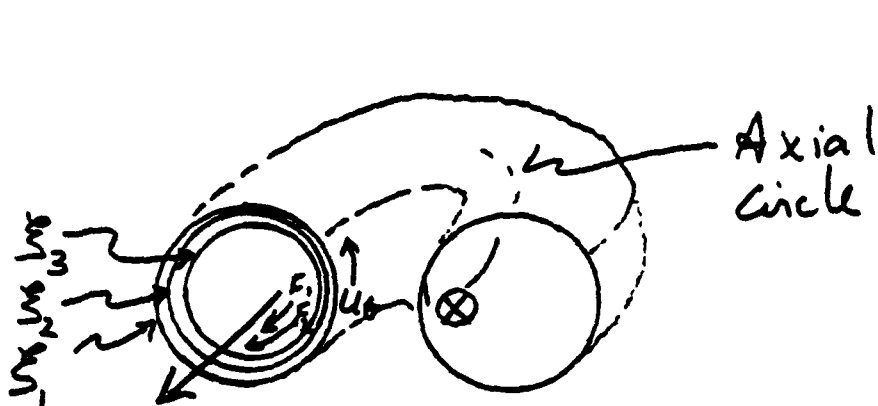
Figure 1. Frictional Curl vanishes in toroidal circulation
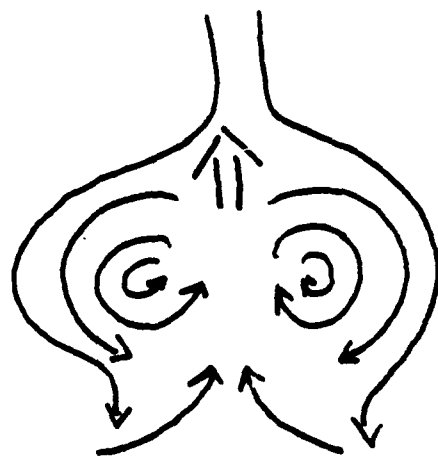
Figure 2. Streamlines of no-slip condition of rising toroidal vortex-cross section.
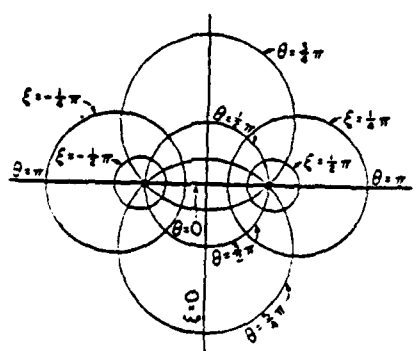
Toroidal Coordinates

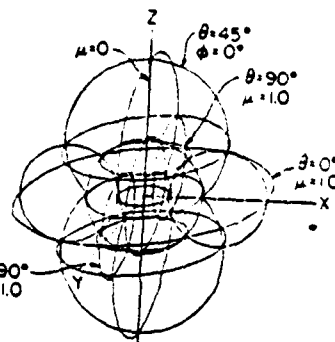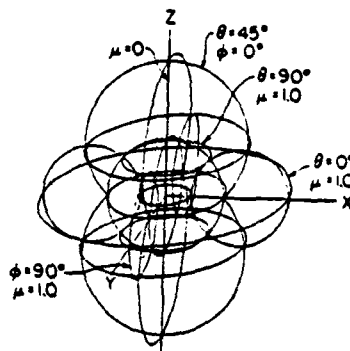Bipolar coordinates ξ and θ.
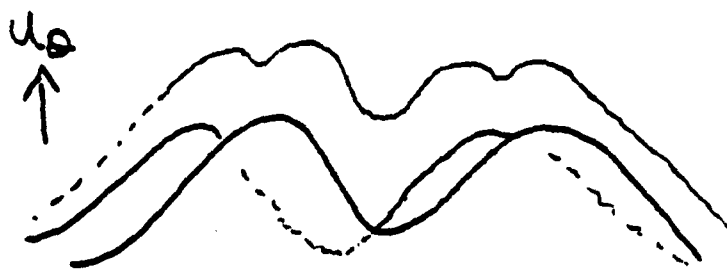
Figure 3. Bipolar and Toroidal Coordinates.
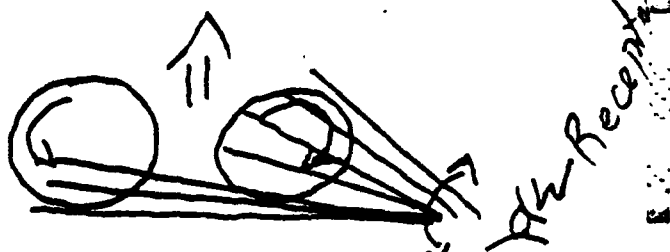
Figure 4. Dual bimodal distribution of velocities

Figure 5. Scanning angle of Doppler radar for far torus.

APPENDIX   E

PRELIMINARY FINDINGS FOR SPIRAL ANALYSIS OF

HURRICANE DAVID 243.6

The orthogonal spiral Fourier analysis technique is designed
to determine the Fourier components of the hurricane's spiral
bands in spiral coordinates and the distribution of the ampli-
tudes. The task is to separate out the spiral amplitudes by
taking cuts along the main axis of the bands. These cuts are
perpendicular to the bands. The sampling along these orthogonal
spirals occurs at regular azimuthal intervals.

The validity of the analysis is dependent on several factors.
First among these is the ability to fit a spherical log spiral
to the spiral bands as observed from the satellite. This means
that the spiral bands must be navigated so that there are no
errors due to foreshortening. This is accomplished in the
program "Tactical Environmental Display System" (TEDS) resident
on the Satellite Processing and Display System (SPADS) at the
Naval Environmental Prediction Research Facility, Monterey,
California.

The pixels from the satellite picture contain both navigational
information and values for the infrared return from cloud tops
to indicate the depths of the cumulonimbi observed. The assump-
tion is that the link between low level divergence, vertical
extent of the cumulus element and infrared return is sufficient-
ly linear that the measurement of the last gives an indication
of the first.

The satellite pictures provide both signal and noise. The signal
is the infrared vaulue of the cloud spiral. The noise enters in
in ground contamination (holes between the spiral bands with the
earth showing through), the graininess due to cumulus and cumulo-
nimbus elements, and the graininess due to pixel size. The first
is particularly evident in the outer part of the spiral band.
The second appears midway through the bands, and the third in
the close quarters near the center of the storm.
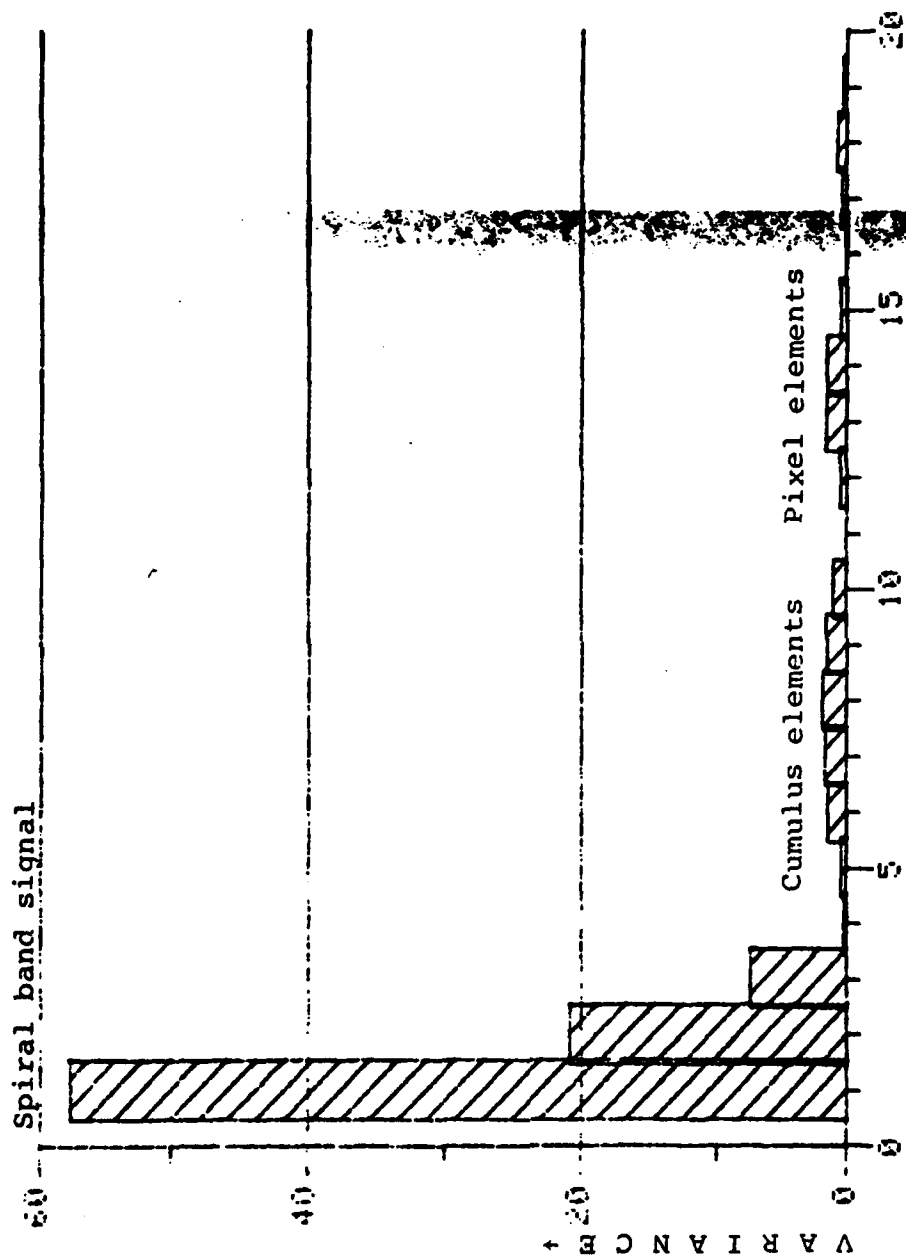
Wave Number →

Figure 1. Plot of logarithm of IR return from cut #1 in hurricane David 243.6 as a function of wave number. The Fourier amplitudes are taken along dotted spirals orthogonal to the main bands shown in Figure 5.
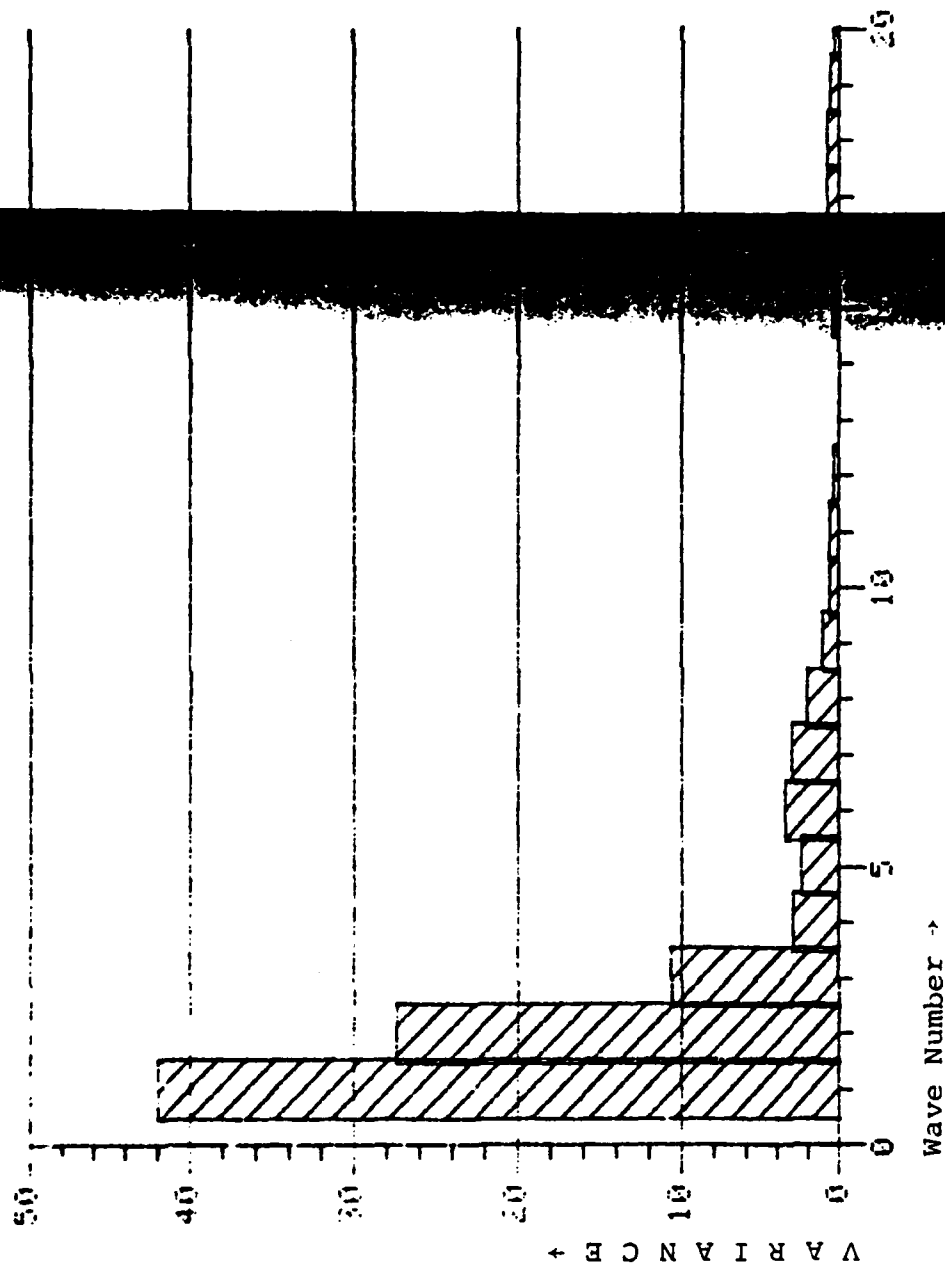
Figure 2. Plot of logarithm of IR return from cut #10 in hurricane David 243.6 as a function of wave number. The Fourier amplitudes are taken along dotted spiral orthogonal to the main bands shown in Figure 5.
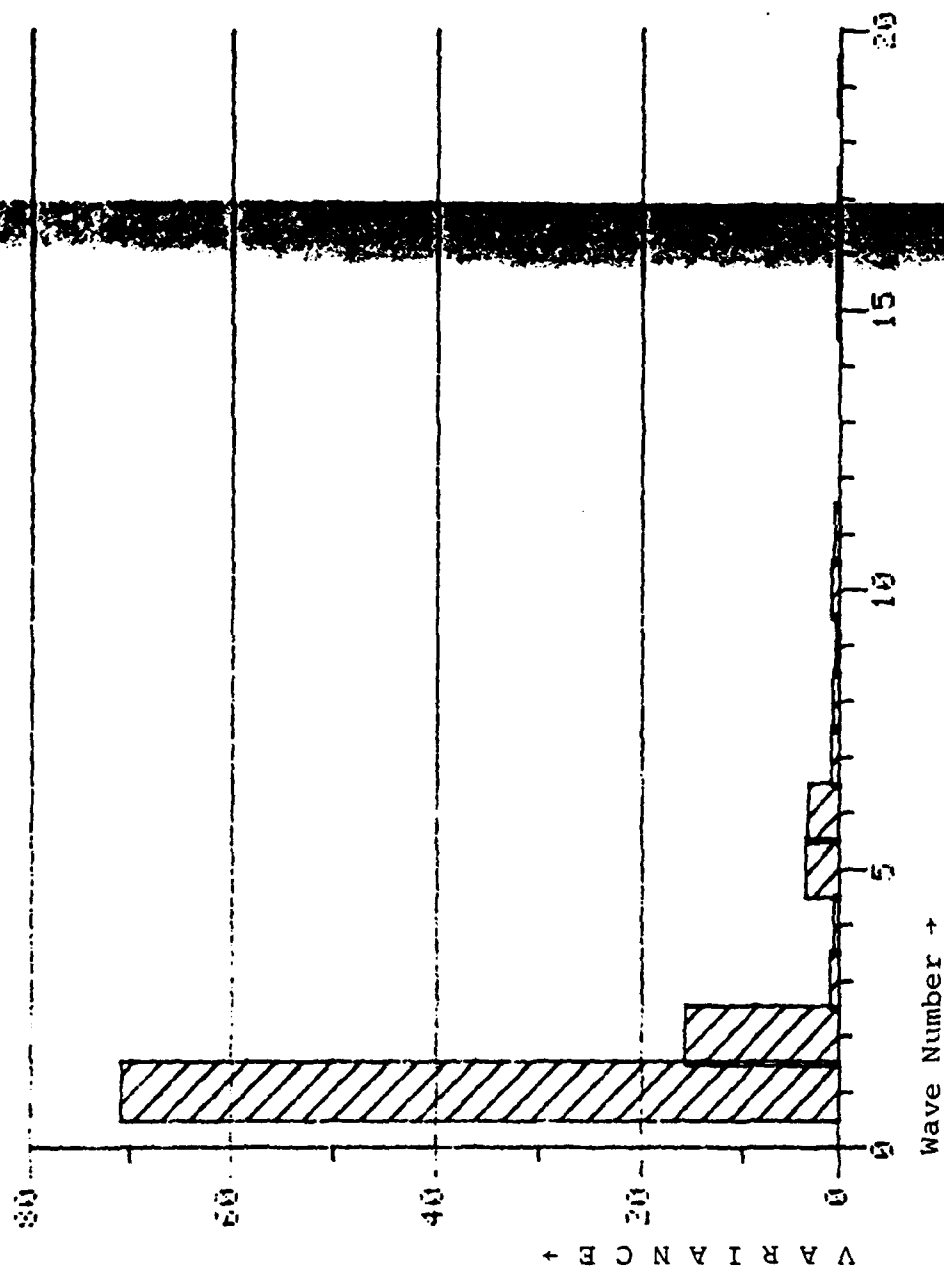
Wave Number →

Figure 3. Plot of variance of IR return from cut 19 in hurricane David 243.6 as a function of wave number. The Fourier amplitudes were taken along dotted spirals orthogonal to the main bands shown in Figure 5.

Three harmonics stand out in the histogram cuts taken at the first, tenth and nineteenth intervals along the main spiral band. Figure 1 shows the histogram at the first cut. The amplitudes for wave numbers one, two and three contain the majority of the signal. These amplitudes are due to the first three spiral bands analysed in David. Thus amplitudes 1-3 predominate in the analysis. Wave numbers 6-10 show a very shallow peak and can be attributed to the graininess due to the convective elements, cumulonimbi and cumuli. Wave numbers 12-15 show another shallow peak attributable to the graininess due to the boxiness of the pixels.

Altogether, in the analysis of David there were forty samplings along each cut, sufficient to provide wave numbers 1-20. A random distribution, indicative of low signal to noise ratio would not have been grouped so distinctly with the great weight of the signal, greater than 90%, grouped in only the first three wave numbers. Moreover, in a random distribution the peaks due to graininess attributable to cumulus elements and pixel size would not have stood out so clearly against a background virtually devoid of signal attributable to the bands themselves.

In cut ten, the logarithmic spacing of the sampling tends to crowd the cumulus and pixel graininess into the signal due to the bands, so that all of the peaks are crowded into the harmonics lower than twelve. All this means is that the separations centered at 4 and 11 are masked due to the shift into the lower wave numbers of the three sets of signals due to the logarithmic sampling necessary in spiral analysis. This is shown in Figure 2.

Figure 3 shows the histogram for cut 19. Again, the variance is predominantly in wave numbers one and two. The only other peak appears in wave numbers five and six.

Thus, at three samplings of the Fourier amplitudes performed
in spiral coordinates, the signal to noise ratio is sufficiently
high that the observed spiral bands are reducible to mathematical
parameterization. There does exist one other test, however.
The field theory specifies that the divergence field satisfies
Laplace's equation. The divergence is given by the infinite
series

$$\delta = \sum_{n=1}^{\infty} e^{nS_\nu} \cos nS_\mu.$$

In this series the amplitude, e^{nS_ν}, is a function of the wave
number, n. If the amplitudes of the wave numbers were plotted
vs. the IR return from the bands then there should be a relation-
ship directly between the two proportional to the wave number.
More simply,

$$\ln \delta = nS_\nu = n\nu \cos \alpha.$$

Thus the logarithm of the IR return is proportional to the
azimuthal displacement of the cut that the amplitude is determined
along. The proportionality is given by the wave number itself.
Therefore, not only should the logarithm of the amplitude be
linear in the azimuth, but the slope of the linearity is given
by the wave number, n. Figure 4 shows the amplitudes plotted
in a semilog scale. The logarithm of the amplitude beyond 0.7
are linear in the azimuth, given by the abscissa. The circles
represent amplitude for wave number 1, x's for number 2, and
triangles for number 3. As can be seen, the slope of the fitted
straight line is directly proportional to the wave number, so that
#2 has twice the slope (albeit negative) as #1 and #3 has
three times the slope. This is precisely what the field theory
predicts.

The data to the left of 0.7 is contaminated by the IR signal
from the surface of the sea, the first set of data contamination
mentioned above. As such it is disregarded in the analysis.

E-6

Figure 4. Plot of Fourier amplitudes vs. azimuth or distance along logarithm of the spiral $e^{S\nu}$. Circles are for wave number 1, x's for wave number 2, and triangles for wave number 3; slopes are proportional to wave number.

Obviously one case study does not constitute proof for the
discovery of a second law of physics. The evidence is promising,
however. The signal to noise ratio is very high. The unexplained
noise in the analysis is vanishingly small. The distribution of
the amplitudes is proportional to the wave number, as predicted
by the field theory and the amplitudes themselves are propor-
tional to the azimuth when plotted in semilog coordinates.

Figure 5 shows the analysis of hurricane David. The bright
white spiral running through the center of the cloud band is
the original fitted spiral. The solid spiral beginning in the
lower left corner of the illustration is the delimiting spiral
and runs parallel to the fitted spiral. The dotted spirals
orthogonal to the delimiting spiral are the spiral "cuts" and
the dots represent the pixel values sampled to obtain the
appropriate Fourier amplitudes. The Fourier amplitudes are
displayed in the picture as being linear in space along the
fitted spiral. The linearity is directly proportional to the
wave number. The center of the spiral is given by the 'x' in
the center of the storm, and the box is a navigational aid
used by TEDS to find the storm center given a user defined spiral
indicated by the rather crooked dashed spiral running through
the fitted spiral.

Part II of the Field Theory will present further analyses of
the amplitudes of various hurricanes in order to determine
the validity of David's representation of the field law
governing the distribution of low level divergence in a
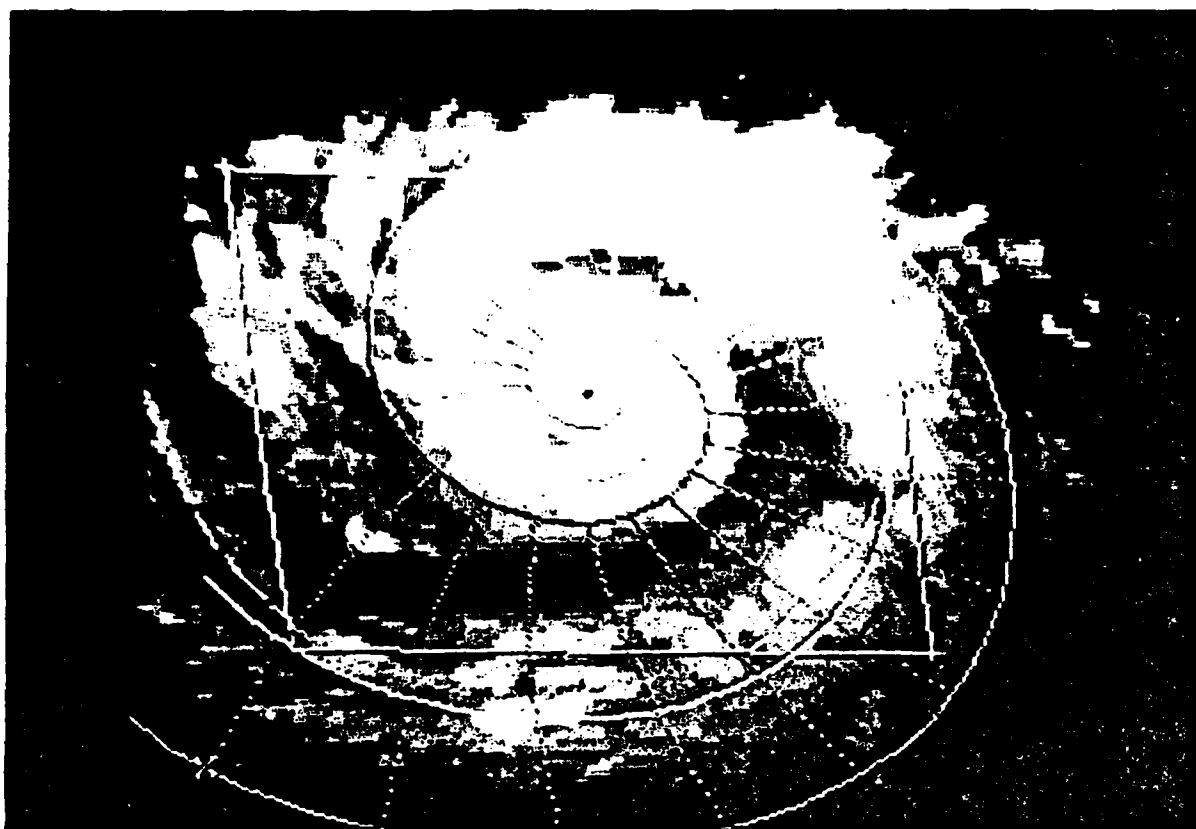hurricane.

Figure 5. Hurricane David 243.6 with spiral analyses.
Axial spiral goes through cloud center.
Delimiting spiral encompasses cloud band
beginning in lower left han corner.
Orthogonal analysis spirals are given by
dotted spirals perpendicualr to delimiting
spiral. Dots are loci for sampling.

END

FILMED

11-83

Date